Online ISSN：2186-490X
Print ISSN：1346-4272
CODEN：CCKHA7

地質調査研究報告

地質調査研究報告

BULLETIN OF THE GEOLOGICAL SURVEY OF JAPAN

Vol. 64　No. 5/6　2013

National Institute of Advanced Industrial Science and Technology
AIST

独立行政法人
産業技術総合研究所
地質調査総合センター

平成25年

地質調査研究報告
Bulletin of the Geological Survey of Japan
Vol. 64, No. 5/6, P. 121−190
2013

地質調査研究報告
BULLETIN OF THE GEOLOGICAL SURVEY OF JAPAN
Vol. 64 No. 5/6 2013

表紙の写真

秋の秋吉台

日本の地球化学図は約 3000 個の河川堆積物を用いて作成した広域元素濃度分布図であり，2004 年に出版された．その 5 年後には，陸海域を含めた包括的な広域元素濃度分布調査を目的として，海洋地球化学図の作成も行った．陸域の元素濃度分布は，地質や鉱山の分布を忠実に反映している．しかし，石灰岩地域は例外であり，大規模石灰岩から供給された河川堆積物中のカルシウムやストロンチウムの濃度は他の河川堆積物に比べ著しく低い．石灰岩地域における粒子移送過程を明らかにするために，日本最大の石灰岩岩体である山口県秋吉台から河川堆積物を採取した．写真はサンプリング終了後，秋吉台カルスト展望台から撮影したものである．風に揺れるススキが秋吉台の秋を感じさせる．

（写真・文：太田充恒）

Cover page

Akiyoshi-dai in autumn

The Japanese geochemical map is the regional spatial distribution pattern of elemental concentrations that was created using about 3000 stream sediment samples and published in 2004. For a comprehensive survey of regional spatial distribution pattern of elemental concentrations both in terrestrial and marine environment, marine geochemical map was further produced after five years. The spatial distribution patterns of elemental concentrations of stream sediments reflect faithfully the distribution of geology and mineral deposits. However, the exception is limestone bedrock. The stream sediments derived from a large-scale limestone bedrock were significantly poorer in calcium and strontium than other sediments. Stream sediments were sampled from Akiyoshi-dai in Yamaguchi Prefecture, where is underlain by the largest-scale limestone bedrock region was selected to elucidate the particle transfer process in limestone region. I took photograph in Akiyoshi-dai from the Akiyoshi-dai karst observation platform after sampling. A Japanese silver grass swing by wind lets you fell autumn of Akiyoshi-dai.

(Photograph and Caption by Atsuyuki Ohta)

Bulletin of the Geological Survey of Japan, vol. 64 (5/6), p. 121 - 138, 2013

Article

Less impact of limestone bedrock on elemental concentrations in stream sediments – Case study of Akiyoshi area –

Atsuyuki Ohta[1, *] and Masayo Minami[2]

Atsuyuki Ohta, Masayo Minami (2013) Less impact of limestone bedrock on elemental concentrations in stream sediments – Case study of Akiyoshi area – *Bull. Geol. Surv. Japan*, vol. 64 (5/6), p. 121-138, 8 figures, 4 tables, 1 appendix.

Abstract: Geological survey of Japan, National Institute of Advanced Industrial Science and Technology has created the nationwide geochemical maps of 53 elements using fine stream sediments (< 180 μm) in Japan. The spatial distribution patterns of elemental concentrations of stream sediments reflect faithfully the distribution of geology and mineral deposits. However, the exception is limestone bedrock, which insignificantly influences on elemental concentrations of stream sediments. To clarify the reason, we collected stream sediments from Akiyoshi-dai, where is underlain by the largest-scale limestone bedrock. Fine stream sediments (< 180 μm), whose drainage basins are occupied by limestones, have high CaO and Sr concentrations and intensive peak of calcite obtained by X-ray diffractometry. Examining variation of elemental concentrations against the particle size of sediments, the finer particle contains a higher proportion of calcite and has higher CaO concentration. However, CaO concentration (10–20 wt. %) in stream sediments is much lower than expected values (~50%); nevertheless limestone outcrops in more than 70 % in their watersheds. The contradictory finding is explained by less contribution of limestone clastics to river system because limestone bedrocks are easily dissolved by water (chemical weathering) but not susceptible to physical weathering and erosion process. In other words, the supply quantity of clastic materials from limestone bedrocks is much smaller than those of other rock types. In addition, Sr concentration in some samples does not correlate with either CaO concentration or the peak intensity of calcite; nevertheless Sr is expected to have similar chemical properties to CaO. The fact suggests that calcite formed from water oversaturated for calcium carbonate is supplied to river system; it has the different Sr concentrations from Akiyoshi Limestone.

Keywords: Akiyoshi-dai; limestone; stream sediment; geochemical map; calcium; strontium

1. Introduction

The Geological Survey of Japan, National Institute of Advanced Industrial Science and Technology prepared nationwide geochemical maps of 53 elements in stream sediments for environmental assessment (Imai *et al*., 2004). Stream sediments are considered to be a composite sample of the products of weathering and erosional of soil and rocks in the catchment area upstream from the sampling site (Howarth and Thornton, 1983). In other words, the spatial distribution patterns of elemental concentrations are controlled conclusively by parent lithology and mineral deposits. Ohta *et al*. (2004a, 2004b, 2005) revealed that this assumption is also reasonable in Japan, where geology has particularly complicated distributions and many mineral deposits occur on a small scale. However, ultramafic rock and limestone associated with accretionary complexes were exceptions. Ultramafic rock elevates highly MgO, Cr, Co, and Ni concentrations in stream sediments, even if it crops out only in a small area (Ohta *et al*., 2004b, 2005). Meanwhile, the contribution of limestone for elemental concentrations in stream sediments was very small in Japan. The stream sediments derived from accretionary complexes associated with a large-scale limestone bedrock were significantly poor in CaO and Sr than other sediments (Ohta *et al*., 2004a). In European countries, extremely high CaO concentration (10–55%) in stream sediments found in the area covered by calcareous sediments and limestone (e.g., De Vos *et al*., 2006; Albanese *et al*., 2007). The sampling density of Japanese geochemical mapping project is low: 1 site per 100 km^2 (Imai *et al*., 2004). Japanese limestone is

[1]AIST, Geological Survey of Japan, Institute of Geology and Geoinformation

[2]Center for Chronological Research, Nagoya University, Chikusa, Nagoya 464-8602, Japan

*Corresponding author: A. OHTA, Central 7, 1-1-1 Higashi, Tsukuba, Ibaraki 305-8567, Japan. E-mail a.ohta@aist.go.jp

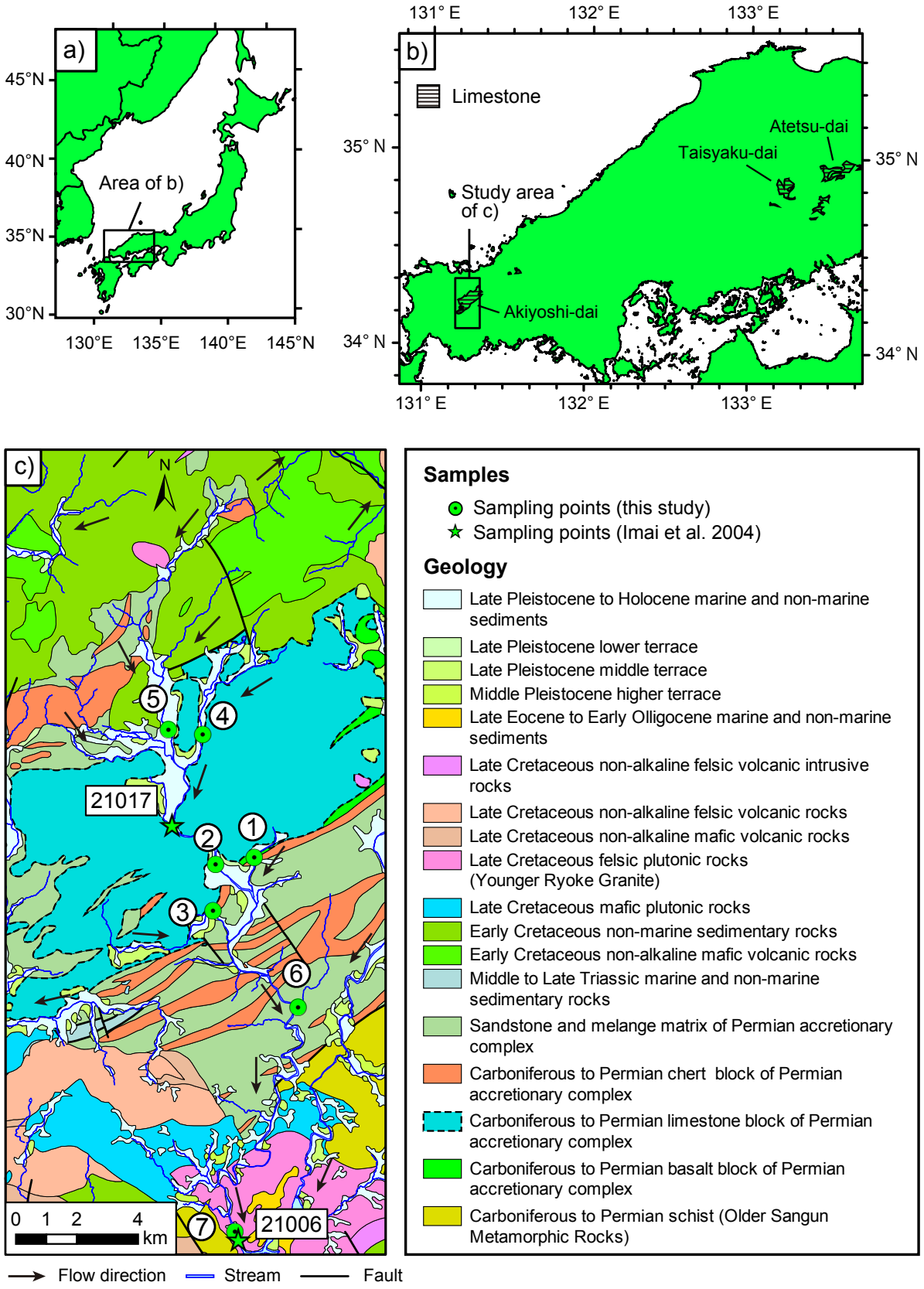

Fig 1. a) Schematic map of the study area. b) Chugoku region with large-scale limestone bedrocks (Akiyoshi-dai, Taisyaku-dai and Atetsu-dai). c) Geological map around the Akiyoshi-dai at a scale of 1:200,000 (Matsuura *et al*., 2007; Geological Survey of Japan, AIST, 2012).

Table 1. Relative ratio by weight of respective grain sizes to sediments less than 2 mm.

	Akiyoshi						
Grain size	1	2	3	4	5	6	7
<180 μm	4.5%	3.6%	6.4%	4.2%	6.1%	4.9%	22%
1-2 mm	33%	43%	41%	42%	31%	42%	12%
500–1000 μm	28%	29%	27%	23%	34%	24%	15%
250–500 μm	25%	19%	19%	23%	24%	26%	21%
125–250 μm	9.2%	6.5%	8.1%	8.5%	8.5%	5.1%	22%
63–125 μm	2.3%	1.2%	3.1%	2.1%	1.9%	1.1%	19%
32–63 μm	0.9%	0.6%	1.1%	1.4%	0.7%	0.8%	8.2%
<32 μm	0.6%	0.6%	0.4%	0.4%	0.3%	0.7%	3.2%

small in size and distributes sporadically. Therefore small limestone-exposed area in watershed might be the reason why the less influence of limestone on elemental concentrations in stream sediments (Ohta *et al*., 2004a). To elucidate the particle transfer process in limestone region, we focus on the Chugoku region where large-scale limestone bedrocks (Akiyoshi-dai, Taisyaku-dai and Atetsu-dai) are exposed (Fig. 1a and b).

2. Study area and samples

2.1 Geology

Figure 1c depicts the geology at a 1:200,000 scale (Matsuura *et al*. 2007; Geological Survey of Japan, 2012). The central part of the study area is covered by Permian accretionary complexes consisting of trench fills (sandstone and mélange matrix) and exotic blocks of oceanic rocks, chert, limestone and metabasalt that range in age mainly through the Carboniferous–Permian. The Akiyoshi Limestone is originated from a Carboniferous-Permian atoll complex upon a seamount (Sano and Kanmera, 1991). They consist of heterogeneous aggregate of the collapsed product during the subducting process in the Middle Permian (Sano and Kanmera, 1991): a complicated mixture of limestone and metabasalt blocks. A surface part of them is covered thinly by the Late Pleistocene to Holocene sediments. Cretaceous non-marine sedimentary rocks (red shale, sandstone, and conglomerate) and Cretaceous basaltic–andesitic lava and tuff are distributed in the northern and southern parts. Rhyolite-dacitic tuffacious rocks cropout in the northeastern and southwestern part. Granitic rocks intruded during Cretaceous time occur mainly in southern part and sporadically in the northern part. High-pressure typed metamorphic rocks distributing on the southeastern side consist mainly of pelitic schist.

2.2 Samples

The Akiyoshi-dai is selected for the study area; stream sediment samples were collected in the high density (Fig. 1c). All samples were collected from the Kotou river system flowing through the Akiyoshi Limestone bedrock. Samples nos. 1, 3, 4, and 5 were collected from the subsidiary stream; samples nos. 2, 6, and 7 were collected from the main river (Fig. 1c). The river sediments at the locations nos. 1 and 3 consisted dominantly of fine sandy sediments. The riverbeds at the locations nos. 2, 4, 5, and 6 were covered by coarse sediment including cobbles and gravels. Especially the riverbed at the location no. 6 was covered dominantly by cobbles and gravels: sandy sediments deposited among them were collected. The location no. 7 is situated at the upper reach of the dam lake. The very fine sandy and silty sediments were deposited there. The star symbols indicate the samples (nos. 21006 and 21017) collected for the nationwide Japanese geochemical mapping (Imai *et al*., 2004).

The collected samples were dried in air and sieved with a 180 μm screen for comparison with the data of Japanese geochemical maps. The duplicated sample was sieved with 7 kinds of screens: 2 mm, 1 mm, 500 μm, 250 μm, 125 μm, 63 μm, and 32 μm screens. The coarser grains over 2 mm were not used for the study. The sieved samples were ground with an agate mortar and pestle. Table 1 summarized the relative ratio by weight of respective grain sizes to samples sieved with 2 mm. The relative ratio by weight of <180 μm is about 4–6% for most cases, but is extremely high for sample no. 7 (22%). Those values do not correlate to a respective catchment area. The 80–90% of stream sediments less than 2 mm is composed of medium to very coarse-grained sands (over 250 μm). However, the coarse sands of sample no. 7 account for just 48% of total sediments sieved with a 2 mm screen. The percentages of fine sands and silty grains (less than 250 μm) of sample no. 7 are extremely higher than those of the other samples.

3. Analytical methods

The degradation of samples follows the method used in Japanese geochemical mapping project (Imai *et al*., 2004). 0.2 g of each sample was digested using HF (5 ml), HNO_3 (3 ml) and $HClO_4$ (2 ml) at 120°C for 3 hr.

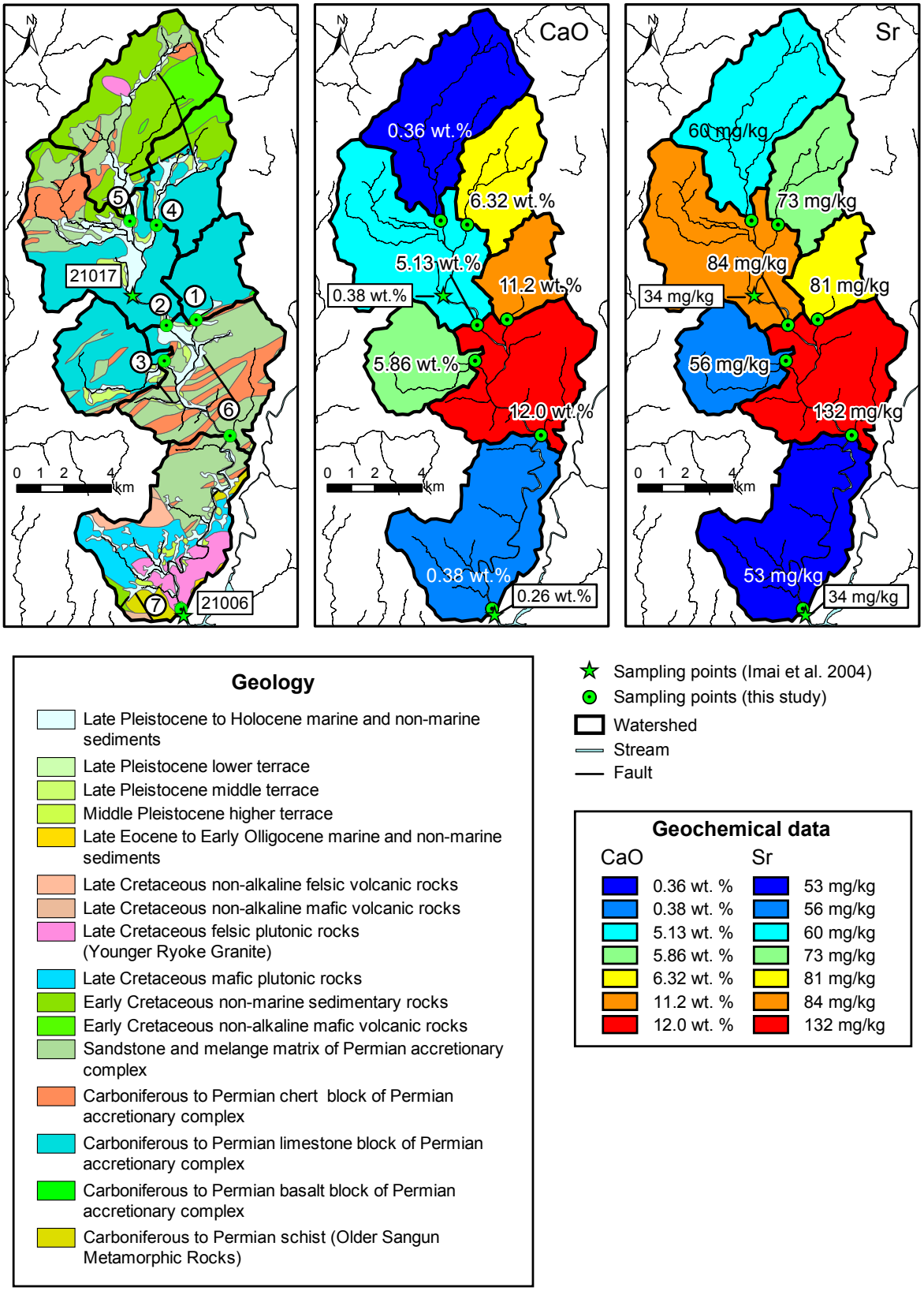

Fig 2. Catchment areas including geology at a scale of 1:200,000 (Matsuura *et al.*, 2007; Geological Survey of Japan, AIST, 2012), and CaO and Sr concentrations of stream sediments sieved with a 180 μm screen.

The degraded product was evaporated to dryness under 180°C and the residue was dissolved with 5 ml of 7 mol/L HNO_3. The dissolved solution was diluted to be 100 mL with deionized water. Concentrations of 51 elements were determined using: ICP-AES (Na_2O, MgO, Al_2O_3, P_2O_5, K_2O, CaO, TiO_2, MnO, Total (T-) Fe_2O_3, V, Sr, and Ba) and ICP-MS (Li, Be, Sc, Cr, Co, Ni, Cu, Zn, Ga, Rb, Y, Zr, Nb, Mo, Cd, Sn, Sb, Cs, La, Ce, Pr, Nd, Sm, Eu, Gd, Tb, Dy, Ho, Er, Tm, Yb, Lu, Hf, Ta, Tl, Pb, Bi, Th, and U). Table 2 summarizes analytical results for the stream sediments.

The samples were further characterized using x-ray powder diffraction (XRD) with CuKα radiation (RIGAKU RINT-2500). The x-ray tube was operated at 40 kV with a 100 mA current. The scanning velocity was 2°(2θ)/min. Sample was placed in a reflection free sample holder (15 mm × 20 mm × 0.2 mm) and pressed vertically using a microscope slide glass to planarize the surface and removed excess sample powders.

4. Results

4.1 Watershed analysis

To elucidate the dominant lithology distributing in respective river system, the watershed stream network was calculated from the digital elevation model (50 m mesh data) provided by the Geographical Survey Institute, Japan. The GIS software (ArcGIS 10.0; Environmental Systems Research Institute) was used for the calculation. Figure 2 portrays the catchment boundary obtained for each sampling location. The area of estimated watershed boundary is summarized in Table 3. The area of watershed of samples nos. 1, 3, 4, and 5 are 10–30 km^2. Those sampling density is 3–10 times as high as those of Japanese geochemical mapping project (1 sample/100 km^2). The catchment areas for samples nos. 2, 6, and 7 include those for samples collected upper stream: these determined areas range from 78 km^2 to 164 km^2.

We assumed that elemental concentrations of stream sediments are determined by the representative lithology, which is the specific rock type exposed in a drainage basin most widely. The intended lithology was Pleistocene-Holocene unconsolidated sediments, Cretaceous sedimentary rocks, Permian accretionary complexes, Cretaceous felsic and mafic volcanic rocks, Cretaceous felsic and mafic plutonic rocks and Carboniferous to Permian metamorphic rocks (mainly pelitic schist). Permian accretionary complexes are further grouped into four: sandstone-mélange matrix, limestone, chert and metabasalt. Table 3 summarizes the relative exposed areas of these lithologies in each drainage basin. Limestone is the dominant lithology in the catchment areas for samples nos. 1, 3, and 4. Pleistocene to Holocene sediments, Cretaceous sedimentary rocks, sandstone and mélange matrix of Permian accretionary complexes are distributed in the watershed of samples nos. 2, 5, 6, and 7. The volcanic, plutonic and metamorphic rocks are the minor lithologies in watershed area of all samples. Table 3 suggests that all samples except for no. 5 contain limestone bedrocks in their river basins. For comparison, the watershed analysis result for samples nos. 21006 and 21017 were also shown in Table 3. The catchment area of sample no. 21006 includes that of 21017. A quarter of those watersheds is covered by limestone bedrocks.

4.2 Spatial distribution patterns of elemental concentrations in stream sediments

Figure 2 portrays the catchment areas, geology within respective watersheds, and CaO and Sr concentrations of stream sediments sieved with 180 μm in order to visualize the relationships between geology and CaO (or Sr) concentration. Five samples out of the newly corrected seven samples have high CaO concentration (5–12 wt. %). However, those values are much lower than 53–55 wt. % of CaO concentration in pure limestone. Sample no. 5 has low CaO concentration (0.36 wt. %) because little limestone distributes in its river basin, where sandstone and mélange matrix of Permian accretionary complexes, Cretaceous sedimentary rocks and Cretaceous mafic volcanic rocks are exposed (Fig. 2a and Table 3). Although sample no. 21017 locates just two km upstream from sample no. 2, its CaO content is no more than 0.38 wt. %. Sample no. 6 has the highest CaO concentration (12.0 wt. %) among 7 samples. Sandstone and chert of Permian accretionary complexes distribute widely around the location no. 6. The fact indicates that calcareous sediment is indeed conveyed from upstream to location no. 6. The samples nos. 7 and 21006 present in the lowest reaches of the Kotou River. Both samples have the quite low CaO concentration, nevertheless their drainage basin contains limestone bedrock as in the case with sample no. 6. The Sr concentration of stream sediments collected in river system underlain by limestone is high (73–132 mg/kg) in analogy with CaO concentration. As exception, Sr content in sample no. 3 is as low as those of samples nos. 5, 21006, and 21017. The Sr concentration of the Akiyoshi Limestone is 80–340 mg/kg (Nakano and Ishihara, 2003). The Sr concentration of stream sediments is somewhat lower than that of limestone bedrocks.

Next, we examined the features of concentrations of the other elements (Table 2). Little variation is observed for Al_2O_3 concentration among seven samples. The samples nos. 1 and 3 have low concentrations of Na_2O, K_2O, Rb, Ba and high concentrations of P_2O_5, TiO_2, T-Fe_2O_3, V, Cr, Co, Ni, Cu, Zn, Y, and lanthanide (La–Lu). The high concentrations of P_2O_5 and 3d transition elements in samples nos. 1 and 3 would be caused by metabasalt associated with the Akiyoshi Limestone (Figs. 1c and 2). The samples nos. 5 and 7 have high K_2O, Rb and Ba concentrations; low MnO and rare earth element concentrations.

4.3 Variation of elemental concentrations in stream sediments according to grain size

Figure 3 shows how CaO and Sr concentrations in stream sediments change according to grain size. Samples nos. 1, 2, 3, 4, and 6 whose CaO concentration is high,

Table 2. Analytical results of fine stream sediments (<180 μm) collected from the Kotou River and those derived from sedimentary rocks in accretionary complexes in Chugoku region.

		Akiyoshi (this study)							Imai et al. (2004)[a]		Ohta et al. (2004)[b]
		1	2	3	4	5	6	7	21006	21017	Med. (min. ~ max.)
Na_2O	wt. %	0.67	1.01	0.49	1.03	1.02	1.05	1.09	0.46	1.00	1.72 (0.46 – 3.00)
MgO	wt. %	0.60	0.70	0.57	0.55	0.78	0.58	0.78	1.08	1.24	1.43 (0.63 – 3.63)
Al_2O_3	wt. %	8.53	9.52	9.05	9.78	8.86	9.13	7.99	10.70	10.37	8.11 (5.57 – 12.1)
P_2O_5	wt. %	0.14	0.11	0.19	0.12	0.10	0.12	0.099	0.085	0.079	0.097 (0.062 – 0.14)
K_2O	wt. %	1.18	1.53	1.18	1.43	1.67	1.30	2.05	2.18	1.78	2.22 (1.60 – 2.81)
CaO	wt. %	11.2	5.13	5.86	6.32	0.36	12.0	0.38	0.26	0.38	0.81 (0.26 – 2.36)
TiO_2	wt. %	1.27	0.79	1.20	0.63	0.77	0.87	0.92	0.71	0.56	0.53 (0.32 – 0.92)
MnO	wt. %	0.26	0.22	0.18	0.19	0.073	0.21	0.070	0.081	0.11	0.12 (0.064 – 0.31)
T-Fe_2O_3	wt. %	7.85	4.41	6.21	3.76	4.20	4.12	4.22	5.85	5.71	4.52 (2.36 – 6.46)
Li	mg/kg	25	29	40	29	33	19	33	67	57	46 (19 – 76)
Be	mg/kg	1.8	1.5	1.6	1.5	1.6	1.1	1.7	2.1	2.2	2.2 (0.80 – 3.3)
Sc	mg/kg	10	9.0	11	8.1	6.8	8.2	6.9	7.4	6.4	7.4 (4.2 – 19)
V	mg/kg	107	78	114	65	78	78	88	119	111	80 (43 – 135)
Cr	mg/kg	95	52	113	59	57	39	56	74	63	54 (24 – 138)
Co	mg/kg	20	13	19	11	11	11	12	14	21	11 (5.0 – 21)
Ni	mg/kg	28	19	46	20	20	14	25	33	27	24 (12 – 39)
Cu	mg/kg	103	23	37	26	25	19	25	31	27	38 (18 – 74)
Zn	mg/kg	232	103	219	107	122	90	110	114	90	130 (90 – 198)
Ga	mg/kg	12	14	15	13	15	11	16	22	19	17 (7.0 – 23)
Rb	mg/kg	62	68	61	73	75	56	99	133	110	127 (67 – 156)
Sr	mg/kg	81	84	56	73	60	132	53	34	34	75 (33 – 125)
Y	mg/kg	26	19	30	19	11	17	10	13	13	15.1 (8.6 – 43)
Zr	mg/kg	90	80	115	85	100	74	97	77	73	67 (37 – 227)
Nb	mg/kg	14	11	12	11	12	10	14	11	8.4	8.3 (4.3 – 14)
Mo	mg/kg	1.7	1.1	1.3	0.96	0.75	0.62	0.75	1.3	0.6	1.2 (0.31 – 13)
Cd	mg/kg	4.0	1.7	6.3	1.3	0.46	0.98	0.61	0.09	0.49	0.29 (0.090 – 0.70)
Sn	mg/kg	19	5.8	7.6	3.1	4.4	2.3	4.4	3.4	2.8	3.8 (2.5 – 9.7)
Sb	mg/kg	4.7	1.8	6.0	2.1	1.4	1.1	1.4	0.97	1.6	1.2 (0.37 – 2.3)
Cs	mg/kg	6.0	8.2	11	9.3	9.3	6.6	7.7	11	13	8.9 (3.3 – 13)
Ba	mg/kg	213	366	192	283	349	295	370	450	388	401 (194 – 460)
La	mg/kg	22	19	24	21	14	17	13	22	18	19 (10 – 69)
Ce	mg/kg	41	34	41	37	29	32	25	31	28	31 (17 – 170)
Pr	mg/kg	5.2	4.5	5.8	4.9	3.5	4.1	3.3	4.7	3.7	4.4 (2.2 – 21)
Nd	mg/kg	19	16	22	17	12	15	12	18	14	17.2 (8.5 – 80)
Sm	mg/kg	3.9	3.3	4.6	3.3	2.4	2.8	2.5	3.3	2.7	3.3 (1.7 – 17)
Eu	mg/kg	0.84	0.73	1.0	0.68	0.50	0.62	0.45	0.67	0.58	0.65 (0.35 – 0.87)
Gd	mg/kg	3.6	2.9	4.0	2.8	2.0	2.5	2.0	2.9	2.5	2.9 (1.6 – 13)
Tb	mg/kg	0.53	0.47	0.62	0.42	0.31	0.38	0.31	0.49	0.41	0.49 (0.26 – 2.0)
Dy	mg/kg	3.2	2.9	3.7	2.7	1.9	2.4	1.8	2.3	2.0	2.4 (1.4 – 9.3)
Ho	mg/kg	0.60	0.54	0.69	0.51	0.35	0.45	0.34	0.43	0.40	0.47 (0.27 – 1.6)
Er	mg/kg	2.0	1.8	2.2	1.7	1.2	1.5	1.1	1.2	1.2	1.4 (0.81 – 4.8)
Tm	mg/kg	0.30	0.29	0.34	0.27	0.19	0.23	0.17	0.19	0.18	0.23 (0.12 – 0.81)
Yb	mg/kg	1.9	1.8	2.2	1.8	1.3	1.5	1.2	1.2	1.1	1.4 (0.83 – 5.3)
Lu	mg/kg	0.30	0.29	0.34	0.29	0.20	0.25	0.19	0.17	0.15	0.22 (0.12 – 0.86)
Hf	mg/kg	2.4	2.2	2.8	2.4	2.7	2.0	2.9	2.1	2.0	1.9 (1.1 – 9.8)
Ta	mg/kg	1.1	0.79	0.38	0.90	0.96	0.78	1.3	0.72	0.69	0.67 (0.39 – 1.7)
Tl	mg/kg	0.49	0.66	0.70	0.60	0.64	0.40	0.77	0.96	0.88	0.82 (0.46 – 1.0)
Pb	mg/kg	49	25	129	43	26	23	36	37	31	37 (24 – 90)
Bi	mg/kg	5.8	0.33	0.67	0.38	0.43	0.29	0.72	0.28	0.28	0.45 (0.19 – 1.4)
Th	mg/kg	8.8	7.3	7.2	8.1	7.5	5.5	9.5	7.3	5.5	7.5 (5.5 – 259)
U	mg/kg	1.8	1.6	1.4	1.5	2.2	1.6	2.6	2.8	2.4	2.2 (1.2 – 32)

[a] Two samples were also collected from Kotou River.

[b] Median (med.), minimum (min.), and maximum (max.) of elemental concentrations were calculated from the data of stream sediments derived from the accretionary complexes in Chugoku region.

Table 3. Area of watershed and estimated ratios of exposed area of lithologies[a] distributed in each watershed.

	Watershed area	Sedimentary rock		Accretionary complex				Volcanic rock		Plutonic rock		Metamorphic rock
		Sed. A	Sed. B	Ss-Mélange	Limestone	Chert	Metabasalt	Felsic	Mafic	Felsic	Mafic	
	km^2	%	%	%	%	%	%	%	%	%	%	%
Akiyoshi												
No. 1	10	2.7	0	0	93	3.2	1.4	0	0	0	0	0
No. 2	78	14	28	12	30	7.6	0	0	7.5	0.9	0	0
No. 3	15	10	0	8.6	77	4.3	0	0	0	0	0	0
No. 4	16	13	24	0	52	0	0	0	10	0	0	0
No. 5	30	10	53	15	1.1	5.7	0	0	14	2.4	0	0
No. 6	131	13	17	19	35	11	0.1	0	4.5	0.5	0	0
No. 7	164	14	14	21	28	10	0.1	1.1	3.9	3.5	4.5	1.4
Imai et al. (2004)												
21006	164	14	14	21	28	10	0.1	1.1	3.9	3.5	4.5	1.4
21017	71	14	31	13	25	8.3	0	0	8.3	1.0	0	0

Sed. A: Pleistocene to Holocene sediments; Sed. B: Cretaceous sedimentary rocks; Ss-Mélange: Sandstone and melange matrix

[a] Geological Survey of Japan, AIST (ed.). 2012. Seamless digital geological map of Japan 1: 200,000. Jul 3, 2012 version. Research Information Database DB084, Geological Survey of Japan, National Institute of Advanced Industrial Science and Technology.

show the similar trends mutually. The CaO concentration is rather constant in very coarse (1–2 mm), coarse (500–1000 μm) and medium sands (250–500 μm): it increases steeply from fine sand (125–250 μm) to coarse silt (32–63 μm): becomes the highest in fine silt (<32 μm). Two samples (nos. 5 and 7) having low CaO content show the different feature: little systematic differences across grain sizes. On the other hands, variation of Sr concentration across the grain sizes is much smaller than those of CaO concentration. The Sr concentration also increases gradually with decreasing grain sizes. Adversely, Sr concentration of sample no. 1 is high in coarser grains except for very coarse sand (1–2 mm). Because Sr(II) has similar ionic radii to Ca(II), both elements are expected to have similar chemical properties mutually. However, this is not true in the study area.

Figure 4 shows the variation of concentrations of elements except for CaO and Sr against grain size of sediments. Al_2O_3 concentration of samples nos. 1, 3, and 6 is constant for all grain sizes, but that of the other samples gradually increases with decreasing grain size. The Na_2O, MgO, K_2O, Rb, and Ba concentrations are almost constant among sandy sediments, but become low in silty sediments (below 63 μm). The Sc, TiO_2, V, T-Fe_2O_3, and Co concentrations have the peak at fine sand (125–250 μm). For sample no. 3, the concentrations of P_2O_5, T-Fe_2O_3, Cr, Co, Cu, and Zn gradually decrease with decreasing the grain size. The concentrations of the other elements increase with decreasing grain size: they steeply increase below very fine sand (63–125 μm) grains (see Y in Fig. 4).

4.4 XRD patterns of stream sediments

Figure 5 shows the XRD patterns of stream sediments under 180 μm. Quartz, plagioclase and clay minerals (kaolinite and chlorite) are recognized in all samples. The high x-ray intensities were observed at 29.4°, 48.5°, 39.4°, 43.2°, and 36.0° (2θ), which are attributed to calcite. The intensities of alkali feldspar are smaller than those of plagioclase. No calcite peak is found for samples nos. 5 and 7. Accordingly, the high CaO concentration in samples nos. 1, 2, 3, 4, and 6 is explained by calcite supplied from limestone bedrocks.

Figures 6 and 7 show the XRD patterns of samples nos. 1 and 7 among various grain sizes, respectively. In sample no. 1, the peak intensities of quartz, plagioclase and K-feldspar decrease with decreasing grain size. The peak intensity of calcite increases steeply below 125 μm of grain size, which corresponds to the steep increase of CaO concentration below 125 μm of grain size (Fig. 3). Accordingly, high CaO concentration in fine grains can be explained by calcite presenting in stream sediment. The peaks of plagioclase and alkali feldspar become less prominent below the 125 μm of grain size. That change found in XRD pattern corresponds to the decrease of Na_2O and K_2O concentrations below the 125 μm of grain size (Fig. 4). The very small peak appears at 35.5° (2θ) for 63–500 μm grain size samples, which may be attributed to magnetite or pyroxene. Sample no. 7 has no peak of calcite but has intensive peaks attributed to plagioclase and alkali feldspar. The peak intensity at 27.5° of alkali feldspar becomes high in middle grain sizes (125–500μm); that at 28.0° of plagioclase becomes high in finer grains (32–125 μm). Especially, the intensive peak of alkali feldspar is notable feature for sample no. 7.

4.5 Relationship between elemental concentrations and XRD peak intensities

Yamamoto *et al*. (1998) reported that elemental concentrations of stream sediments have a good correlation to peak intensities of minerals obtained by XRD. The correlation between elemental concentrations and peak intensities of minerals were also estimated in this study. We assumed that the intensities of 12.4°, 26.6°,

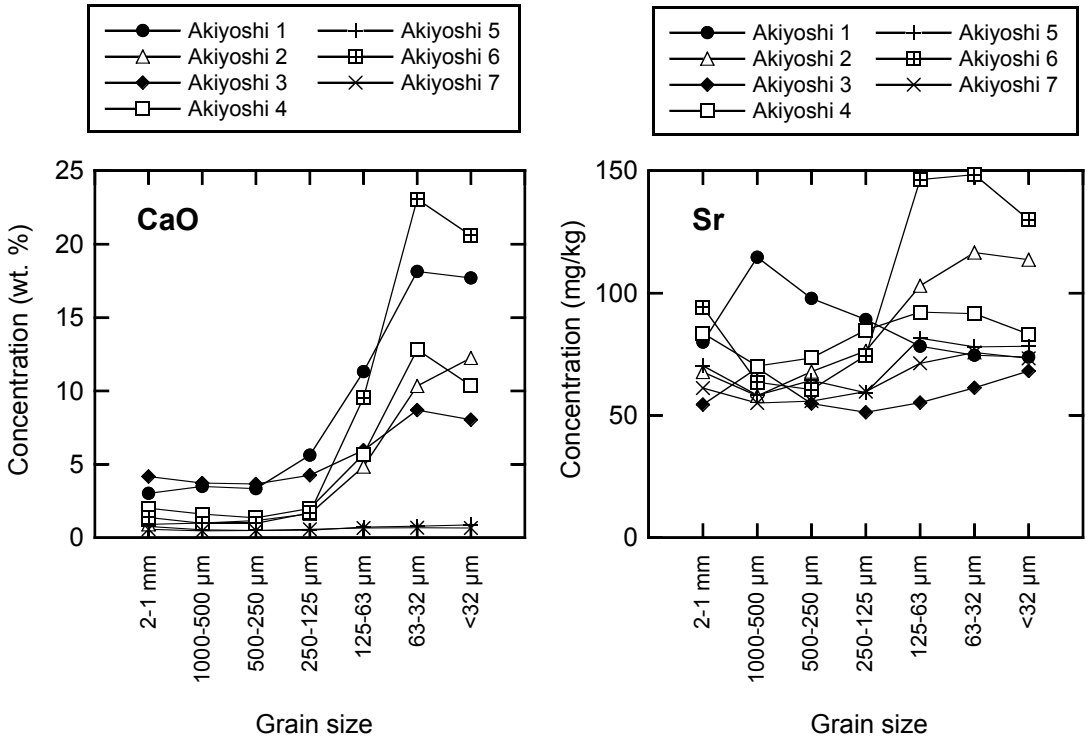

Fig 3. CaO and Sr concentrations of stream sediments according to particle size classification.

27.4°, 28.0°, and 29.4° (2θ) indicate the abundance of clay mineral, quartz, plagioclase, alkali feldspar and calcite, respectively. The peak intensities of corresponding minerals relate to their weight fractions in samples. Sample was put on a sample holder in equal amount for XRD measurement. Actually, a standard powder having object minerals (known mixing ratios) is needed for quantification of mineralogical composition (e.g., Nelson and Cochrane, 1970). Therefore, relationship between elemental concentrations and XRD peak intensities of corresponding minerals is semiquantitative evaluation.

Table 4 shows the correlation coefficients between concentrations of 12 elements and peak intensities of minerals. The peak intensity of quartz correlates negatively to P_2O_5, CaO, and MnO concentrations. The peak intensity of alkali feldspar has positive correlation with K_2O and Rb concentrations; that of plagioclase correlates to Na_2O, MgO, and Ba concentrations. The peak intensity of calcite correlates positively to CaO and Sr concentrations. The MgO, K_2O, and Rb concentrations also have positive correlation to the peak intensity of clay minerals.

Figure 8 shows the relationships between concentrations of Na_2O, K_2O, CaO, and Sr and the peak intensities of calcite, plagioclase, and alkali feldspar for all samples. There is very strong positive correlation between CaO concentration and peak intensity of calcite. On the contrary, the correlation between Sr concentration and the peak intensity of calcite is weak compared with the case of CaO. Especially, samples nos. 1 and 3 are plotted out of the positive correlation of Sr concentration and peak intensity of calcite. The Na_2O and K_2O concentrations increase gradually with increasing the peak intensities of plagioclase and K-feldspar, respectively.

5. Discussion

5.1 Small supply of limestone clastics to river system

As we described above, the stream sediments collected in the drainage basin including Akiyoshi Limestone bedrock have high CaO concentration (5–12 wt. %). The CaO concentration is much higher than the CaO data of stream sediments derived from accretionary complexes including limestone bedrocks, which has been reported by Japanese geochemical mapping (Table 2). Thus, we confirmed the influence of limestone bedrock to river system in this study area. However, the impact on CaO abundance in stream sediments is unexpectedly small.

Watershed analysis suggests that 93% of the catchment area in the location no. 1 is occupied by limestone and that the rest is covered by Pleistocene to Holocene sediments and the chert and metabasalt of Permian accretionary complexes (Table 3). The river is an underground river for the most part, which flows through calcareous caves in Akiyoshi-dai. The river on the ground is just a few km long (around the location no. 1). Accordingly, most detritus materials would be conveyed from calcareous cave: they must consist dominantly of calcite. Because limestone has 53–55 wt. % of CaO concentration, the sample is expected to have no fewer than 50 wt. %. Actually, CaO concentration of stream sediments under 180 µm is just 12 wt. % and that of silt particle (< 63 µm) is about 18 wt. % (see Table 2 and Fig. 3). In contrast,

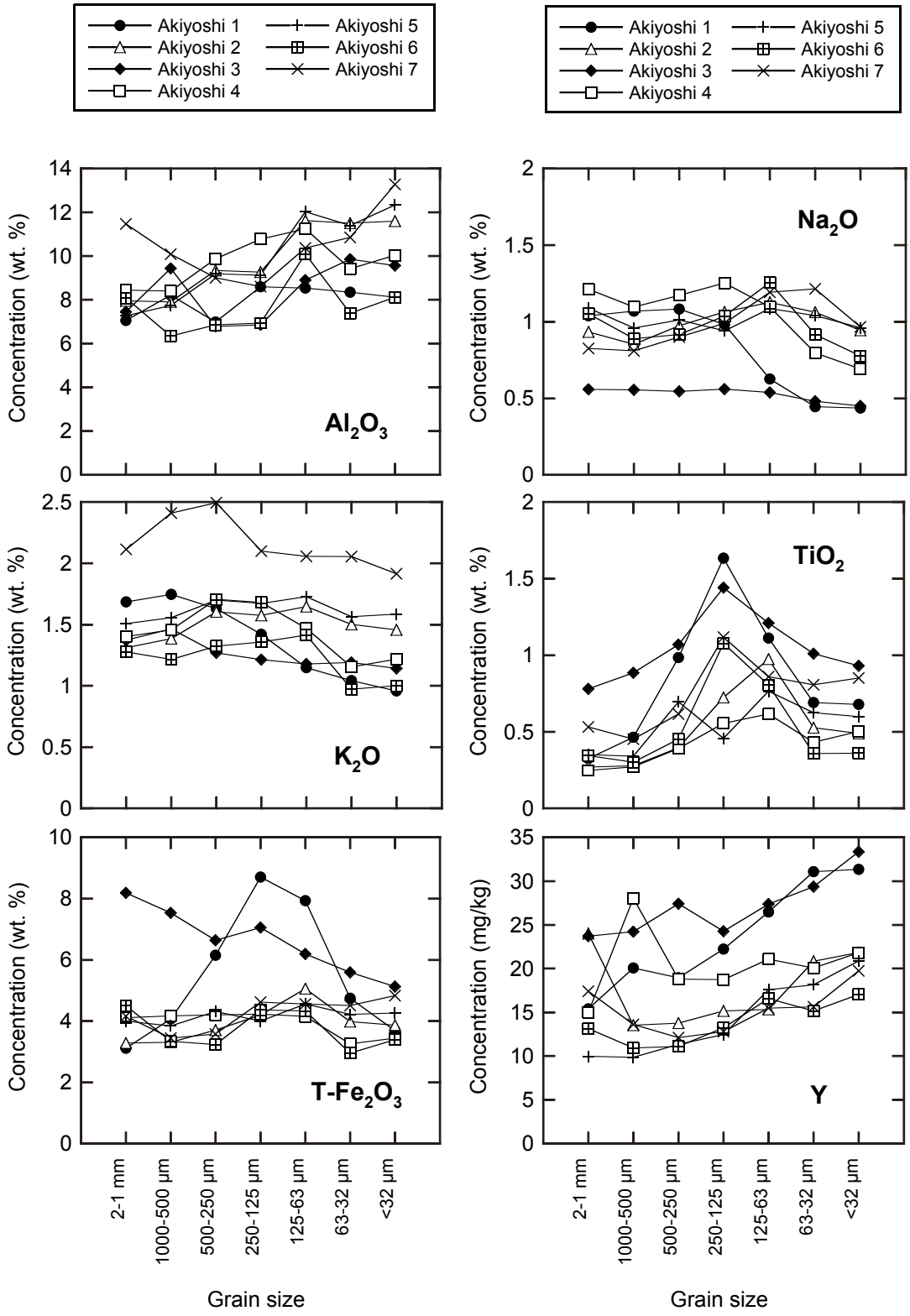

Fig 4. Elemental concentrations of stream sediments according to particle size classification.

Al_2O_3 concentrations of sample no. 1 are constant to be 7.0–8.6 wt. % irrespective to grain size (Fig. 4). In addition, the concentrations of P_2O_5 and 3d transition elements of sample no. 1 show the highest class, although these elements are not abundant in Akiyoshi Limestone (e.g., Nakano and Ishihara, 2003) (Table 2). These results suggest that particles derived from metabasalt existing narrowly are particularly significant for stream sediments

Table 4. Correlation coefficients between elemental concentrations and peak intensities of minerals.

	Q	Pl	Kf	Cc	Cl	Na_2O	MgO	Al_2O_3	P_2O_5	K_2O	CaO	TiO_2	MnO	T-Fe_2O_3	Rb	Sr
Pl	0.38															
Kf	0.20	0.14														
Cc	-0.77	-0.46	-0.29													
Cl	0.11	0.44	0.51	-0.39												
Na_2O	0.34	0.61	0.22	-0.39	0.28											
MgO	0.14	0.66	0.25	-0.49	0.66	0.60										
Al_2O_3	-0.31	0.21	-0.09	0.00	0.37	0.24	0.47									
P_2O_5	-0.66	-0.44	-0.26	0.41	-0.14	-0.68	-0.18	0.17								
K_2O	0.38	0.49	0.67	-0.61	0.67	0.49	0.58	0.36	-0.39							
CaO	-0.77	-0.45	-0.31	0.99	-0.40	-0.43	-0.51	-0.04	0.42	-0.64						
TiO_2	-0.41	-0.10	0.20	0.12	0.12	-0.35	0.12	0.00	0.56	-0.10	0.13					
MnO	-0.72	-0.42	-0.32	0.83	-0.38	-0.29	-0.31	0.21	0.50	-0.54	0.78	0.28				
T-Fe_2O_3	-0.28	-0.15	-0.02	0.05	-0.02	-0.44	0.02	-0.11	0.64	-0.23	0.08	0.78	0.23			
Rb	0.17	0.40	0.51	-0.47	0.64	0.33	0.53	0.56	-0.23	0.91	-0.49	-0.08	-0.36	-0.21		
Sr	-0.44	0.10	-0.20	0.57	-0.14	0.39	0.08	0.21	-0.02	-0.23	0.55	-0.11	0.51	-0.17	-0.28	
Ba	0.41	0.52	0.31	-0.48	0.47	0.76	0.62	0.49	-0.63	0.74	-0.54	-0.45	-0.36	-0.58	0.68	0.10

Q: quartz, Kf: alkali feldspar, Pl: plagioclase, Cc: calcite, Cl: clay minerals

in Akiyoshi Limestone bedrocks (Fig. 1). The similar results are found in sample no. 3.

Both samples nos. 6 and 7 were collected from the main stream of Kotou River and contain wide distribution of limestone in their catchment area. Sample no. 6 has high CaO concentration but sample no. 7 has quite the low concentration. Various lithologies (granite, granodiorite, rhyorite-dacitic welded tuff, gabbro, and pelitic schist) present near the location no. 7. Sample no. 7 consists dominantly of fine sands and silt and is abundant in alkali feldspar and clay minerals (Fig. 7). The source of supply of alkali feldspar would be granite or granodiorite. The abundant clay minerals such as chlorite would be caused by weathering, which produces biotite, amphiborite, and pyroxene that are hosted in granite, granodiorite, gabbro, and politic schist. As a result, geochemistry of stream sediment is more strongly influenced by nearby lithologies in the study area. In contrast, the river basin around the location no. 6 is covered widely by sandstone and chert of Permian accretionary complexes, which are highly resistant to physical weathering. The reason why sample no. 6 has high CaO content is that the dilution effect of particles derived from those lithologies on calcite particles may be small in extent.

The Akiyoshi Limestone hardy contains any lithic fragments, because it is originated from an isolated atoll. The pure limestone is more likely to be dissolved by chemical weathering process (Fujii, 2009): the physical weathering process exercises less slight influence on limestone than chemical weathering process. Fall rains dissolve limestone bedrocks and seep into the bedrocks to form underground riverine system. Accordingly, the supply quantity of clastic materials from limestone bedrocks is much smaller than those of other rock types. In other words, most fine-sand-sized clastics of limestone may be dissolved before arriving to river system. This is the main reason why the impact of limestone on CaO abundance in stream sediments is unexpectedly small. Most limestone bedrocks in Japan are very pure because of isolated atoll-origin as with the case of the Akiyoshi. The less influence of limestone on geochemical maps would be explained by the same reason. Incidentally, it is unlikely that calcite clastics in stream sediments are totally dissolved between locations nos. 6 and no. 7 because the total stream length between two points is just 13 km. If calcite clastics were dissolved in such short distances, significant loss of CaO in stream sediments would be also found between sampling locations nos. 6 and 1 (or nos. 2 and 3).

5.2 Influence of calcite formed secondarily

Figures 3 and 5 reveal that calcite debris supplied from host rocks to river system is abundant in finer particles. However, it is expected that finer calcite particle is dissolved in stream water faster than coarser calcite because fine particle has a larger surface area than coarse grain. Finer calcite particles may be supplied through limestone mine activity. However, digging area of limestone is found only in the watershed of sample no. 3. Accordingly we assumed that calcite is formed secondarily in limestone cave or in river system to which groundwater flowing through limestone bedrock is supplied because calcium carbonate is oversaturated by CO_2 degassing process (e.g., Kashima, 2010). Calcite aggregated may cover fine clastic materials and clay minerals. Calcite formed secondarily can explain the different behavior of Sr from CaO in sample no. 1 (also no. 3). The origin of ground water in Akiyoshi-dai is meteoric water. The Sr concentration in ground water possibly changes largely based on the rainfall level. As a result, Sr concentration of calcite formed secondarily changes largely from that in limestone. The Sr concentration does not have good positive correlation

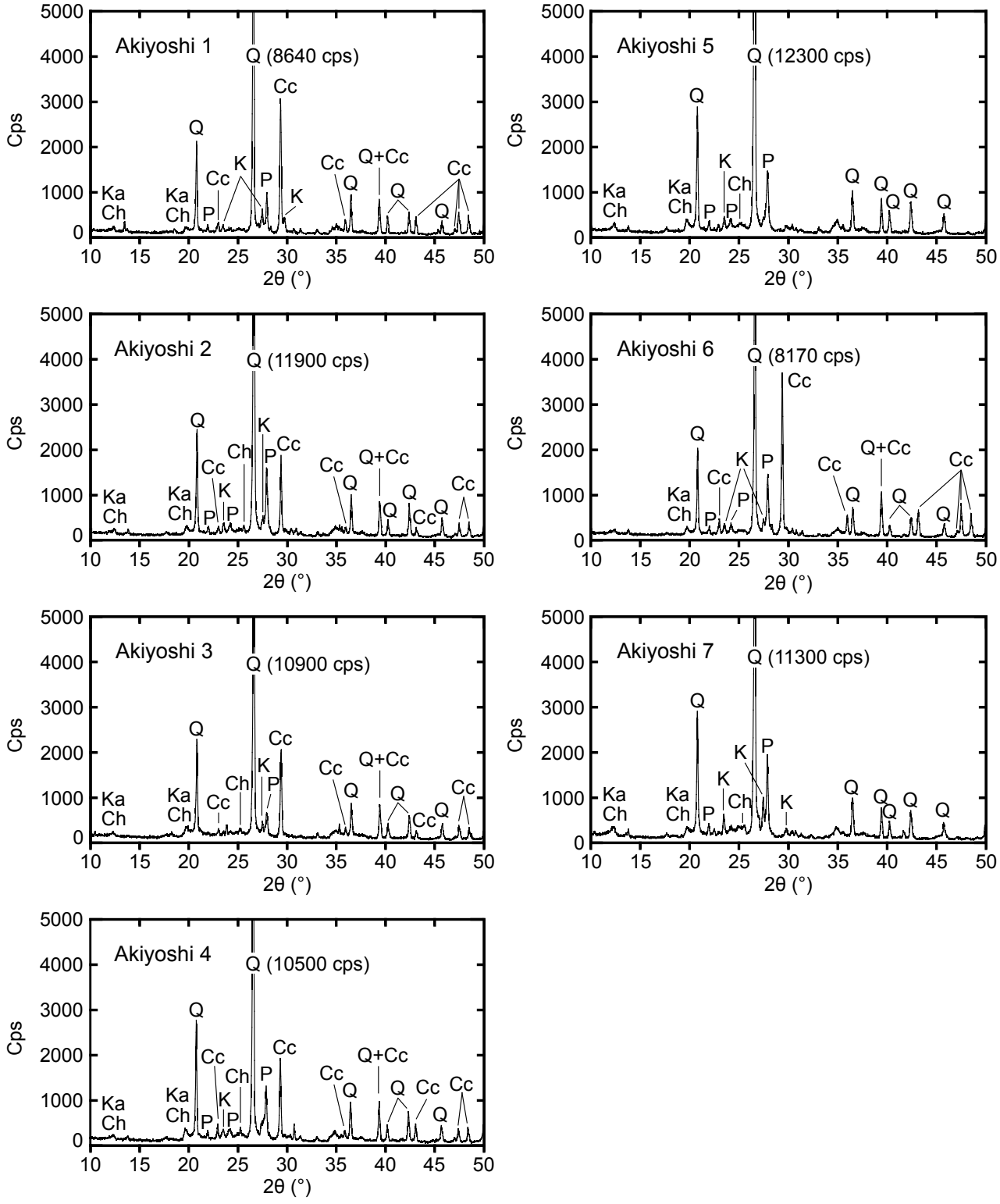

Fig 5. XRD patterns of stream sediments sieved with a 180 μm screen. Abbreviation Q, P, K, Cc, Ka, and Ch indicate quartz, plagioclase, alkali feldspar, calcite, kaolinite and chlorite, respectively.

to CaO concentration because stream sediments derived from limestone bedrock area are composed of the mixture of limestone clastics, calcite formed secondarily, and clastics except for limestone. The hypothesis proposed here will be validated in the following paper using Sr isotope ratio of stream sediments in this study area.

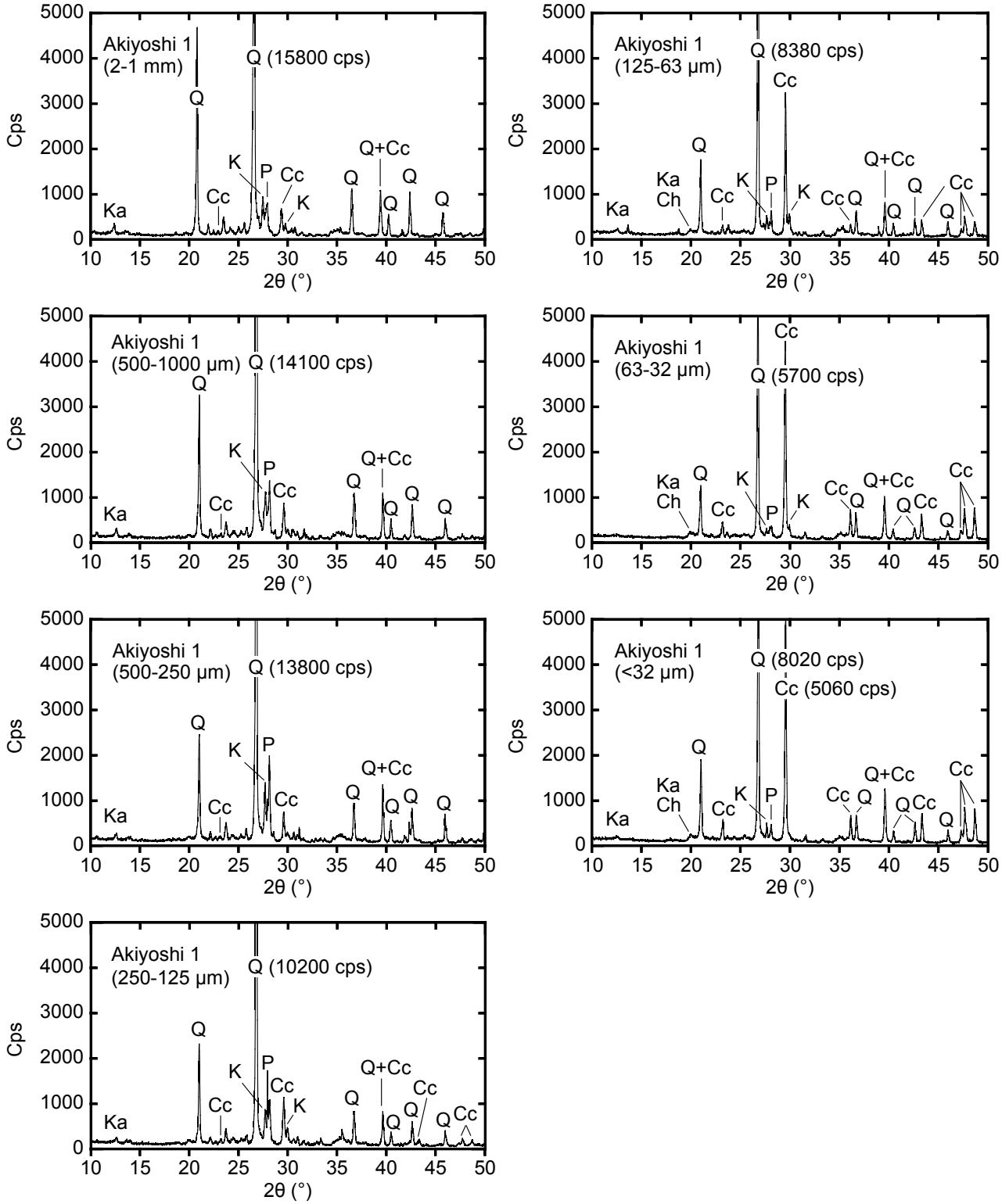

Fig 6. XRD patterns of stream sediment (sample no. 1) grouped into 7 grain sizes. Abbreviation Q, P, K, Cc, Ka, and Ch are the same as Fig. 4.

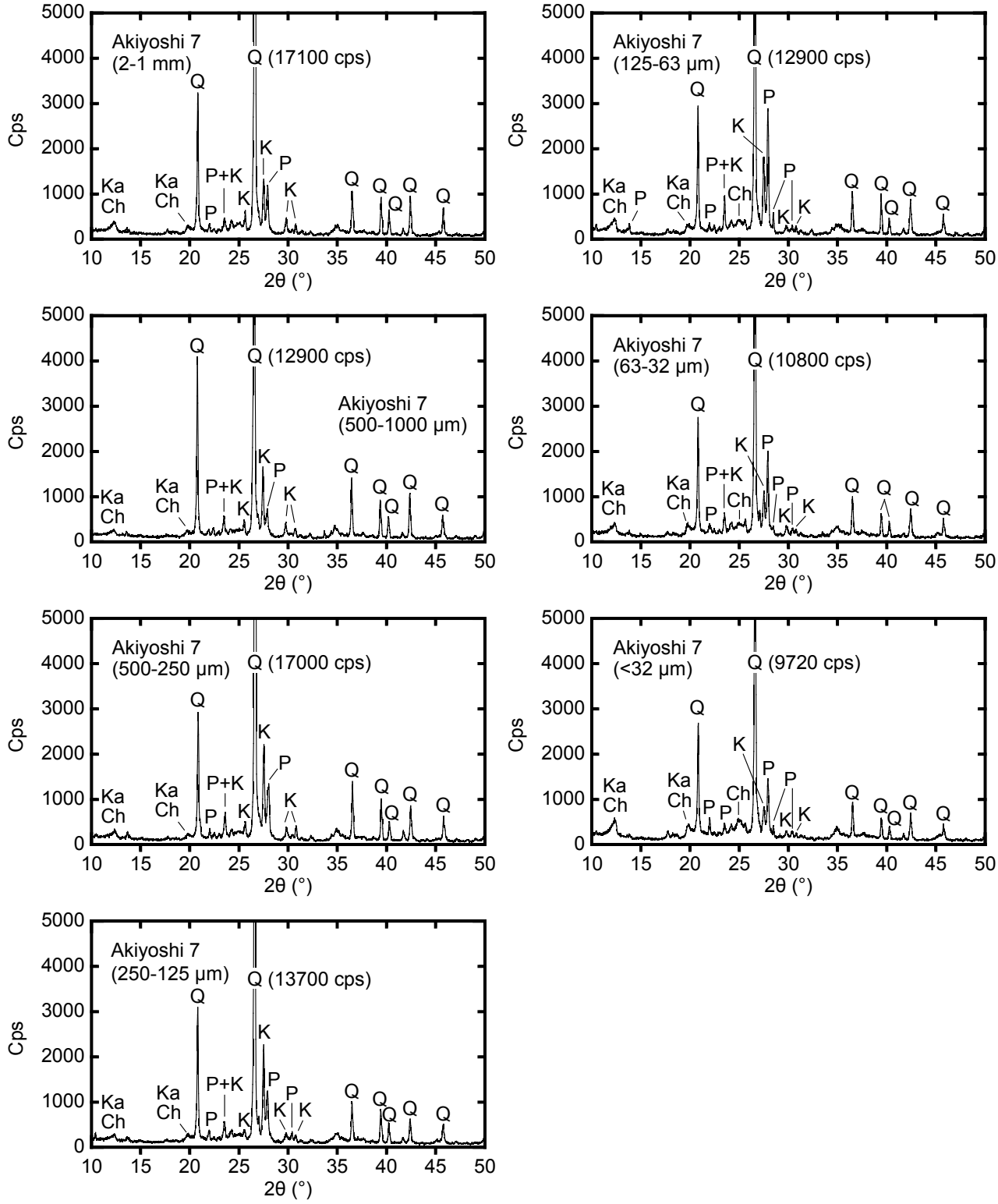

Fig 7. XRD patterns of stream sediment (sample no. 7) grouped into 7 grain sizes. Abbreviation Q, P, K, Cc, Ka, and Ch are the same as Fig. 4.

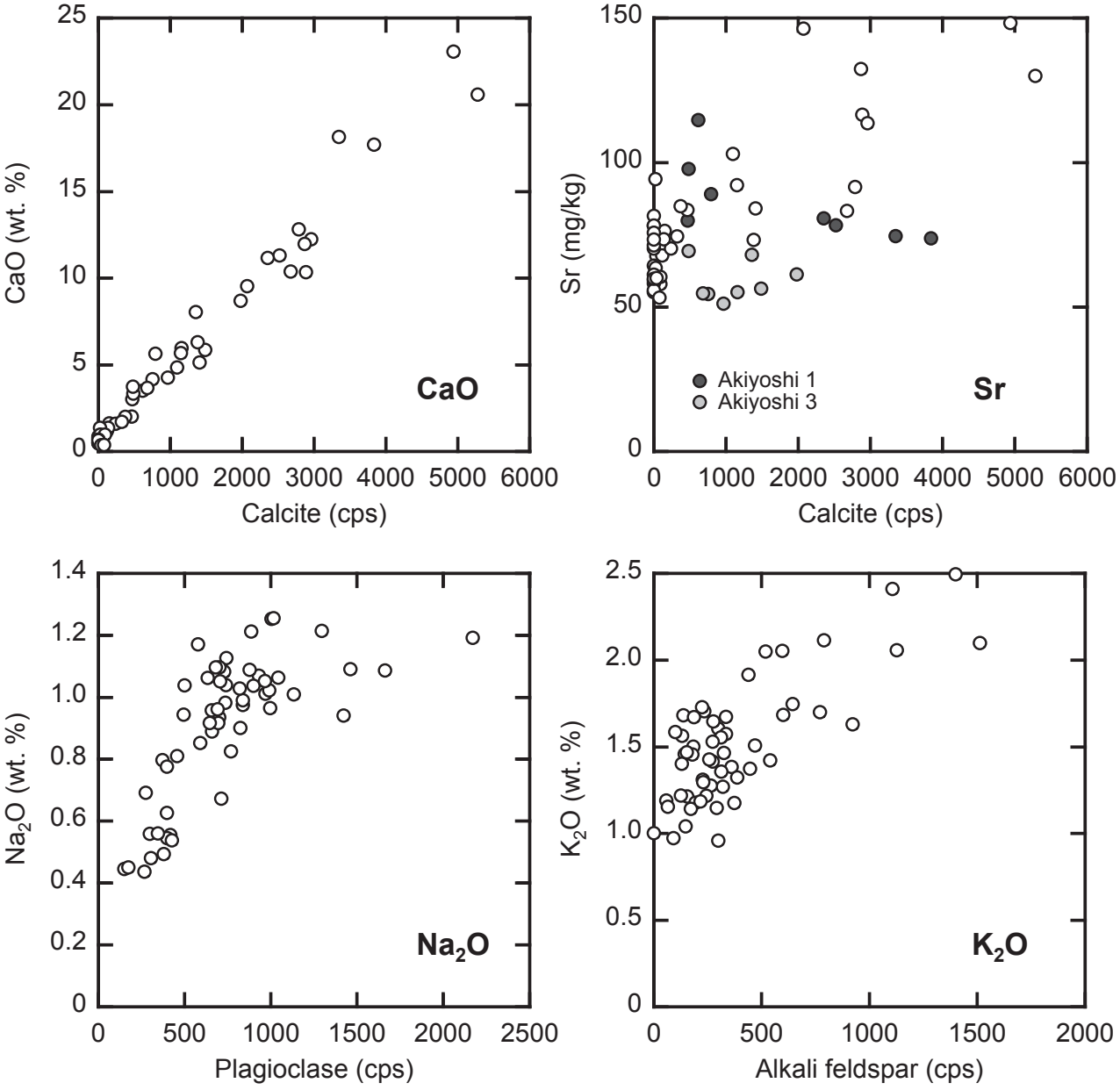

Fig 8. Relationships between elemental concentrations and peak intensities of minerals obtained by XRD. The intensities of the peaks at 27.4°, 28.0° and 29.4° (2θ) are assigned as plagioclase, alkali feldspar and calcite, respectively.

6. Summary

We elucidated why the impact of limestone to nationwide CaO and Sr maps in Japan is obscured. Seven stream sediment samples were collected from the Akiyoshi-dai that is underlain by the largest limestone bedrock in Japan. The 51 elemental concentrations and mineralogical compositions were determined for these samples. Stream sediments derived from the Akiyoshi-dai area have the high CaO concentration and the intensive peak of calcite in the XRD pattern. However the contribution is restricted to a small area. High concentrations of elements except for CaO and Sr such as Al_2O_3 (8.5–9.0 wt. %) and T-Fe_2O_3 (6.2–7.9 wt. %) are found even in samples whose drainage basins dominantly expose limestone. Eventually, it is concluded that small amount of limestone clastics is supplied to river system because pure limestone originated from an isolated atoll is more likely to be subjected to chemical weathering process more than physical weathering and erosion processes. Geochemical maps have been created on the assumption that stream sediment is a composite sample of the materials distributing in the catchment area: its geochemistry is controlled conclusively by parent lithology. We have assumed that the influence of parent

lithology on elemental abundance of stream sediments correlates simply to its exposed area in each watershed of samples. The rule is inapplicable to limestone.

Acknowledgements: The authors grateful to Masaya Suzuki for his technical support for XRD measurement. This work was supported by JSPS KAKENHI Grant Number 22300308.

References

Albanese, S., De Vivo, B., Lima, A. and Cicchella, D. (2007) Geochemical background and baseline values of toxic elements in stream sediments of Campania region (Italy). *J. Geochem. Explor*. **93**, 21-34.

De Vos, W., Tarvainen, T., Salminen, R., Reeder, S., De Vivo, B., Demetriades, A., Pirc, S., Batista, M. J., Marsina, K., Ottesen, R.-T., O'Connor, P. J., Bidovec, M., Lima, A., Siewers, U., Smith, B., Taylor, H., Shaw, R., Salpeteur, I., Gregorauskiene, V., Halamic, J., Slaninka, I., Lax, K., Gravesen, P., Birke, M., Breward, N., Ander, E. L., Jordan, G., Duris, M., Klein, P., Locutura, J., Bel-lan, A., Pasieczna, A., Lis, J., Mazreku, A., Gilucis, A., Heitzmann, P., Klaver, G. and Petersell, V. (2006) *Geochemical atlas of Europe. Part 2 - Interpretation of Geochemical Maps, Additional Tables, Figures, Maps, and Related Publications*. Geological Survey of Finland, Espoo, Finland, 692 pp.

Fujii, A. (2009) A Report on the Public Symposium "Mammal fossils in the Cenozoic Era preserved in limestone caves of the Akiyoshi-dai Plateau" at the Annual Meeting of the Mammalogical Society of Japan (2008): Caves of the Akiyoshi-dai Plateau and their chronology based on the rate of downward erosion of the Koto-gawa River. *Honyurui Kagaku (Mammalian Science)* **49**, 91-95 (in Japanese).

Geological Survey of Japan, AIST (2012) Seamless digital geological map of Japan 1: 200,000. Jul 3, 2012 version. (Geological Survey of Japan, A., ed.). *Research Information Database DB084, Geological Survey of Japan, National Institute of Advanced Industrial Science and Technology*. Geological Survey of Japan, AIST, Tsukuba.

Howarth, R. J. and Thornton, I. (1983) Regional Geochemical Mapping and its Application to Environmental Studies. Applied *Environmental Geochemistry*. (Thornton, I., ed.), 41-73, Academic Press London.

Imai, N., Terashima, S., Ohta, A., Mikoshiba, M., Okai, T., Tachibana, Y., Togashi, S., Matsuhisa, Y., Kanai, Y. and Kamioka, H. (2004) *Geochemical map of Japan*. Geological Survey of Japan, AIST, 209 pp (in Japanese with English astract).

Kashima, N. (2010) Speleominerals and *Cave Environment. Cave Environmental NET Society (CENS)* **1**, 3-6 (in Japanese with English astract).

Matsuura, H., Ozaki, M., Wakita, K., Makimoto, H., Mizuno, K., Kametaka, M., Sudo, S., Morijiri, R. and Komazawa, M. (2007) Yamagushi and Mishima. *Geological Map of Japan 1:200,000*. Geological Survey of Japan, AIST, Tsukuba.

Nakano, T. and Ishihara, S. (2003) Geochemical characteristics of the Akiyoshi limestones, Japan and their bearing on exploration for blind skarn deposits. *Resour. Geol*. **53**, 29-36.

Nelson, C. S. and Cochran, R.H.A. (1970) A rapid x-ray method for the quantitative determination of selected minerals in fine-grained and altered rocks. *Tane* **16**, 151-162.

Ohta, A., Imai, N., Terashima, S. and Tachibana, Y. (2004a) Investigation of elemental behaviors in Chugoku region of Japan based on geochemical map utilizing stream sediments. *Chikyukagaku (Geochemistry)* **38**, 203-222 (in Japanese with English astract).

Ohta, A., Imai, N., Terashima, S. and Tachibana, Y. (2005) Application of multi-element statistical analysis for regional geochemical mapping in Central Japan. *Appl. Geochem*. **20**, 1017-1037.

Ohta, A., Imai, N., Terashima, S., Tachibana, Y., Ikehara, K. and Nakajima, T. (2004b) Geochemical mapping in Hokuriku, Japan: influence of surface geology, mineral occurrences and mass movement from terrestrial to marine environments. *Appl. Geochem*. **19**, 1453-1469.

Sano, H. and Kanmera, K. (1991) Collapse of ancient oceanic reef complex -What happened during collision of Akiyoshi reef complex?- Sequence of collisional collapse and generation of collapse products. *Journal of Geological Society of Japan* **97**, 631-644.

Yamamoto, K., Tanaka, T., Kawabe, I., Iwamori, H., Hirahara, Y., Asahara, Y., Kim, K. H., Richardson, C., Ito, T., Dragusanu, C., Miura, N., Aoki, H., Ohta, A., Sakakibara, T., Tanimizu, M., Mizutani, Y., Miyanaga, N., Murayama, M., Senda, R., Takayanagi, Y., Inoue, Y., Kawasaki, K., Takagi, M., Kawasaki, K., Nebu, S. and Inayoshi, M. (1998) Geochemical map of the Ryoke granitic area in the northeastern part of Toyota City, Aichi Prefecture. *Jour. Geol. Soc. Japan* **104**, 688-704 (in Japanese with English astract).

Received March 29, 2013
Accepted September 20, 2013

Appendix Table. Elemental concentrations of stream sediments groupded into 7 grain sizes.

		Akiyoshi 1							Akiyoshi 2							Akiyoshi 3							Akiyoshi 4						
		A	B	C	D	E	F	G	A	B	C	D	E	F	G	A	B	C	D	E	F	G	A	B	C	D	E	F	G
Na_2O	wt. %	1.04	1.07	1.08	0.98	0.63	0.45	0.44	0.93	0.85	0.98	1.06	1.13	1.06	0.94	0.56	0.56	0.55	0.56	0.54	0.48	0.45	1.21	1.10	1.17	1.25	1.10	0.80	0.69
MgO	wt. %	0.63	0.71	0.85	0.86	0.55	0.39	0.35	0.56	0.57	0.64	0.70	0.83	0.76	0.73	0.64	0.60	0.57	0.61	0.52	0.57	0.49	0.57	0.57	0.64	0.68	0.66	0.57	0.59
Al_2O_3	wt. %	7.05	8.22	6.99	8.60	8.54	8.35	8.13	7.96	7.91	9.35	9.27	11.6	11.5	11.6	7.45	9.44	6.78	6.86	8.90	9.86	9.57	8.44	8.41	9.88	10.8	11.2	9.43	10.0
P_2O_5	wt. %	0.079	0.091	0.11	0.13	0.14	0.13	0.12	0.070	0.069	0.079	0.082	0.12	0.14	0.15	0.23	0.21	0.17	0.18	0.19	0.21	0.20	0.073	0.076	0.085	0.092	0.13	0.13	0.15
K_2O	wt. %	1.68	1.75	1.63	1.42	1.15	1.04	0.96	1.31	1.38	1.61	1.58	1.65	1.50	1.46	1.37	1.47	1.27	1.21	1.18	1.19	1.14	1.40	1.46	1.71	1.68	1.47	1.16	1.22
CaO	wt. %	3.03	3.50	3.34	5.64	11.3	18.1	17.7	0.92	1.01	1.17	1.63	4.85	10.3	12.2	4.17	3.74	3.67	4.26	5.97	8.70	8.04	2.02	1.61	1.37	2.00	5.69	12.8	10.4
TiO_2	wt. %	0.32	0.46	0.98	1.63	1.11	0.69	0.68	0.27	0.28	0.40	0.72	0.97	0.53	0.49	0.78	0.88	1.07	1.44	1.21	1.01	0.93	0.25	0.27	0.39	0.56	0.62	0.43	0.50
MnO	wt. %	0.063	0.091	0.13	0.22	0.28	0.20	0.19	0.089	0.077	0.10	0.14	0.24	0.29	0.36	0.12	0.12	0.12	0.16	0.18	0.19	0.18	0.12	0.099	0.096	0.13	0.21	0.25	0.34
$T\text{-}Fe_2O_3$	wt. %	3.12	4.07	6.15	8.70	7.94	4.75	3.69	3.29	3.31	3.71	4.19	5.06	3.98	3.87	8.18	7.54	6.64	7.06	6.19	5.59	5.13	4.11	4.17	4.21	4.23	4.15	3.26	3.45
Li	mg/kg	25	28	30	49	35	34	32	35	35	40	41	46	41	43	51	49	47	55	56	57	55	34	35	41	41	42	37	40
Be	mg/kg	1.1	1.3	1.5	1.7	1.8	1.6	1.5	1.3	1.3	1.3	1.4	1.5	1.5	1.6	1.5	1.4	1.4	1.5	1.5	1.6	1.4	1.4	1.4	1.5	1.6	1.6	1.4	1.5
Sc	mg/kg	7.0	8.7	9.2	11.9	9.8	8.4	8.3	5.9	5.8	6.6	8.0	10	9.8	9.6	10	11	9.9	11	11	12	11	5.7	6.0	6.4	7.5	8.7	7.3	8.2
V	mg/kg	51	58	93	134	98	68	60	45	46	56	73	92	67	61	112	111	116	136	115	101	87	44	50	56	62	66	51	55
Cr	mg/kg	39	57	71	82	122	105	99	37	40	49	47	60	51	54	134	135	113	117	110	133	131	42	50	49	50	58	55	63
Co	mg/kg	11	13	17	20	21	18	17	7.6	8.8	11	11	13	12	14	22	19	17	20	18	17	16	8.1	8.7	10	10	11	11	12
Ni	mg/kg	14	17	19	23	27	27	35	14	14	15	16	20	19	23	46	44	39	43	43	50	51	13	13	16	18	20	19	24
Cu	mg/kg	27	38	41	50	76	88	87	18	17	19	19	26	28	28	35	34	31	38	40	41	38	24	20	20	24	32	35	41
Zn	mg/kg	78	113	172	220	236	217	202	52	59	77	85	110	101	101	183	181	185	226	221	206	183	89	77	88	95	105	92	105
Ga	mg/kg	10	11	12	13	12	11	11	10	10	12	13	15	14	14	14	14	13	15	14	14	13	11	12	13	14	14	12	13
Rb	mg/kg	70	73	69	68	61	59	58	64	67	78	75	80	78	78	64	70	63	61	54	67	68	71	74	88	86	88	72	79
Sr	mg/kg	80	115	98	89	78	75	74	68	58	68	76	103	117	114	55	69	55	51	55	61	68	84	70	73	85	92	92	83
Y	mg/kg	15	20	19	22	26	31	31	24	14	14	15	15	21	22	24	24	27	24	27	29	33	15	28	19	19	21	20	22
Zr	mg/kg	59	60	64	76	98	107	102	66	65	70	73	94	88	90	98	100	95	109	125	124	129	61	64	73	78	94	84	95
Nb	mg/kg	4.8	6.3	7.7	15	14	12	12	5.4	5.6	6.8	9.8	13	8.4	8.1	10	11	9.8	9.5	12	13	14	5.6	6.3	7.7	9.9	11	8.3	10
Mo	mg/kg	0.47	0.60	0.69	1.1	0.95	1.2	1.7	0.35	0.38	0.41	0.49	0.83	0.64	0.77	1.4	1.2	1.3	1.2	1.1	1.2	1.6	0.56	0.55	0.47	0.50	0.82	0.63	0.84
Cd	mg/kg	1.0	1.5	2.0	2.7	4.0	5.4	5.8	0.65	0.61	0.80	1.1	1.8	2.1	2.6	2.9	3.4	4.0	5.7	6.4	6.8	5.6	0.57	0.51	0.64	0.84	1.4	1.6	2.0
Sn	mg/kg	2.9	8.1	11	20	20	12	14	1.8	2.0	2.2	3.1	3.0	3.3	4.6	5.1	5.3	6.6	6.3	9.7	7.9	9.4	2.1	2.6	2.6	3.1	3.7	3.1	5.3
Sb	mg/kg	1.5	2.4	2.7	3.4	5.5	5.3	4.3	1.6	1.3	1.5	1.6	2.0	1.6	1.6	6.0	5.8	4.6	5.1	5.9	5.9	5.4	3.6	2.2	2.0	2.1	1.9	1.6	1.7
Cs	mg/kg	3.4	4.1	4.3	5.2	6.3	6.7	6.6	5.6	5.8	7.1	7.3	9.6	9.8	10	8.5	9.1	8.4	10	11	11	11	5.4	6.1	7.9	9.0	10	9.3	10
Ba	mg/kg	316	343	289	238	209	201	212	371	350	375	362	401	392	403	209	222	202	202	194	197	211	351	334	356	342	308	255	287
La	mg/kg	14	15	14	19	23	25	30	38	15	14	14	15	24	23	34	17	19	17	19	24	29	16	17	14	16	21	22	26
Ce	mg/kg	27	28	25	35	44	47	57	66	25	25	25	26	44	43	68	31	37	28	31	39	43	27	30	26	31	41	44	53
Pr	mg/kg	3.4	3.7	3.7	4.5	5.3	5.9	7.1	7.3	3.4	3.2	3.2	3.4	5.4	5.3	8.8	4.2	4.7	4.1	4.7	5.8	6.9	3.4	3.6	3.2	3.7	4.7	5.0	6.0
Nd	mg/kg	12	14	14	16	19	21	25	26	12	11	12	12	19	19	32	16	18	16	18	21	26	12	13	12	13	17	18	21
Sm	mg/kg	2.6	3.1	2.9	3.4	3.9	4.3	4.9	2.4	2.3	2.3	2.4	3.7	3.8	4.1	3.5	3.8	3.3	3.7	4.3	5.0	5.3	2.3	2.6	2.3	2.5	3.3	3.4	4.0
Eu	mg/kg	0.57	0.76	0.70	0.76	0.83	0.92	1.0	0.51	0.48	0.51	0.57	0.77	0.84	0.88	0.87	0.96	0.84	0.90	1.0	1.1	1.2	0.50	0.53	0.48	0.57	0.68	0.70	0.77
Gd	mg/kg	2.5	2.9	2.8	3.1	3.6	3.9	4.3	2.2	2.0	2.2	2.3	3.2	3.4	3.7	3.4	3.7	3.2	3.5	4.0	4.6	4.8	2.2	2.6	2.1	2.2	2.8	3.0	3.5
Tb	mg/kg	0.37	0.45	0.43	0.48	0.54	0.59	0.62	0.33	0.32	0.35	0.35	0.50	0.52	0.55	0.53	0.58	0.50	0.55	0.59	0.68	0.68	0.34	0.49	0.38	0.39	0.46	0.44	0.50
Dy	mg/kg	2.2	2.8	2.6	2.8	3.2	3.6	3.7	2.0	2.0	2.2	2.3	3.0	3.1	3.3	3.1	3.4	3.0	3.3	3.6	4.0	4.0	2.1	3.6	2.6	2.5	2.8	2.6	2.9
Ho	mg/kg	0.40	0.51	0.49	0.54	0.62	0.69	0.68	0.38	0.39	0.44	0.45	0.58	0.58	0.60	0.58	0.64	0.56	0.61	0.67	0.74	0.73	0.43	0.84	0.54	0.51	0.53	0.48	0.53
Er	mg/kg	1.3	1.6	1.5	1.7	1.9	2.2	2.1	1.3	1.3	1.5	1.5	1.8	1.8	1.9	1.9	2.1	1.8	2.1	2.2	2.4	2.4	1.4	3.0	1.8	1.7	1.7	1.6	1.7
Tm	mg/kg	0.20	0.25	0.24	0.27	0.31	0.34	0.34	0.19	0.21	0.24	0.25	0.29	0.29	0.30	0.29	0.31	0.28	0.30	0.33	0.37	0.36	0.23	0.50	0.30	0.29	0.28	0.24	0.27
Yb	mg/kg	1.3	1.6	1.5	1.7	1.9	2.1	2.1	1.3	1.4	1.6	1.6	1.9	1.9	1.9	1.8	1.9	1.8	1.9	2.1	2.3	2.3	1.6	3.4	2.0	1.9	1.8	1.6	1.7
Lu	mg/kg	0.21	0.25	0.25	0.27	0.31	0.34	0.33	0.21	0.23	0.26	0.26	0.30	0.29	0.30	0.30	0.32	0.29	0.32	0.36	0.37	0.36	0.25	0.55	0.32	0.31	0.30	0.25	0.28
Hf	mg/kg	1.6	1.7	1.8	2.1	2.8	3.0	2.7	1.8	1.8	2.0	2.0	2.7	2.5	2.5	2.5	2.4	2.3	2.7	3.1	3.1	3.3	1.8	1.9	2.1	2.2	2.6	2.3	2.5
Ta	mg/kg	0.36	0.38	0.24	0.99	1.1	0.94	1.1	0.51	0.52	0.60	0.70	0.87	0.79	0.76	0.40	0.65	0.17	0.18	0.32	0.94	1.1	0.52	0.59	0.71	0.86	0.97	0.77	0.94
Tl	mg/kg	0.44	0.49	0.52	0.52	0.49	0.49	0.48	0.52	0.53	0.61	0.62	0.69	0.67	0.67	0.61	0.64	0.61	0.69	0.70	0.71	0.67	0.51	0.51	0.62	0.63	0.63	0.54	0.60
Pb	mg/kg	87	32	33	43	52	55	61	13	15	18	21	32	25	30	136	128	114	124	131	128	107	28	30	30	31	36	37	44
Bi	mg/kg	0.90	2.1	2.9	6.0	8.8	5.6	4.8	0.25	0.21	0.23	0.27	0.36	0.34	0.36	0.46	0.49	0.49	0.66	0.77	0.66	0.57	0.26	0.28	0.25	0.29	0.39	0.35	0.40
Th	mg/kg	5.8	5.7	5.9	8.0	8.8	8.0	8.9	6.2	6.3	6.9	6.7	9.2	8.0	8.3	5.4	6.2	5.5	6.0	7.0	8.7	8.4	6.8	6.6	7.5	7.8	8.6	8.0	8.9
U	mg/kg	1.3	1.4	1.2	1.7	1.9	2.0	1.8	1.6	1.6	1.7	1.8	2.1	1.9	1.8	1.4	1.4	1.3	1.5	1.4	1.5	1.9	1.8	1.8	1.8	1.9	2.1	1.7	1.8

A: 1-2mm, B: 500–1000 μm, C: 250–500 μm, D: 125–250 μm, E: 63–125 μm, F: 32–63 μm, G: <32 μm

Appendix Table. continued.

		Akiyoshi 5							Akiyoshi 6							Akiyoshi 7						
		A	B	C	D	E	F	G	A	B	C	D	E	F	G	A	B	C	D	E	F	G
Na_2O	wt. %	1.09	0.96	1.01	0.94	1.09	1.04	0.96	1.05	0.89	0.92	1.04	1.26	0.92	0.78	0.83	0.81	0.90	0.99	1.19	1.21	0.97
MgO	wt. %	0.85	0.78	0.87	0.81	0.93	0.88	0.92	0.68	0.55	0.56	0.67	0.73	0.55	0.61	0.68	0.59	0.66	0.79	0.92	1.01	1.04
Al_2O_3	wt. %	7.27	7.75	9.18	9.14	12.0	11.4	12.3	8.09	6.35	6.86	6.94	10.1	7.39	8.13	11.5	10.1	9.01	8.61	10.4	10.9	13.3
P_2O_5	wt. %	0.085	0.077	0.086	0.080	0.11	0.13	0.15	0.089	0.065	0.064	0.074	0.12	0.12	0.18	0.11	0.087	0.080	0.096	0.10	0.11	0.12
K_2O	wt. %	1.51	1.56	1.70	1.67	1.73	1.56	1.59	1.28	1.22	1.32	1.36	1.42	0.97	1.00	2.11	2.41	2.49	2.10	2.06	2.05	1.92
CaO	wt. %	0.77	0.54	0.51	0.52	0.73	0.80	0.88	1.38	0.99	0.98	1.71	9.55	23.1	20.6	0.58	0.47	0.49	0.58	0.67	0.70	0.66
TiO_2	wt. %	0.35	0.34	0.70	0.46	0.76	0.63	0.60	0.34	0.30	0.45	1.08	0.81	0.36	0.36	0.53	0.45	0.62	1.12	0.86	0.81	0.85
MnO	wt. %	0.060	0.054	0.065	0.057	0.083	0.087	0.11	0.068	0.056	0.071	0.11	0.20	0.22	0.29	0.079	0.059	0.059	0.082	0.075	0.071	0.076
T-Fe_2O_3	wt. %	4.00	3.84	4.31	4.00	4.56	4.22	4.27	4.50	3.34	3.23	4.36	4.33	2.95	3.40	4.17	3.45	3.58	4.62	4.56	4.51	4.83
Li	mg/kg	39	38	45	42	48	48	50	31	30	32	31	30	21	24	39	33	33	37	48	48	56
Be	mg/kg	1.3	1.3	1.4	1.4	1.6	1.6	1.7	1.2	1.0	1.1	1.1	1.2	0.9	1.0	1.6	1.4	1.4	1.6	1.7	1.8	2.0
Sc	mg/kg	5.6	5.2	6.8	6.0	10	9.3	10	6.7	5.1	5.4	7.1	8.6	6.0	6.9	8.2	6.3	5.7	7.1	8.1	9.1	12
V	mg/kg	56	54	74	63	78	75	69	64	48	49	80	75	47	52	68	57	62	96	85	85	89
Cr	mg/kg	36	37	54	43	54	59	60	28	30	30	46	47	32	35	43	36	36	49	53	57	64
Co	mg/kg	9.6	9.8	10	10	11	11	12	9.5	8.6	8.8	10	12	8.2	10	11	8.9	9.1	11	12	12	13
Ni	mg/kg	17	15	18	16	21	22	26	14	13	12	13	16	7.9	13	20	17	18	20	24	26	31
Cu	mg/kg	22	22	26	23	32	39	43	19	16	16	18	28	23	28	30	25	26	31	36	40	46
Zn	mg/kg	82	96	113	109	121	124	135	59	56	63	80	98	74	88	87	74	68	95	105	110	125
Ga	mg/kg	12	12	14	13	16	15	16	11	9.3	9.8	11	12	8.7	10	15	13	13	14	17	17	20
Rb	mg/kg	70	75	85	83	87	83	91	57	52	57	57	60	43	48	113	126	128	108	108	111	112
Sr	mg/kg	70	58	64	59	82	78	78	94	64	61	74	146	148	130	61	55	56	60	71	76	73
Y	mg/kg	10	9.9	11	12	18	18	21	13	11	11	13	17	15	17	17	14	12	13	16	16	20
Zr	mg/kg	71	74	89	81	101	108	105	69	63	71	75	86	67	60	88	62	66	80	106	135	145
Nb	mg/kg	6.1	6.3	11	7.6	12	11	11	5.4	4.8	6.2	11	10	4.8	5.0	8.8	7.9	10	16	13	13	14
Mo	mg/kg	0.41	0.42	0.60	0.46	0.62	0.64	1.1	0.48	0.38	0.36	0.50	0.74	0.47	0.65	0.59	0.70	0.59	0.80	0.65	0.59	0.64
Cd	mg/kg	0.23	0.25	0.40	0.32	0.53	0.61	0.76	0.27	0.30	0.42	0.57	1.0	1.2	1.5	0.46	0.42	0.41	0.58	0.67	0.68	0.76
Sn	mg/kg	2.3	2.6	3.8	6.7	3.6	4.7	6.1	1.5	1.5	1.7	2.2	2.7	1.7	2.9	3.4	2.8	3.2	4.6	4.6	4.6	5.5
Sb	mg/kg	1.7	1.5	1.2	1.4	1.4	1.4	1.4	1.2	0.99	1.0	1.1	1.3	0.91	1.1	1.2	1.0	1.0	1.1	1.3	1.4	1.4
Cs	mg/kg	6.0	6.5	9.0	8.1	11	11	12	5.0	4.5	5.1	5.3	7.4	5.6	6.6	8.1	7.1	7.0	7.4	8.3	8.7	9.7
Ba	mg/kg	338	334	347	342	365	351	388	304	285	297	305	326	237	257	384	394	394	362	377	404	422
La	mg/kg	12	11	14	12	20	21	25	14	11	9.9	11	15	14	17	22	17	16	16	19	18	25
Ce	mg/kg	22	22	27	26	39	40	48	25	21	20	22	29	26	32	45	35	33	32	39	36	50
Pr	mg/kg	3.0	2.6	3.0	2.8	4.6	4.9	5.9	3.4	2.7	2.4	2.7	3.8	3.4	4.1	5.2	4.0	3.7	4.0	4.8	4.6	6.4
Nd	mg/kg	10	9.2	10	9.9	17	18	21	12	9.9	8.5	9.5	13	12	15	19	15	13	15	17	17	23
Sm	mg/kg	2.0	1.8	2.0	1.9	3.3	3.5	4.1	2.5	1.9	1.7	1.9	2.7	2.5	3.0	3.7	2.9	2.6	2.9	3.5	3.4	4.6
Eu	mg/kg	0.45	0.37	0.45	0.42	0.69	0.76	0.86	0.55	0.44	0.41	0.47	0.64	0.57	0.69	0.76	0.66	0.54	0.53	0.62	0.65	0.81
Gd	mg/kg	1.7	1.6	1.8	1.8	2.8	3.0	3.6	2.1	1.7	1.6	1.8	2.5	2.3	2.8	3.3	2.6	2.4	2.4	3.0	3.0	3.8
Tb	mg/kg	0.27	0.25	0.28	0.29	0.44	0.46	0.54	0.34	0.27	0.25	0.30	0.39	0.35	0.40	0.47	0.38	0.34	0.36	0.44	0.45	0.57
Dy	mg/kg	1.6	1.5	1.8	1.9	2.7	2.8	3.1	2.1	1.7	1.7	2.0	2.4	2.1	2.4	2.7	2.2	2.0	2.1	2.6	2.6	3.3
Ho	mg/kg	0.30	0.29	0.34	0.36	0.49	0.51	0.56	0.38	0.33	0.33	0.39	0.45	0.38	0.44	0.49	0.39	0.36	0.38	0.47	0.48	0.59
Er	mg/kg	1.0	0.99	1.2	1.2	1.6	1.7	1.8	1.3	1.1	1.1	1.3	1.5	1.3	1.4	1.6	1.3	1.2	1.2	1.5	1.6	1.9
Tm	mg/kg	0.16	0.17	0.20	0.20	0.26	0.26	0.29	0.20	0.18	0.18	0.22	0.24	0.19	0.22	0.26	0.20	0.19	0.20	0.24	0.25	0.30
Yb	mg/kg	1.1	1.1	1.3	1.4	1.7	1.7	1.9	1.3	1.2	1.2	1.6	1.6	1.3	1.4	1.7	1.3	1.2	1.3	1.6	1.7	2.0
Lu	mg/kg	0.18	0.18	0.22	0.22	0.29	0.29	0.30	0.21	0.19	0.20	0.25	0.26	0.20	0.21	0.26	0.20	0.19	0.21	0.26	0.27	0.32
Hf	mg/kg	1.9	2.1	2.4	2.2	2.8	2.9	2.9	1.9	1.7	1.9	2.0	2.3	1.8	1.6	2.7	1.8	2.0	2.4	3.2	4.1	4.2
Ta	mg/kg	0.56	0.57	0.89	0.71	1.0	0.99	1.0	0.45	0.43	0.53	0.53	0.76	0.45	0.47	0.94	0.84	1.1	1.5	1.3	1.3	1.4
Tl	mg/kg	0.55	0.57	0.62	0.61	0.64	0.63	0.67	0.41	0.40	0.45	0.42	0.43	0.30	0.35	0.70	0.72	0.76	0.72	0.74	0.75	0.81
Pb	mg/kg	16	17	22	20	54	28	33	15	14	15	18	27	20	28	36	34	31	34	35	34	38
Bi	mg/kg	0.26	0.26	0.33	0.29	0.44	0.52	0.59	0.19	0.18	0.18	0.22	0.30	0.26	0.36	0.63	0.51	0.48	0.59	0.68	0.80	0.98
Th	mg/kg	5.7	5.9	6.4	6.4	8.7	8.9	10	5.8	4.8	5.0	5.2	5.8	4.5	5.2	9.9	8.1	9.0	9.6	11	11	15
U	mg/kg	1.6	1.7	2.1	1.9	2.3	2.4	2.5	1.5	1.3	1.5	1.6	1.7	1.2	1.2	2.5	2.0	2.2	2.5	3.1	3.4	4.0

A: 1-2mm, B: 500–1000 μm, C: 250–500 μm, D: 125–250 μm, E: 63–125 μm, F: 32–63 μm, G: <32 μm

Bulletin of the Geological Survey of Japan, vol. 64 (5/6), 2013

石灰岩が河川堆積物中の元素濃度に与える影響の低さについて —秋吉地域の例—

太田充恒・南　雅代

要　旨

地質調査総合センターは日本において，細粒砂（< 180 μm）を用いた全国規模の53元素濃度の地球化学図を作成してきた．河川堆積物中の元素濃度の空間分布は地質や鉱山の分布を忠実に反映している．しかし，石灰岩岩体は例外であり，河川堆積物中の元素濃度にほとんど影響を与えていない．そこで我々は，この理由を明らかにすべく，日本最大規模の石灰岩岩体である秋吉台から採取した河川堆積物中の元素濃度並びに鉱物組成を調べた．流域に石灰岩を含む地域で採取された細粒砂（< 180 μm）は，CaO濃度が高く，そのX線回折データには強い方解石のピークが存在した．堆積物中の元素濃度の粒径依存性を調べたところ，粒径が細かくなるほど方解石の存在度が高くなりかつCaO濃度も増加した．しかし，石灰岩が流域に70%を超える面積を占める試料が示すCaO濃度は，予想される値（~50 wt. %）に比べて，10–20 wt. %と非常に低い．この矛盾した結果は，石灰岩岩体は化学風化によって水に溶けやすいが，物理風化・削剥を受けにくい事によって説明できる．すなわち，石灰岩岩体から供給される砕屑粒子の供給量が他の岩体の供給量に比べ圧倒的に低い事を意味する．また，SrはCaとよく似た化学的挙動を示す事が期待されるにもかかわらず，一部の試料中のSr濃度はCaO濃度や方解石のピーク強度とは良い相関関係を示さなかった．これは，炭酸カルシウムに対して過飽和な水から、秋吉石灰岩とは異なるSr濃度を持つ方解石が形成され、河川系に供給されたことを意味する．

キーワード：秋吉台；石灰岩；河川堆積物；地球化学図；カルシウム；ストロンチウム

地質調査研究報告 , 第 64 巻，第 5/6 号 , p. 139 − 150, 2013

論文 - Article

GSJ におけるエアロゾル中放射性核種の 2012 年観測と環境要因の再検討

金井　豊 [1, *]・土井妙子 [2]・桝本和義 [3]

Yutaka Kanai, Taeko Doi and Kazuyoshi Masumoto (2013) Observation of radionuclides transported with aerosols at the GSJ in 2012 and re-examination of meteorological factors. *Bull. Geol. Surv. Japan*, vol. 64 (5/6), p. 139−150, 9 figs, 3 tables.

Abstract: In order to obtain the geochemical knowledge of material cycle as a tracer and to contribute the concern of inhabitant about safety after the accident of the Fukushima Dai-ichi Nuclear Power Plant (FDNPP), the aerosol observation at the GSJ was continued and the new data in 2012 are reported in this paper.

The Cs radioisotope concentrations in the air decreased from April 2012 when the southerly wind often blew instead of northerly wind and rainy day increased. Several increases in the observed concentration were ascribed to the re-suspension of deposited particles by strong wind. The meteorological effect on variation of Cs-137 concentration in 2011 was re-examined in this study by the use of back trajectory analysis, which clarified that the air mass which had passed over the FDNPP arrived at the GSJ when the high concentration was observed. Measurement of the samples with known concentration showed that there seemed to be no problem on measurement system in this study.

Keywords: Aerosol, Fukushima Dai-ichi Nuclear Power Plant, Cs-134, Cs-137, Pb-210, Be-7, Geological Survey of Japan, 2012, Meteorological factor, Back trajectory

要　旨

物質循環のトレーサーとしての地球科学的知見を得ると同時に，福島第一原子力発電所事故後の地域住民の不安感の払拭にも貢献するため，地質調査総合センターにおいてエアロゾル中の放射性核種の観測を2012年も継続して行った．前報告（本誌，63，107-118）に引き続き2012年1月から2012年12月までの観測データを報告する．放射性Cs同位体のエアロゾル濃度は，2012年4月より低下しており，北よりの風から南よりの風に変わり降雨の日が多くなったことと良く対応していた．また、幾つかの濃度増加は強風時の再飛散によるものと推定された．前報告では2011年のエアロゾル中Cs-137濃度に対する気象の影響は不明瞭であったが，本研究では後方流跡線解析を適用することで，濃度変化が気象状況の影響を受けていたことをより明瞭に示すことができた．また，濃度既知の試料を本研究において再測定した結果，測定上の大きな問題点は無いものと考えられた．

1．はじめに

2011年3月11日14時46分に発生したM 9.0の東北地方太平洋沖地震とその後におそった大津波によって起きた東京電力株式会社福島第一原子力発電所（FDNPP）の事故により，環境中にヨウ素-131(I-131)やセシウム-137(Cs-137)などの大量の人工放射性核種が放出された（例えば，内閣官房内閣広報室，2011a；経済産業省，2011）．地質調査総合センター（GSJ）では，環境中の放射性核種の動態を解明する研究の一環として，また，事故後の放射性核種のモニタリングを通じて地域住民の放射線被ばくに対する不安感を払拭するため，事故後20日経過した3月末から大気中エアロゾルの放射性核種の観測を開始し，2011年の観測結果を報告してきた（金井，2012a；Kanai，2012）．2011年12月には放出量が事故直後の1/1300万に収まり（経済産業省，2011），「冷温停止状態」宣言もなされたが(内閣官房内閣広報室，2011b)，FDNPPでは依然として放射性核種の放出が続いていたため，2012年も継続して観測を行った．

[1] 地質情報研究部門 (AIST, Geological Survey of Japan, Institute of Geology and Geoinformation)
[2] 国立環境研究所 (National Institute for Environmental Studies)
[3] 高エネルギー加速器研究機構 (High Energy Accelerator Research Organization, KEK)
[*] Corresponding author: Y. KANAI, Central 7, 1-1-1 Higashi, Tsukuba, Ibaraki 305-8567, Japan. E-mail: y.kanai@aist.go.jp

第1表　GSJにおけるエアロゾル採取日とエアロゾル中の放射性核種の濃度.

Table 1　Aerosol sampling dates and radioactive nuclide concentrations in aerosols collected at the GSJ in 2012.

No.*	Start		Stop		Volume	Activity (Bq / m^3)			
	Y / M / D	H : M	Y / M / D	H : M	(m^3)	Cs-134 605 keV	Cs-137 662 keV	Be-7 478 keV	Pb-210 46.5 keV
66	2011/12/28	14:27	2012/1/4	16:14	10187	5.3E−05 ± 3E−06	7.0E−05 ± 4E−06	3.6E−03 ± 6E−05	6.7E−04 ± 5E−05
67	2012/1/4	16:16	2012/1/12	11:05	11209	5.5E−05 ± 3E−06	7.1E−05 ± 4E−06	2.9E−03 ± 5E−05	4.2E−04 ± 5E−05
68	2012/1/12	11:08	2012/1/19	11:50	10122	9.5E−05 ± 4E−06	1.3E−04 ± 5E−06	4.7E−03 ± 7E−05	8.4E−04 ± 6E−05
69	2012/1/19	11:52	2012/1/26	14:26	10234	4.4E−05 ± 3E−06	4.8E−05 ± 4E−06	2.7E−03 ± 6E−05	7.4E−04 ± 5E−05
70	2012/1/26	14:27	2012/2/2	10:56	9869	8.6E−05 ± 4E−06	1.1E−04 ± 5E−06	3.5E−03 ± 6E−05	9.8E−04 ± 6E−05
71	2012/2/2	10:59	2012/2/10	13:35	11676	5.6E−05 ± 3E−06	7.7E−05 ± 4E−06	3.2E−03 ± 6E−05	5.7E−04 ± 5E−05
72	2012/2/10	13:59	2012/2/16	16:53	8814	1.2E−04 ± 5E−06	1.5E−04 ± 6E−06	5.0E−03 ± 8E−05	6.1E−04 ± 7E−05
73	2012/2/16	16:55	2012/2/24	15:05	11409	7.8E−05 ± 3E−06	9.5E−05 ± 4E−06	4.8E−03 ± 6E−05	8.2E−04 ± 5E−05
74	2012/2/24	15:06	2012/3/2	9:37	9751	9.0E−05 ± 4E−06	1.0E−04 ± 4E−06	4.8E−03 ± 7E−05	7.0E−04 ± 6E−05
75	2012/3/2	9:40	2012/3/8	14:42	8942	4.3E−05 ± 3E−06	4.5E−05 ± 4E−06	2.9E−03 ± 5E−05	6.1E−04 ± 6E−05
76	2012/3/8	14:44	2012/3/13	15:07	7223	2.8E−05 ± 3E−06	3.4E−05 ± 5E−06	1.7E−03 ± 6E−05	4.6E−04 ± 7E−05
77	2012/3/13	15:09	2012/3/22	15:01	12952	8.9E−05 ± 3E−06	1.2E−04 ± 4E−06	5.3E−03 ± 6E−05	8.8E−04 ± 5E−05
78	2012/3/22	15:03	2012/4/2	8:53	15469	6.4E−05 ± 3E−06	8.2E−05 ± 4E−06	4.9E−03 ± 6E−05	9.6E−04 ± 7E−05
79	2012/4/2	8:54	2012/4/13	7:42	15768	9.1E−05 ± 3E−06	1.3E−04 ± 3E−06	5.9E−03 ± 6E−05	6.4E−04 ± 4E−05
80	2012/4/13	7:45	2012/4/25	17:17	17852	2.4E−05 ± 2E−06	3.6E−05 ± 2E−06	4.0E−03 ± 5E−05	6.1E−04 ± 4E−05
81	2012/4/25	17:19	2012/5/7	11:44	16945	2.6E−05 ± 2E−06	3.5E−05 ± 2E−06	3.4E−03 ± 5E−05	4.5E−04 ± 4E−05
82	2012/5/7	11:45	2012/5/21	10:36	19674 1)	2.6E−05 ± 2E−06	3.5E−05 ± 2E−06	3.4E−03 ± 5E−05	4.5E−04 ± 4E−05
83	2012/5/21	10:38	2012/6/6	13:21	23203	2.4E−05 ± 1E−06	3.4E−05 ± 2E−06	5.4E−03 ± 4E−05	7.4E−04 ± 4E−05
84	2012/6/6	13:23	2012/6/20	10:26	19983	2.1E−05 ± 9E−07	3.0E−05 ± 1E−06	3.0E−03 ± 2E−05	3.0E−04 ± 2E−05
85	2012/6/20	10:29	2012/7/4	15:13	20444	2.5E−05 ± 1E−06	3.5E−05 ± 2E−06	1.8E−03 ± 2E−05	2.1E−04 ± 3E−05
86	2012/7/4	15:18	2012/7/19	8:44	21206	2.3E−05 ± 2E−06	2.7E−05 ± 2E−06	1.7E−03 ± 3E−05	3.1E−04 ± 4E−05
87	2012/7/19	8:46	2012/8/1	14:40	19074	1.9E−05 ± 1E−06	3.0E−05 ± 2E−06	2.1E−03 ± 2E−05	3.7E−04 ± 2E−05
88	2012/8/1	14:42	2012/8/15	10:52	19930	3.0E−05 ± 1E−06	4.6E−05 ± 2E−06	2.4E−03 ± 3E−05	3.2E−04 ± 3E−05
89	2012/8/15	10:54	2012/8/29	14:39	20385	1.9E−05 ± 8E−07	3.1E−05 ± 1E−06	2.9E−03 ± 2E−05	2.8E−04 ± 2E−05
90	2012/8/29	14:42	2012/9/13	14:37	21595	2.3E−05 ± 8E−07	3.4E−05 ± 1E−06	3.1E−03 ± 2E−05	3.6E−04 ± 1E−05
91	2012/9/13	14:39	2012/9/28	10:35	21356	1.8E−05 ± 1E−06	3.1E−05 ± 2E−06	3.6E−03 ± 4E−05	4.2E−04 ± 3E−05
92	2012/9/28	10:42	2012/10/11	15:03	18981	4.4E−05 ± 2E−06	7.5E−05 ± 2E−06	3.0E−03 ± 4E−05	4.0E−04 ± 4E−05
93	2012/10/11	15:10	2012/10/25	11:21	18853 2)	1.1E−05 ± 8E−07	2.3E−05 ± 8E−07	5.0E−03 ± 2E−05	8.5E−04 ± 2E−05
94	2012/10/25	11:23	2012/11/8	11:19	20156	1.3E−05 ± 8E−07	2.4E−05 ± 8E−07	4.6E−03 ± 2E−05	7.8E−04 ± 2E−05
95	2012/11/8	11:22	2012/11/28	9:47	28705	1.3E−05 ± 8E−07	2.4E−05 ± 9E−07	3.3E−03 ± 2E−05	5.9E−04 ± 2E−05
96	2012/11/28	9:50	2012/12/12	11:55	20285	1.6E−05 ± 2E−06	2.7E−05 ± 2E−06	2.9E−03 ± 4E−05	5.5E−04 ± 5E−05
97	2012/12/12	11:57	2012/12/26	10:43	20086	2.0E−05 ± 1E−06	3.7E−05 ± 2E−06	3.5E−03 ± 4E−05	6.1E−04 ± 4E−05

* "No." continues from Table 1 in the previous report (Kanai, 2012a)

1) stopped on 20 May during electric power failure

2) stopped on 13 and 21 October during electric power failure

第2表　本研究で測定した国立環境研究所で2011年採取されたエアロゾル試料.

Table 2　Aerosol samples collected at the National Institute for Environmental Studies in 2011.

No.	Start	Stop	Velocity (l / m)	Volume (m^3)	Number of ACF *
1	2011/3/15 14:39	～ 2011/3/15 17:34	600	105	1
2	2011/3/15 17:48	～ 2011/3/16 8:48	600	540	1
6	2011/3/18 10:16	～ 2011/3/20 9:55	600	1715	1
7	2011/3/20 10:00	～ 2011/3/22 9:54	600	1724	2
10	2011/3/24 11:15	～ 2011/3/25 10:43	600	845	2
14	2011/3/28 10:59	～ 2011/3/30 10:10	600	1698	2
18	2011/4/5 11:18	～ 2011/4/7 10:24	600	1691	2

＊ ACF : Activated Carbon Fiber filter (for collection of gaseous iodine)

前報（金井，2012a）では，エアロゾル中の人工放射性核種濃度が発生源での放出量変化や気象条件などによって変動すると考え検討を行ったが，サンプリング期間中の雨量や風向が影響している傾向は認められたものの，明瞭にそれを示すことができなかった．そこで，濃度の変動要因をより明らかにするため，新たに後方流跡線解析の適用を試みてその一部を発表した（金井，2013）．

本報告では，金井(2012a)以降に継続してエアロゾル中の放射性核種の監視を続けた2012年の観測結果と共に，2011年の観測結果に対して後方流跡線解析を適用して詳細に検討した事項を報告する．更に，測定値の信頼性向上のために，濃度既知試料を用いてデータの比較検討した結果についても報告する．

２．試料と実験装置

２．１　試料採取

試料採取に用いた装置・用具等は，前報(金井，2012a；2012b；Kanai，2012)と同様で，産業技術総合研究所地質調査総合センター第７事業所C-8棟の屋上(地上14 m)に設置されたハイボリュームエアサンプラー (HV-1000F, Shibata Scientific Co., Ltd.)を用いた．2012年に観測されるエアロゾル中の人工放射性核種は，放射性セシウム同位体（Cs-137，Cs-134）に限定されてきているので，その濃度レベルを考慮し，試料採取時間は3月中旬あたりまでは1週間前後，その後は10日前後，5月中旬あたりからは2週間前後に設定して採取した．各試料の採取開始時間，終了時間，採取空気量などを第1表に示した．エアロゾルを採取したポリフロンフィルター（ADVANTEC製PF040；約25 cm x 20 cm x 0.95 mm厚）は，1/16のサイズに折りたたんでポリエチレン袋に封入し，更にポリエチレン容器に入れて放射能測定に供した．

２．２　測定装置と測定試料

放射能測定装置も前報と同様で，井戸型Ge半導体検出器を備えたMCA7600システムを使用した（金井，2012a）．測定時間は，おおむね1日から4日間である．測定結果は，崩壊補正してサンプリングの開始時間における核種濃度として求めた．測定試料には，GSJで採取した試料の他に，今回は濃度既知の比較試料として，国立環境研究所において採取された7試料も同様に測定を行った．国立環境研究所では，地上から10mの屋上において，当所で使用したポリフロンフィルターと異なる石英繊維フィルター（ADVANTEC製QR-100；約25 cm x 20 cm）を用い，気体状放射性ヨウ素の採取に用いる活性炭フィルターとの2段組で，毎分600 lの吸引速度で空気が採取された（国立環境研究所，2011；土井，2012；Doi *et al*., 2013）．主にGSJが観測を開始する以前に採取された試料で，その試料採取の詳細を第2表に示した．更に，参考のために日本分析化学会(2012)で発行しているU8容器（(外径50 mm ϕ x 高さ55 mm）に入った放射能分析用土壌標準物質3試料（JSAC0471 ～ JSAC0473）も測定を行った．

３．結果と考察

３．１　エアロゾル試料による測定値の相互比較

FDNPP事故後には，数多くの放射能測定機関において環境試料の放射能測定がなされ，多くの報告値がある．しかし，これらは測定手法や精度などに問題のあることが多く，信頼性向上のために相互比較は有効な方法である．

国立環境研究所においては，原発事故直後の2011年3月15日からエアロゾルを採取し，高エネルギー加速器研究機構と共同で放射性核種濃度を報告した（国立環境研究所，2011；高エネルギー加速器研究機構，2011；土井，2012；Doi *et al*., 2013）．そこで，測定値の相互比較のために，国立環境研究所において採取された濃度既知の7試料について，当所の測定装置を用いて測定を行った．測定時には採取後1年半近く経過していたことから短寿命核種はほとんど消失しており，検出された核種は放射性セシウム同位体（Cs-134，Cs-137）と鉛-210に限定されていた．

第1図には，試料厚みによる自己吸収が未補正の当所で測定した形式的な放射性セシウム同位体の計測値と高エネルギー加速器研究機構で報告された定量値との関係を示した．Cs-134，Cs-137のいずれについても両者の測定値の相関係数が0.999と良い比例関係にあることから，測定機器類や試料の保存に特に大きな問題は無いと考えられる．しかし，未補正の形式的な計測値と高エネルギー加速器研究機構による定量値との間には平均約1.4倍の開きがある．国立環境研究所でのフィルターは石英繊維フィルター製のものであり，本装置での測定時における形状(フィルターの厚みなど)も当所で設定した観測試料の形状と異なっているため，定量のためには形状等による補正を必要とする．

当所での測定の標準的な形状（1/16に折りたたみ）は，おおよそ15 mmの厚みであった(金井，2012a)．一方，国立環境研究所での試料は1/16にたたんだ時の厚みは平均で約7.5-9 mmであった．ここで，JSACから発行されているU8容器に入った標準試料を用いて算出した検出効率の試料量による変化を第2図に示した．検出効率の逆数が試料の厚み（容器内の試料の高さ）と一次関係にあるとして(科学技術庁，1992)，近似直線が示されている．試料の違い（エアロゾルフィルターと土壌）と容器形状の違い（約5.5 cm x 6.5 cmの長方形底面と直径43 mmの円形底面）からこの第2図の関係を直接利用できないものの，これから試料の厚みが15 mmと7.5-9 mmの検出効率の違いを計算すると，その比は約1.2となった．

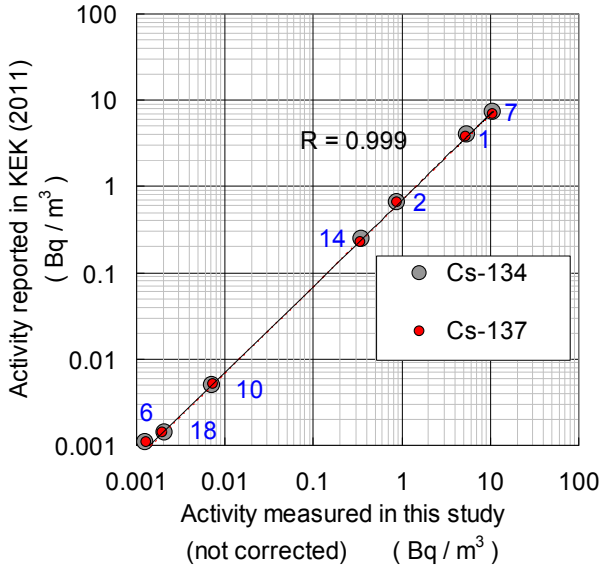

第1図　本研究での測定値とKEKでの報告値の関係．数字は第2表の試料番号．

Fig. 1　Correlation between activities measured in this study and those reported by KEK. Number indicates the sample number in Table 2.

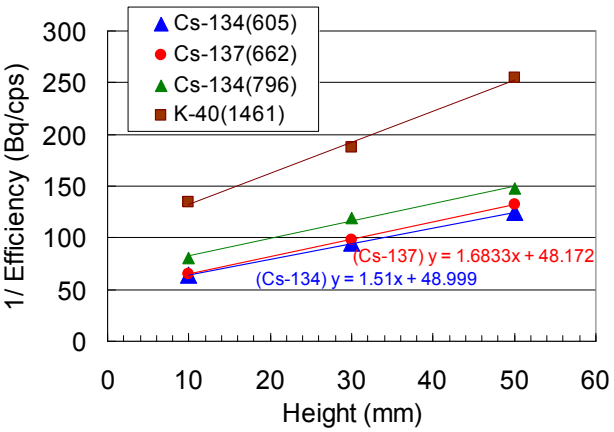

第2図　JSAC標準試料(U8容器)を用いて算出した検出効率と試料厚みとの関係．

Fig. 2　Correlation between detection efficiency of standard sample provided by JSAC (U8 container) and sample thickness.

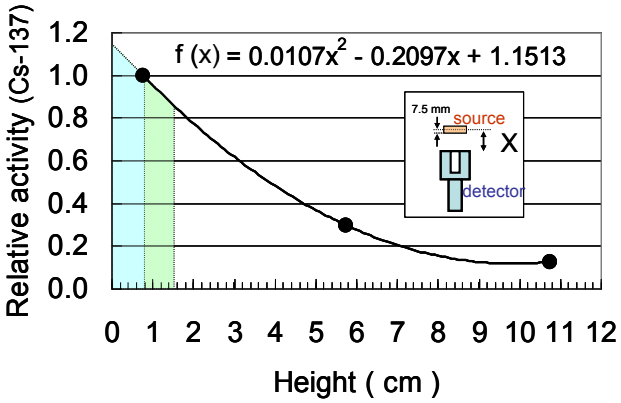

第3図　面線源と仮定してCs-137の相対検出効率と検出器からの距離の関係．

Fig. 3　Correlation between relative efficiency of Cs-137 and distance from detector.

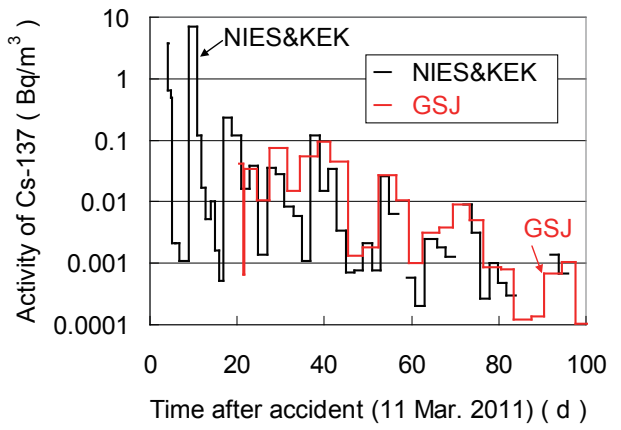

第4図　国立環境研究所で観測された2011年のCs-137濃度変化(“NIES&KEK”と表示；高エネルギー加速器研究機構(2011)による)とGSJでの観測結果(“GSJ”と表示；金井(2012a)，Kanai(2012)による)．

Fig. 4　Variations of Cs-137 concentrations in 2011 observed at the National Institute for Environmental Studies (denoted by “NIES&KEK”; from KEK(2011)) and the GSJ (denoted by “GSJ”; from Kanai(2012a) and Kanai(2012)).

前報(金井，2012a)では，折りたたんだ試料を用い検出器からの距離と放射線強度の関係を報告した．金井(2012a)のデータから，厚みのある試料の中央を面線源と仮定して計算した，実試料の面線源の相対的な放射線強度と距離(検出器の上に直接載せた場合を高さ7.5 mm，相対放射線強度の基準としている)の関係を第3図に示した．実際の厚みのある試料における検出効率は，その厚みまでの面線源の効率を積算して平均化したものと近似的に同じとみなせる(Average efficiency = $\frac{1}{x}\int_0^x f(x)dx$)ことから，第3図を用いて15 mmと7.5-9 mmの相対検出効率の比を計算するとその比の値は約1.5-1.3，約8 mmとすると約1.4となった．この値は，

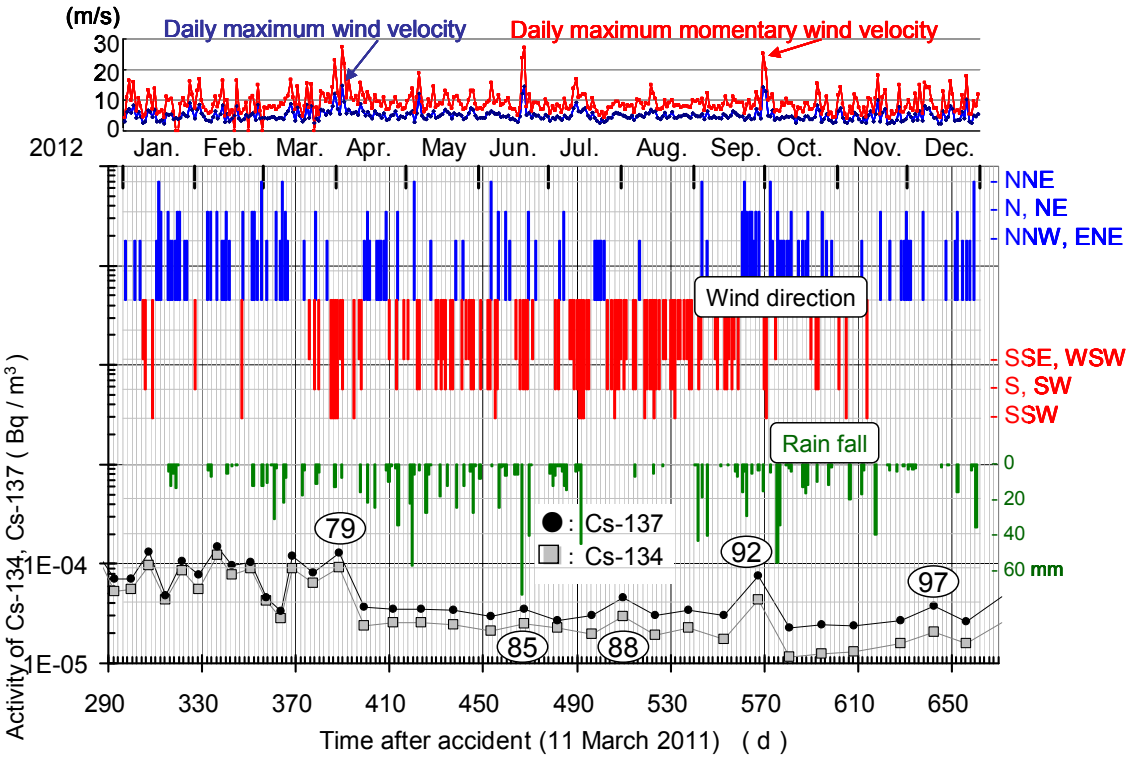

第5図 GSJにおけるエアロゾル中の放射性セシウム同位体の2012年濃度変化と気象状況．丸の中の数字は，第1表の試料番号を示す．

Fig. 5 Variations of radioactive Cs in aerosols collected at the GSJ and weather condition in 2012. Number in circle denotes the sample number in Table 1.

未補正の形式的な計測値と高エネルギー加速器研究機構による定量値との比と整合的である．折りたたんだ実試料と同じ面サイズの試料を用いて計算しているので，この比は実際の試料の厚みに起因する検出効率の違いをより正しく反映しているものと考えられる．

KEKでの報告値でも20％以下の不確かさが見積もられており（Doi *et al*, 2013），標準線源における不確かさでも±3～6％程度(k=2)が一般的であることから(山田･中村, 2005)，試料厚みの誤差や測定の再現性なども含めて放射線計測の全体の誤差を考えると，当所での測定値は高エネルギー加速器研究機構での報告値とは大きくは矛盾していないと推定され，本研究でのこれまでの報告値に測定上の大きな問題点は無いものと考えられる．

第4図には，国立環境研究所で採取観測された3月からのCs-137濃度の変化（高エネルギー加速器研究機構, 2011）と，GSJでの観測結果(金井，2012a；Kanai，2012)とを重ねて表示した．試料採取地点や採取時間が異なるため，大きな変動パターンは類似しているが，細かな測定結果は異なっている．同一観測地点でも3－4桁に及ぶような桁違いに大きな時間変動があることから，高濃度エアロゾルを含むプルームが不均一で，空間的にも時間的にも変動が大きかったために，第4図に示されるように観測期間の長短や時間差・採取場所の違いなどで両者間に相違ができたのではないかと考えられる．

3．2　2012年におけるエアロゾル中の人工放射性核種の観測結果

2012年1月から12月末までのGSJにおける観測結果を第1表及び第5図に示す．2011年の観測結果は金井(2012a)で報告済みである．放射性セシウム同位体の濃度は，2011年の10月あたりから10^{-4} Bq/m^{3}前後の濃度レベルを保ちながら変化してきたが，2012年の4月中旬あたりから約半分のレベルに低下し，その後もそのレベルを保ってきている．

GSJで観測されたエアロゾル中の放射性セシウム濃度の変動要因としては，冷温停止状態になったとはいえ未だ続く環境への放出量変化，FDNPPから拡散・移流を支配する気象条件，そして事故時の大量放出で飛散・沈積した粒子の再飛散と移動などが考えられる．発生源であるFDNPPにおいては，2011年12月に6x10^7 Bq/h，2012年の9月時点でも1x10^7 Bq/hの放射性物質が放出されているとされている(経済産業省，2011；東京電力株式会社, 2012a)．東京電力株式会社によると，4号機の原子炉建屋に燃料取り出し用カバー設置の本工事を4月17日に開始し，このカバーは放射性物質の放出拡散を防ぎ，換気設備によって内部の放射性物質の大気への放出を低減で

きるとしているが(東京電力株式会社，2012b)，完成は2013年度半ばを目指しており，また，1-3号機からの大量の放出はあったものの(大原ほか，2011；鶴田・中島，2012) 4号機は放出の可能性も指摘されたが(Stohl *et al*., 2012)災害時に停止中であったためにおそらく低いであろうから，これが観測値の低下の原因とは考えられない．ちなみに，4号機南方のモニタリング地点MP8において，4月16日の朝に42 μSv/hであった空間線量率が午後には8 μSv/hに低下していることが報告されているが(東京電力株式会社，2012c)，これも周辺域の森林伐採・表土除去・遮へい壁設置等の工事の影響とみられている(東京電力株式会社，2012d)．4月に観測された濃度低下の原因としては，工事に関連する事項は不明である．FDNPPにおいては，既に1号機の原子炉建屋に放射性物質飛散防止のカバー掛け工事が2011年10月14日に行われ，10月28日に排気設備等の工事も完了している(東京電力株式会社，2011)．しかし，その前後においては，周辺の放射線量の大幅な低下はみられず，また，GSJにおけるエアロゾルの観測データにおいても，大きな変動はなくなったものの濃度低下は認められておらず(第8図を参照のこと)，当時の1号機では放射性物質の放出拡散は他の原子炉ほど多量ではなかったと推定される．

第5図には，つくば市館野における最大風速の風向・降雨などの気象状況(気象庁，2012)も図示してある．これをみると，4月以降は北よりの風が少なく南向きに変わり，降雨が多い気候になっていることから，4月以降の濃度低下はFDNPP経由した空気塊の到来が少なく，また降雨の影響で空気中濃度が低濃度となったためではないかと定性的に説明される．

2012年の9月末から10月にかけて濃度が一時的に上昇し(試料No.92)，その後10月中旬からは以前よりも幾分低下している傾向がみられる．これに関しては，2号機で9月9日にダクト損傷が報告されているが(東京電力株式会社，2012e)，発電所内のモニタリング地点ではバックグラウンドが高いためか有意な変動は認められておらず，GSJでの濃度変化と時間的なずれもあることから今のところその影響は不明である．また，3号機でも6月19日にダクト損傷が見つかっているが(東京電力株式会社，2012f)，GSJでの観測値の僅かな濃度変動(No.85)がこれに起因するかも不明である．

これらに関しては，工事に関連する事項よりは，むしろ強風による再飛散を考慮した方が合理的である．つくばでは最大風速が10 m/sを超える気象状況の日が，3月31日(風向(以下同様)：SSW，降雨有り)，4月3日(S)，5月6日(S，降雨有り)，6月19日(S，降雨有り)，6月20日(S)，9月30日(S，降雨有り)，10月1日(SSW)，12月26日(NNW)であった(第5図参照)．12月26日を除くとほとんどが南よりの強風であり，FDNPPからの直接的な飛散は考えにくい．強風に伴って降雨もあるため土壌が湿って飛散しにくい環境となるため単純に結論づけられないが，4月初め(試料No.79)や微増ではあるが6月末(No.85)，9月末(No.92)等で観測された高濃度は，このような強風による近傍からの再飛散が一つの原因であった可能性が高い．

3．3　2012年におけるエアロゾル中の天然放射性核種

エアロゾル中には，天然起源の核種としてウラン系列・トリウム系列の核種や大気上層部において宇宙線による酸素·窒素の核破砕反応によって生じるベリリウム-7(Be-7)が観測されるので，ここでは半減期の比較的長いPb-210とBe-7について報告する．

2012年におけるPb-210とBe-7の観測結果を，第6図及び第1表に示す．Pb-210は0.2－1.0 mBq/m^3，Be-7は1.7－5.8 mBq/m^{3}の範囲にあり，2011年よりもその変動幅は小さかった．全体でも両者の間に1％の危険率で有意な相関が認められた(相関係数R=0.72)．両者の起源が異なるにもかかわらず高い相関を示すことから，エアロゾルに対する両者の挙動が類似していることが推定される．

3月から5月までを春季，6月から8月までを夏季，9月から11月までを秋季，12月から2月を冬季として2012年の測定結果を分類して図示すると，第7図に示されるように両者とも夏季に低くなるパターンが認められた．全体の変動幅が小さく春季・秋季・冬季の広がりが大きいために，2011年のように春季・秋季に高く夏季・冬季に低下するという明確なパターンは確認できなかった．しかし，平均値で見ると，Pb-210は春季4.1 mBq/m^3 > 冬季3.8 mBq/m^3 ≒ 秋季3.8 mBq/m^3 > 夏季2.3 mBq/m^3，Be-7は春季0.64 mBq/m^3 > 冬季0.58 mBq/m^3 ≒ 秋季0.57 mBq/m^3 > 夏季0.30 mBq/m^3 となっており，平均として春季に高濃度であったことが確認できる．2012年は冬季のエアロゾル中の濃度が2011年よりも高い傾向にあったこと，夏には低濃度の気団が優勢であったことなどが推定される．

このように，GSJで観測されたエアロゾル中の天然放射性核種であるPb-210とBe-7は，冬季を除くとこれまでとほぼ同様の季節変動パターンを示していることが確認された．

ちなみに，分析の信頼性向上のために行った3月に国立環境研究所で採取された試料における鉛-210の測定は，エアロゾル試料の採取時間(約3時間～2日)が短かったために検出限界以下である試料が多く，2試料(第2表のNo.6，18)についてのみ検出が可能であった．これらの測定値(未補正で0.6-0.9 mBq/m^3)は試料形状の補正を必要とするが，おおむねこれまでに報告してきたGSJでの採取試料の濃度範囲 (0.2-1.0 mBq/m^3；本研究，0.2-3.2 mBq/m^3；金井，2012a) にあり，前報(金井，2012a)と同様に原発事故によってエアロゾル中の鉛-210濃度は影響を受けないことを裏付ける結果が得られた．

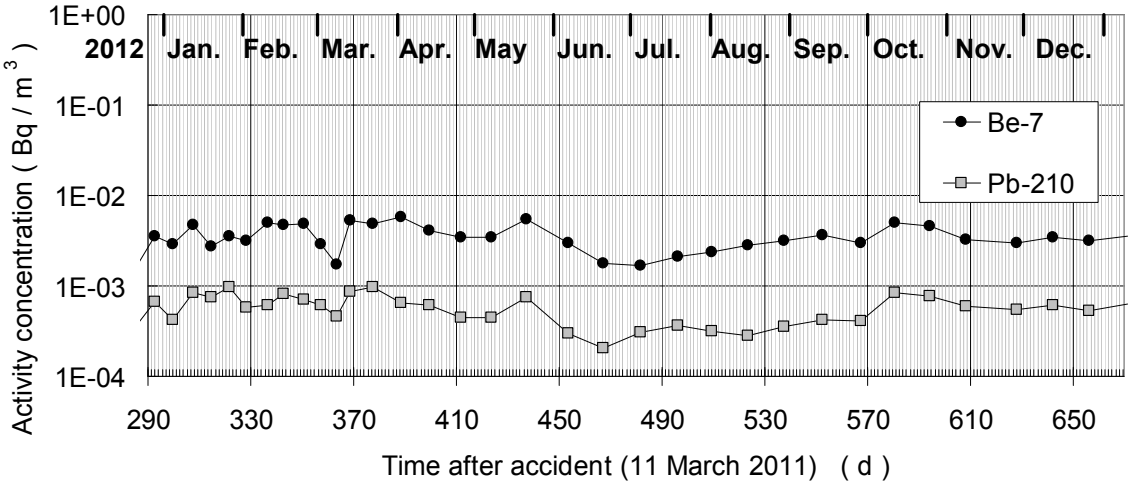

第6図 GSJにおけるエアロゾル中のPb-210，Be-7の2012年濃度変化.

Fig. 6 Variations of Pb-210 and Be-7 in aerosols collected at the GSJ in 2012.

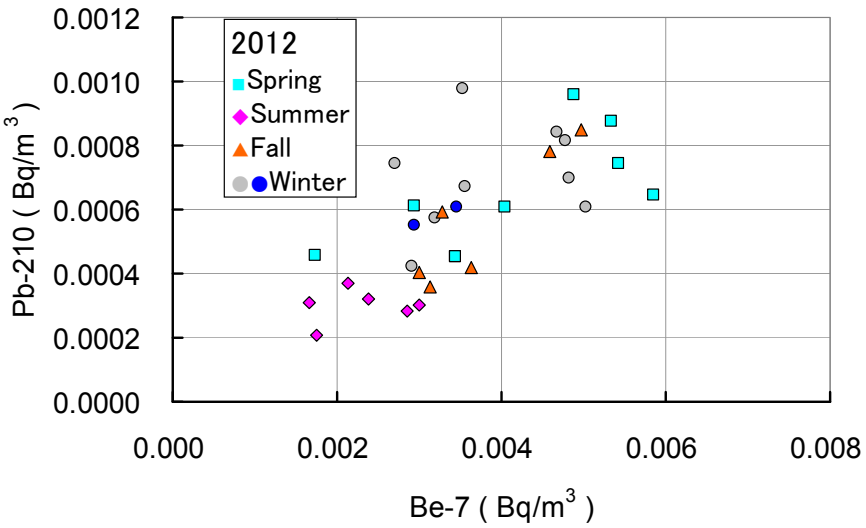

第7図 2012年におけるエアロゾル中のPb-210とBe-7の季節変動.

Fig. 7 Seasonal variation of Pb-210 and Be-7 in aerosols collected in 2012.

３．４ 後方流跡線解析によるエアロゾル濃度変動の検討

2011年のエアロゾル中の人工放射性核種濃度，特に放射性セシウム同位体(Cs-137，Cs-134)濃度は，第8図に示すように低下傾向にあるものの大きな変動を示し，これらの変動は9月末までにおおよそ12回ほど確認された．その観測試料番号，観測期間などを第3表に示した．濃度変動は発生源での放出量変化や気象条件などの影響を受けると考えられ，前報(金井，2012a)では雨量や風向を検討した結果．これらが影響している傾向は認められたものの，明瞭に示すことができなかった．

ところで物質移動を伴う気象モデルでは，時々刻々変動する風向，風速などの気象条件を考慮して，ある空気塊が大気の流れによって移動する軌跡である「流跡線」を利用するのが便利である．その解析手法には，ある地点の空気塊がその後に各地の風速風向によってどのような経路で輸送されるのかを推測する「前方流跡線解析」と，ある地点に到達した空気が，風の流れをさかのぼりどのような経路を通ってきたかを推測する「後方流跡線解析」とがあり，定点での汚染物質の起源を探るような場合には後者の解析手法が有効であるため，本研究にそれを適用した．

本研究における後方流跡線解析には，NOAA HYSPLIT model (Draxler and Rolph，2012；Rolph，2012)を利用し

第3表　2011年にGSJで高濃度となった観測期間と，FDNPPを経由した空気塊がGSJを通過したとみられる推定日．

Table 3　Supposed transit date when the air mass via the FDNPP passed over the GSJ in 2011.

No.	Sample collection (JST) Start		～	Stop		Supposed transit date of high content aerosol at the GSJ
	M/D	H:M		M/D	H:M	
3	4/1	16:03	～	4/4	9:44	4/3
5	4/7	9:50	～	4/11	9:50	4/10
8	4/18	10:31	～	4/21	10:32	4/19-21
12	5/2	11:42	～	5/6	9:20	5/3-5
17	5/19	10:27	～	5/23	10:07	5/22-23
24	6/13	10:39	～	6/16	16:19	6/15
28	6/27	10:02	～	6/30	10:34	?
30	7/4	10:13	～	7/7	10:45	7/6
34	7/19	10:47	～	7/25	10:22	7/24-25
41	8/22	11:58	～	8/26	15:12	8/22
46	9/9	15:09	～	9/12	17:19	?
50	9/26	13:13	～	9/30	13:28	9/27-29

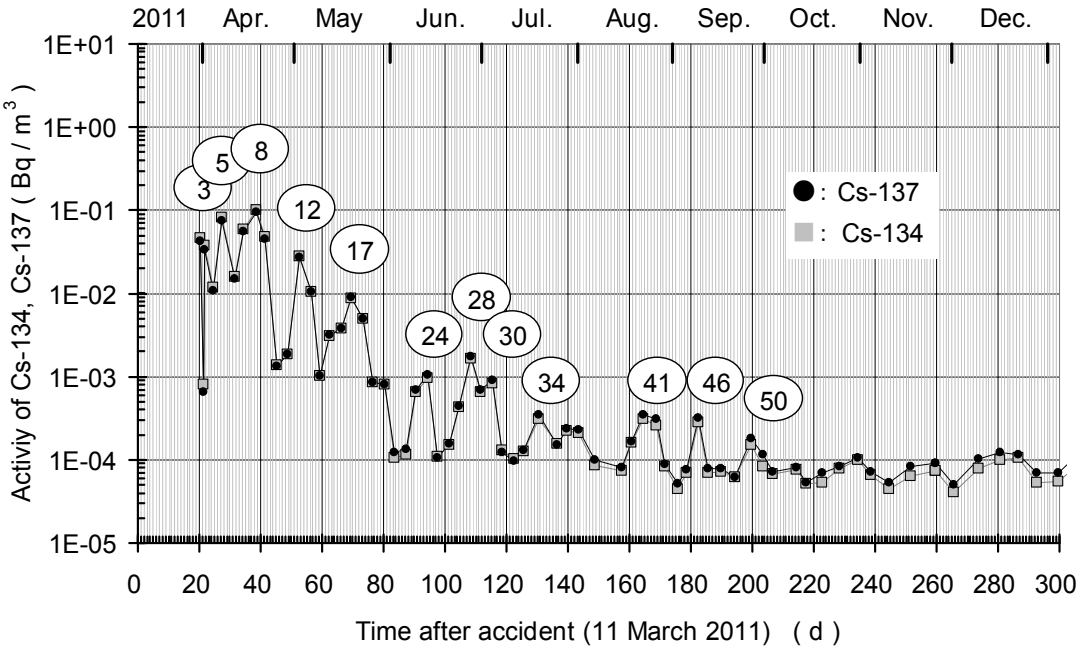

第8図　GSJにおける2011年放射性Cs同位体の観測値の変動(金井，2012a)．丸の中の数字は試料番号を示す．

Fig. 8　Variation of radioactive Cs concentrations at the GSJ in 2011 (Kanai, 2012a). Number in circle indicates the sample number.

て気象との関係を検討した．Air Resources Laboratory (ARL) のウェブページ(http://ready.arl.noaa.gov/HYSPLIT.php) から，「HYSPLIT-WEB (Internet-based) Run HYSPLIT Trajectory Model」に進み，各種条件を選択して計算させ図化した．気象データとしては，「GDAS(global, 2006-present)」を用い，鉛直移動計算方法として気象学モデルの鉛直速度場を用いる「Model Vertical Velocity」を選択し，地表から500 m，100 m，50 mの高さ条件とした．対象とした事象は，第8図と第3表で示した高濃度ピークとなった12回の観測期間で，この期間にGSJ(緯度: 36.06°N，経度: 140.13°E)に到達した空気塊がFDNPPを経過してきたかを検討した．その結果，高濃度となった12回のうち，試料番号28と46を除き，その多くはFDNPP付近の上空を経由した気団が観測期間中にGSJを通過し

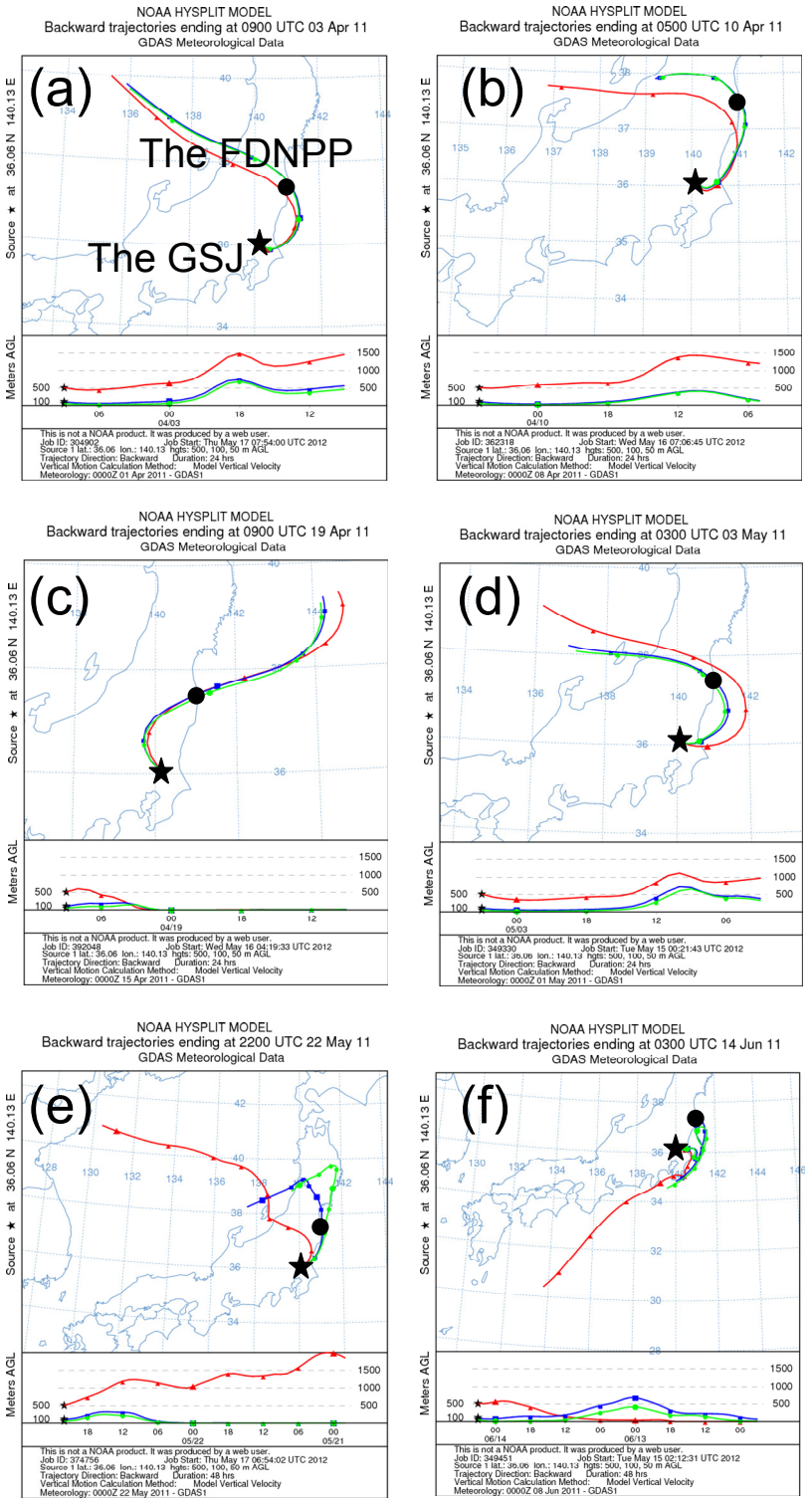

第9図　逆流跡線解析の結果の一例．★：GSJ，●：FDNPP.
(a) 18:00 JST on 3 April 2011
(b) 14:00 JST on 10 April 2011
(c) 18:00 JST on 19 April 2011
(d) 12:00 JST on 3 May 2011
(e) 7:00 JST on 23 May 2011
(f) 12:00 JST on 14 June 2011
(g) 15:00 JST on 6 July 2011
(h) 0:00 JST 24 July 2011
(i) 12:00 JST on 22 August 2011
(j) 12:00 JST on 27 September 2011

Fig. 9　Examples of back trajectory analysis. ★：GSJ, ●：FDNPP.
(a) 18:00 JST on 3 April 2011
(b) 14:00 JST on 10 April 2011
(c) 18:00 JST on 19 April 2011
(d) 12:00 JST on 3 May 2011
(e) 7:00 JST on 23 May 2011
(f) 12:00 JST on 14 June 2011
(g) 15:00 JST on 6 July 2011
(h) 0:00 JST 24 July 2011
(i) 12:00 JST on 22 August 2011
(j) 12:00 JST on 27 September 2011

ていたことが判明した．この推定されたGSJの通過日を第3表に示した．また，この観測期間における逆流跡線解析の結果の一例を第9図に示した．そのほとんどは北よりの風に乗ってGSJに到達しているが，(f)のように風向変化で一度南下した空気塊が南よりの風で到達する場合もあることが示された．また，モデル計算では地球規模での気象データを使用しているが，非常にローカルな気象変動もありうるので，今回の後方流跡線解析で解明できなかったケースではそうしたローカルな気象が影響していたのかも知れない．

前回解析したように濃度変化に降雨の影響もあるだろうが（金井，2012a），エアロゾルは空気塊と共に移動するので，大きな放出源であるFDNPP付近の上空を経由した気団が観測期間中にGSJを通過したためにGSJでの観

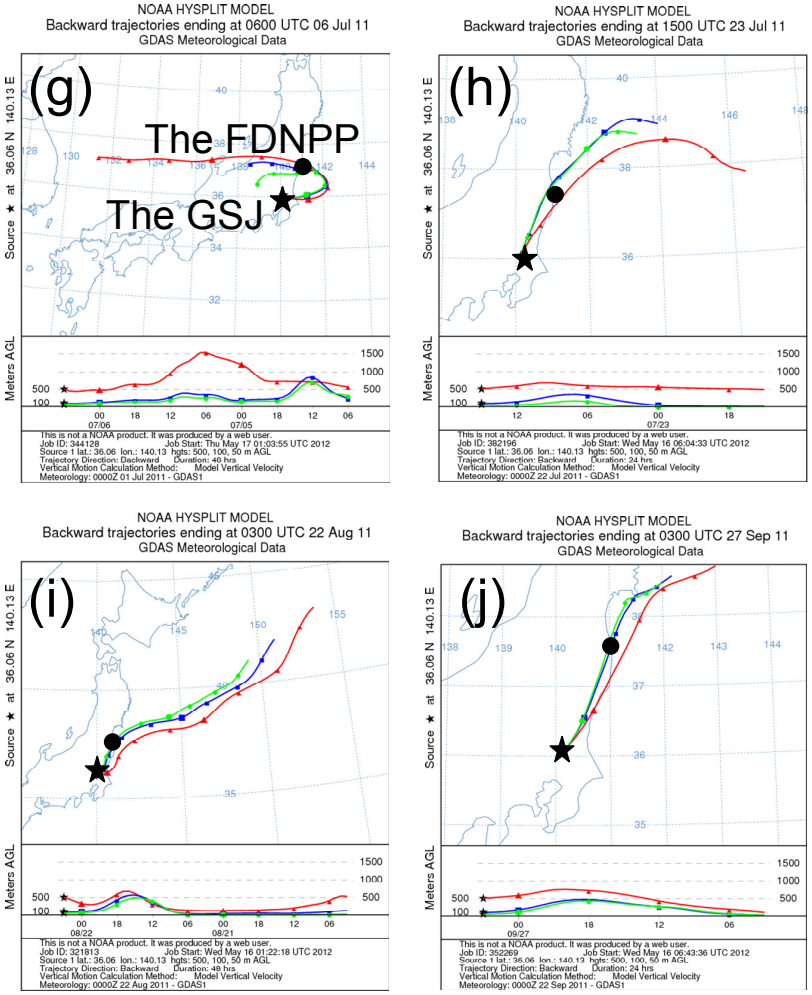

第9図　続き.
逆流跡線解析の結果の一例. ★：GSJ, ●：FDNPP.
(a) 18:00 JST on 3 April 2011
(b) 14:00 JST on 10 April 2011
(c) 18:00 JST on 19 April 2011
(d) 12:00 JST on 3 May 2011
(e) 7:00 JST on 23 May 2011
(f) 12:00 JST on 14 June 2011
(g) 15:00 JST on 6 July 2011
(h) 0:00 JST 24 July 2011
(i) 12:00 JST on 22 August 2011
(j) 12:00 JST on 27 September 2011

Fig. 9　continued.
Examples of back trajectory analysis. ★: GSJ, ●：FDNPP.
(a) 18:00 JST on 3 April 2011
(b) 14:00 JST on 10 April 2011
(c) 18:00 JST on 19 April 2011
(d) 12:00 JST on 3 May 2011
(e) 7:00 JST on 23 May 2011
(f) 12:00 JST on 14 June 2011
(g) 15:00 JST on 6 July 2011
(h) 0:00 JST 24 July 2011
(i) 12:00 JST on 22 August 2011
(j) 12:00 JST on 27 September 2011

測値が高濃度となったことが，このような逆流跡線解析の結果から明らかにすることができた.

4．まとめ

大気中エアロゾルの放射性核種のモニタリングは，物質循環や堆積物への物質移動のトレーサーとして地球科学的に有用であるばかりでなく，地域住民の放射能被爆に対する不安感の払拭，万が一の場合の線量評価にも貢献する．このため，著者らは2011年に引き続き2012年も大気中のエアロゾルの放射性核種の観測を継続した.

原発事故で環境中に放出された人工放射性核種のCs-137は，2011年10月あたりから10^{-4} Bq/m^{3}前後を推移してきたが，2012年4月中旬あたりから約半分のレベルに低下し，その後もそのレベルを保ってきている．これは北よりの風から南よりの風に変わり降雨の日が多くなったことと良く対応しており，2012年の変動はFDNPPでの工事等の影響よりも気象条件や再飛散が大きく作用していたものと考えられる．また，天然放射性核種であるPb-210とBe-7は，2011年よりも変動幅が幾分小さく冬季が高濃度であった点を除くと，これまでとほぼ同様の季節変動パターンを示した.

2011年の観測で放射性セシウム同位体濃度の比較的大きなピークが期間中約12回確認されたが，NOAA HYSPLIT modelを利用して逆流跡線解析を行い気象との関係を再検討したところ，その多くはFDNPP付近の上空を経由した気団であり，降雨の影響も受けたことが判明した.

また，濃度既知の試料を本研究において再測定して相互比較した結果，これまでの報告値に測定上の大きな問題点は無いものと考えられた.

謝辞：本論文をとりまとめる上で，研究環境安全本部環境安全管理部の上岡　晃氏及び資源環境研究部門の月村勝宏氏から貴重なコメントをいただいた．ここに記して，深く感謝申し上げる.

文　献

土井妙子(2012)　放射線　第3講－大気中の放射能の測定・モニタリング－．大気環境学会誌，**47**，A29-A36.

Doi, T., Masumoto, K., Toyoda, A., Tanaka, A., Shibata, Y. and Hirose, K. (2013) Anthropogenic radionuclides in the atmosphere observed at Tsukuba: characteristics of the radionuclides derived from Fukushima. *J. Environ. Radioact*., **122**, 55-62.

Draxler, R.R. and Rolph, G.D. (2012) HYSPLIT (HYbrid Single-Particle Lagrangian Integrated Trajectory) Model access via NOAA ARL READY Website (http://ready.arl.noaa.gov/HYSPLIT.php). NOAA Air Resources Laboratory, Silver Spring, MD.

科学技術庁(1992)　放射能測定法シリーズ　7 ゲルマニウム半導体検出器によるガンマ線スペクトロメトリー，日本分析センター発行，平成4年改訂(1992).

Kanai, Y. (2012) Monitoring of aerosols in Tsukuba after Fukushima Nuclear Power Plant incident in 2011. *J. Environ. Radioact*., **111**, 33-37.

金井　豊(2012a)　エアロゾルにより輸送された放射性核種の観測(2011)－福島第一原子力発電所事故に関連して－．地質調査研究報告，**63**，107-118.

金井　豊(2012b)　エアロゾル中の人工放射性核種に関する観測・測定の試み．Proceedings of the 13th Workshop on Environmental Radioactivity, KEK Proceedings **2012-6**, 108-116.

金井　豊(2013)　地質調査総合センターにおけるエアロゾル中放射性核種の継続観測．第14回「環境放射能」研究会要旨論文集，P-30.

経済産業省(2011)　添付2　福島第一原子力発電所における現状の放射性物質の放出量評価及び敷地境界における被ばく線量評価について，http://www.meti.go.jp/earthquake/nuclear/pdf/111216e.pdf (2013/4/25)

気象庁(2012)　気象統計情報，過去の気象データ検索，http://www.data.jma.go.jp/obd/stats/etrn/index.php (2013/4/25)

国立環境研究所(2011)　Ⅰ-7. (1) つくば市内における放射性物質及び放射線の測定，1. 高エネルギー加速器研究機構との協力による，大気中の放射性物質の測定，http://www.nies.go.jp/shinsai/1-7-1.html (2013/4/25)

高エネルギー加速器研究機構(2011)　環境放射線の測定結果，(1)つくば市で観測された空気中の放射性物質の種類と濃度の測定結果，http://www.kek.jp/ja/Research/ARL/RSC/Radmonitor/ (2013/4/25)

内閣官房内閣広報室(2011a)　Ⅵ. 放射性物質の環境への放出．内閣官房内閣広報室，http://www.kantei.go.jp/jp/topics/2011/pdf/06-kankyo.pdf (2013/4/25)

内閣官房内閣広報室(2011b)　平成23年12月16日 野田内閣総理大臣記者会見．内閣官房内閣広報室，http://www.kantei.go.jp/jp/noda/statement/2011/1216kaiken.html (2013/4/25)

日本分析化学会(2012)　放射能分析用土壌標準物質の頒布開始について，http://www.jsac.jp/sites/default/files/20120605.pdf (2013/4/25)

大原利眞・森野　悠・田中　敦(2011)　福島第一原子力発電所から放出された放射性物質の大気中の挙動．保健医療科学，**60**，292－299.

Rolph, G.D. (2012) Real-time Environmental Applications and Display sYstem (READY) Website (http://ready.arl.noaa.gov). NOAA Air Resources Laboratory, Silver Spring, MD.

Stohl, A., Seibert, P., Wotawa, G., Arnold, D., Burkhart, J.F., Eckhardt, S., Tapia, C., Vargas, A. and Yasunari, T.J. (2012) Xenon-133 and caesium-137 releases into the atmosphere from the Fukushima Dai-ichi nuclear power plant: determination of the source term, atmospheric dispersion, and deposition. *Atmos. Chem. Phys*., **12**, 2313–2343.

東京電力株式会社(2011)　プレスリリース 2011年「福島第一原子力発電所１号機原子炉建屋カバー工事の完了について」．平成23年10月28日，東京電力株式会社，http://www.tepco.co.jp/cc/press/11102804-j.html (2013/4/25)

東京電力株式会社(2012a)　東京電力(株)福島第一原子力発電所１～４号機の廃止措置等に向けた中長期ロードマップ進捗状況(概要版)，http://www.tepco.co.jp/nu/fukushima-np/roadmap/images/m120924_06-j.pdf (2013/4/25)

東京電力株式会社(2012b)　プレスリリース「2012年福島第一原子力発電所４号機燃料取り出し用カバー計画概要と本工事の着手について」．平成24年４月16日，東京電力株式会社，http://www.tepco.co.jp/cc/press/2012/1201925_1834.html (2013/4/25)

東京電力株式会社(2012c)　福島第一原子力発電所構内での計測データ 2012年｜アーカイブ．2012年4月16日 福島第一原子力発電所の現状について【午後11時50分 時 点 】，http://www.tepco.co.jp/nu/fukushima-np/f1/data/2012/index-j.html (2013/4/25)

東京電力株式会社(2012d)　福島第一原子力発電所構内でのモニタリングポスト計測状況．お知らせ，http://www.tepco.co.jp/nu/fukushima-np/f1/index-j.html (2013/4/25)

東京電力株式会社(2012e)　福島第一原子力発電所　２号機の現状，原子炉格納容器ガス管理システムのダクト損傷について(10月15日追記)，http://www.tepco.

co.jp/nu/fukushima-np/f1/genkyo/fp_reactor/fp_no02/index.html （2013/4/25）

東京電力株式会社(2012f)　福島第一原子力発電所　３号機の現状，原子炉格納容器ガス管理システムのダクト修理作業について，http://www.tepco.co.jp/nu/fukushima-np/f1/genkyo/fp_reactor/fp_no03/index.html（2013/4/25）

鶴田治雄・中島映至(2012)　特集「東日本大震災から１年」福島第一原子力発電所の事故により放出された放射性物質の大気中での動態．地球化学，**46**，99-111.

山田崇裕・中村吉秀(2005)　放射能標準体積線源に用いるポリプロピレン製U8容器の検討．Radioisotopes, **54**，105-110.

（ 受　付：2013年5月1日；　受　理：2013年8月21日 ）

Bulletin of the Geological Survey of Japan, vol. 64 (5/6), p. 151 - 190, 2013

Report

Triassic to Middle Jurassic radiolarians from pelagic cherts in the Nanjō Mountains, Southwest Japan – Part 2. Kanmuri Yama district

Satoshi Nakae

Satoshi Nakae (2013) Triassic to Middle Jurassic radiolarians from pelagic cherts in the Nanjō Mountains, Southwest Japan – Part 2. Kanmuri Yama district. *Bull. Geol. Surv. Japan*, vol. 64 (5/6), p. 151-190, 3 figures, 2 tables, 8 plates.

Abstract: The Nanjō Mountains located in the central region of Fukui Prefecture, Southwest Japan, are chiefly underlain by the sedimentary complex of various rock-types such as basalt, limestone, chert, mudstone and sandstone. Among these rocks within the mountains, twenty-seven chert outcrops (localities) were explored for their radiolarian content. Twenty-six rock samples from seventeen localities in the studied Kanmuri Yama district yielded moderately- to poorly-preserved radiolarian remains as a result. Most of the samples contain Triassic to Middle Jurassic species, with Spumellaria and Entactinaria dominant among the Triassic faunas and with Nassellaria dominant among the Jurassic faunas. The description and faunal analysis of these radiolarians revealed that the cherts in the Kanmuri Yama district span a wide range of age from the Late Olenekian to Middle Bathonian stages.

Keywords: radiolaria, Triassic, Middle Jurassic, Nanjō Mountains, Mino belt, Kanmuri Yama district, Fukui Prefecture, Southwest Japan

1. Introduction

The Nanjō Mountains, which extend over an area of ca. 40 km x 20 km in the central region of Fukui Prefecture, are geotectonically divided into the Mino and Ultra-Tamba belts of the Inner Zone of Southwest Japan. The lithologic assemblages of each belt differ from one other; the accretionary complex of the Mino belt is regarded as one of the Jurassic accretionary complexes that formed along the eastern margin of the paleo-Asian continent (*e.g.*, Wakita, 1988), conversely the accretionary complex of the Ultra-Tamba belt is dominated by pale or greenish gray sandstone with subordinate chert and phyllitic mudstone of Permian age (Umeda *et al.*, 1996; Nakae, 2012). The Mino belt consists of thrust-bounded units of basalt and limestone of oceanic island/seamount origin, cherts of pelagic origin and terrigenous clastic rocks (Wakita, 1988; Nakae *et al.*, 2013). 1:50,000 scale maps of the "Imajō" and "Kanmuri Yama" districts almost cover the entire area of the Nanjō Mountains (Fig.1).

The age of the cherts in the Nanjō Mountains has so far been determined to be Triassic to Jurassic (*e.g.*, Hattori and Yoshimura, 1982; Takamura and Hayami, 1985; Taga, 1997; Umeda and Taga, 2003). Through this present study, additional extraction of radiolarians from the accretionary complex of the Mino belt in the Nanjō Mountains was therefore conducted for detailed age determination of its component rocks. Consequently, this study presents a systematic description of all radiolarian species extracted from the cherts in the Kanmuri Yama district as the second report. Those from the Imajō district have already been described in the first report by Nakae (2013).

2. Materials and Method

Through the course of this study, 530 samples were collected in the Nanjō Mountains (222 from the Imajō district, and 308 from the Kanmuri Yama district). The samples were undertaken using an usual technique for radiolarian extraction; briefly, the rock samples were individually soaked in dilute hydrofluoric acid (HF) solution (5%) for 10 to 15 hours, before being washed through a 62μm mesh sieve (235#). As a result, age-diagnostic radiolarians representative of Triassic to Middle Jurassic ages recovered from forty chert samples (from twenty-seven localities), twenty-six of which were from the Kanmuri Yama district. The residues of each processed sample were then examined under a stereomicroscope, and radiolarian remains were selected for examination by scanning electronic microscope (SEM). All figured specimens were deposited and registered with the Geological Museum, Geological Survey of Japan under catalogue numbers (GSJ F).

AIST, Geological Survey of Japan, Institute of Geology and Geoinformation
Author: S. NAKAE, Central 7, 1-1-1 Higashi, Tsukuba 305-8567, JAPAN. Email: nakae-satoshi@aist.go.jp

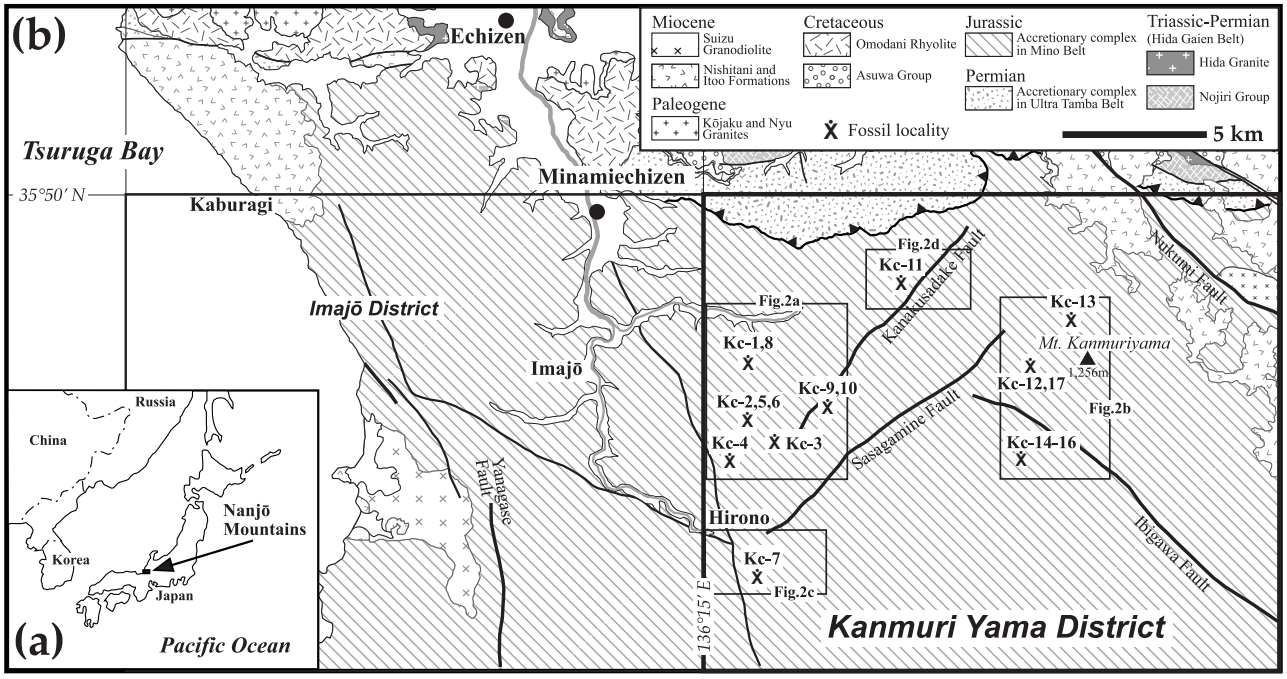

Fig. 1 Index map of the Kanmuri Yama district in Nanjō Mountains.
(a): The Nanjō Mountains are situated in a central part of Fukui Prefecture. (b): A simplified geological map of the mountains, most part of which geotectonically belongs to the Mino belt, Southwest Japan. The Kanmuri Yama district contains the eastern part of the Nanjō Mountains. Detailed radiolarian localities with symbols are given in Fig. 2.

3. Radiolarian locality and fauna

Twenty-six chert samples comprising part of a suite of 308 samples that were collected from the Kanmuri Yama district in the Nanjō Mountains yielded moderately- to poorly-preserved radiolarian faunas. Radiolarian localities (Kc-1 – Kc17) are shown in Figs. 1 and 2, and the identified species are listed in Table 1. Below is a detailed description of each locality investigated and their faunal contents.

(1) Locality Kc-1 (Fig. 2a)
Location: Tarumi-gawa, Minamiechizen Town.
(lat. 35º46’31.3” N, long. 136º16’57.4” E)
Sample number: KJ 0301.
Lithology: Thinly bedded light gray to pale gray chert.
Fauna: *Cryptostephanidium*? sp., *Palaeosaturnalis* sp., *Haeckelicyrtium*? spp. (Plate 1).
Age: Probably Carnian.

(2) Locality Kc-2 (Fig. 2a)
Location: Northeast of Masudani, Minamiechizen Town.
(lat. 35º45’23.8” N, long. 136º16’40.6” E)
Sample number: KJ 0402
Lithology: Thinly bedded light pale gray chert.
Fauna: *Eptingium nakasekoi* Kozur and Mostler, *Pseudostylosphaera japonica* (Nakaseko and Nishinura), *Pseudostylosphaera*? sp., *Triassocampe deweveri* (Nakaseko and Nishimura), *Triassocampe* spp., Poulpidae gen. et sp. indet., Spumellaria gen. et sp. indet. (Plate 1).
Age: Late Anisian.

Sample number: KJ 0403
Lithology: Thinly bedded light pale gray chert.
Fauna: *Pseudostylosphaera*? sp., *Triassocampe* sp. cf. *T. myterocorys* Sugiyama, *Multimonilis* sp. (Plate 1).
Age: Probably Ladinian – Early Carnian.

Sample number: KJ 0404
Lithology: Thinly bedded light pale gray chert.
Fauna: *Triassocampe deweveri* (Nakaseko and Nishimura), *Triassocampe* sp., Nassellaria gen. et sp. indet. (Plate 1).
Age: Late Anisian – middle Late Ladinian.

(3) Locality Kc-3 (Fig. 2a)
Location: East of Masudani, Minamiechizen Town.
(lat. 35º44’58.4” N, long. 136º17’9.1” E)
Sample number: KJ 0410c.
Lithology: Thinly bedded reddish brown chert.
Fauna: *Droltus* sp. cf. *D. hecatensis* Pessagno and Whalen, Entactinaria gen. et sp. indet., Nassellaria gen. et sp. indet. (Plate 1).
Age: Probably Hettangian – Early Pliensbachian.

(4) Locality Kc-4 (Fig. 2a)
Location: Masudani, Minamiechizen Town.
(lat. 35º44’28.5” N, long. 136º15’38.5” E)
Sample number: KJ 0810e.
Lithology: Thinly bedded gray chert.

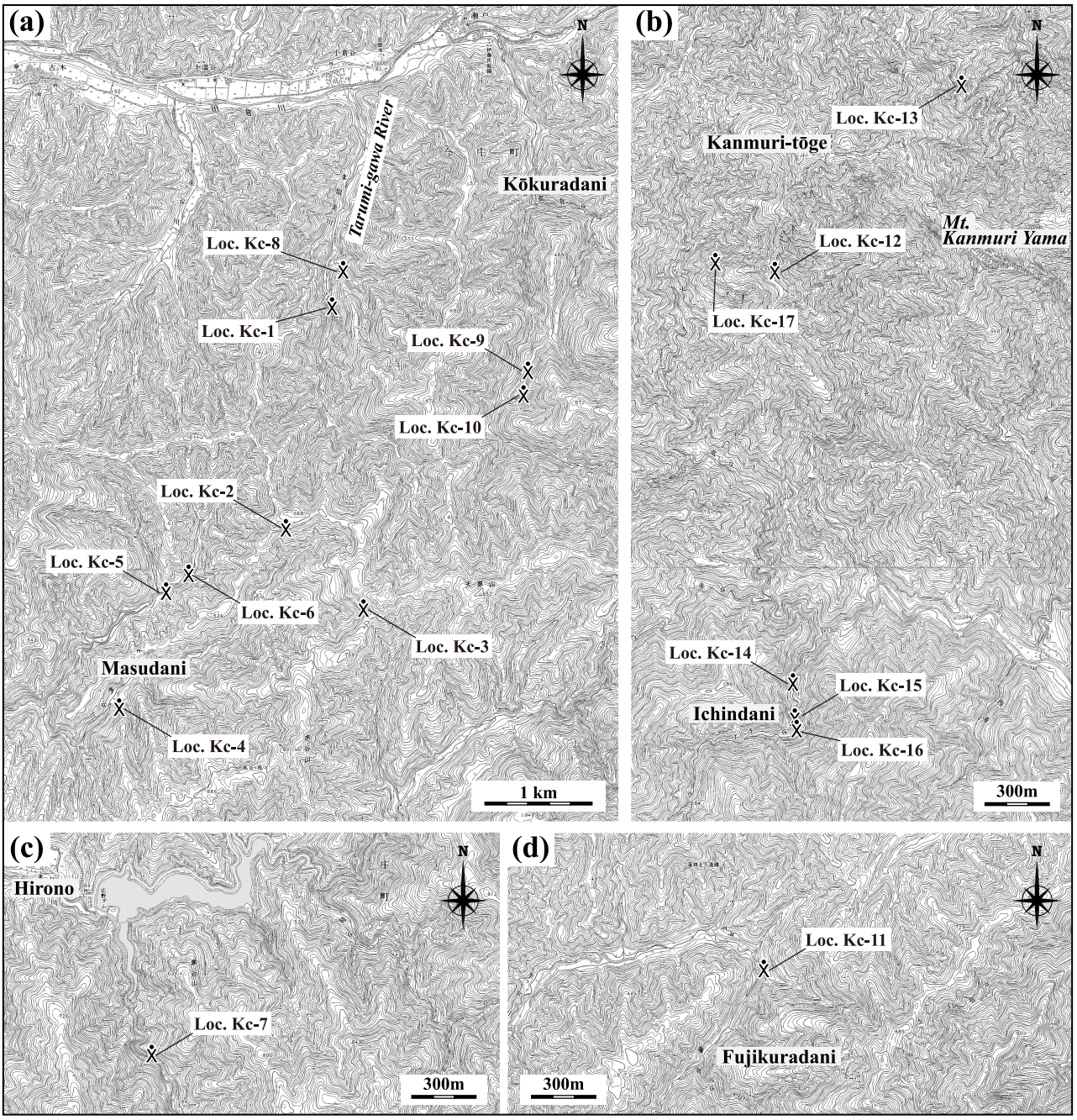

Fig. 2 Localities of chert samples yielding Triassic to Middle Jurassic radiolarians.
Parts of topographic maps of "Furuki" is used for figures (a) and (d), "Kanmuri Yama" and "Mino Tokuyama" for figure (b) and "Hirono" for figure (c). These maps are published from the Geospatial Information Authority of Japan.

Fauna: *Archaeocenosphaera*? sp., *Pseudostylosphaera*? spp., *Tirodella*? sp., *Celluronta* sp., Spumellaria gen. et sp. indet., Nassellaria gen. et sp. indet. (Plate 2).
Age: Early Anisian – Middle Anisian.

Sample number: KJ 0810f.
Lithology: Thinly bedded gray chert.
Fauna: *Eptingium*? sp., *Pseudostylosphaera* spp., Spumellaria gen. et sp. indet., Nassellaria gen. et sp. indet. (Plate 2).
Age: Probably Early Anisian – Early Carnian.

Sample number: KJ 0810g.
Lithology: Thinly bedded gray chert.
Fauna: *Cryptostephanidium*? sp., *Eptingium* sp., *Pseudostylosphaera compacta* (Nakaseko and Nishimura), *Parasepsagon* sp., *Triassocampe* spp., Spumellaria gen. et sp. indet., Entactinaria gen. et sp. indet., Nassellaria gen. et sp. indet. (Plate 2).
Age: Middle Anisian – Late Anisian.

Table. 1 List of radiolarian species detected from the Kanmuri Yama district in the Nanjō Maountains.

	Locality Number (Kc-)	1	2		3	4			5			6		7	8			9	10	11	12	13	14	15	16	17
	Sample Number	KJ 0301	KJ 0402	KJ 0403	KJ 0404	KJ 0410c	KJ 0810e	KJ 0810f	KJ 0810g	KJ 0904a	KJ 0904b	KJ 0904c	KJ 0905b	KJ 0905c	KJ 1904a	KJ 2206a	KJ 2206h	KJ 2206i	KJ 2412	KJ 2413	KJ 2902c	KJ 3701	KJ 3907	KJ 4401a	KJ 4405	KJ 4406a	KJ 5904
SPUMELLARIA	*Pantanellium*? *virgeum* Sashida														+											
	Pantanellium spp.																							+		+
	Zartus sp.																								+	
	Trillus elkhornensis Pessagno and Blome													+												
	Archaeocenosphaera? spp.						+			+	+															
	Udalia spp.															+										
	Protopsium spp.																				+					
	Spongoxystris? sp.																			+						
	Oertlispongus sp.																				+					
	Palaeosaturnalis sp.	+																					+			
	Praemesosaturnalis spp.																						+			
	Patulibracchiidae gen. et sp. indet.																								+	
	Spumellaria gen. et sp. indet.		+				+	+	+		+	+	+		+			+			+					
ENTACTINARIA	*Spongostephanidium* spp.																+				+					
	Cryptostephanidium? spp.	+							+								+		+							
	Eptingium nakasekoi Kozur and Mostler		+																			+				
	Eptingium spp.								+									+				+				
	Eptingium? spp.							+			+										+					
	Pentabelus sp. cf. *P. furutanii* Sugiyama																				+					
	Pseudostylosphaera compacta (Nakaseko and Nishimura)								+		+						+									
	Pseudostylosphaera helicata (Nakaseko and Nishimura)										+															
	Pseudostylosphaera japonica (Nakaseko and Nishimura)		+																	+			+			
	Pseudostylosphaera sp. aff. *P. tenuis* (Nakaseko and Nishimura)											+														
	Pseudostylosphaera spp.							+									+		+		+					
	Pseudostylosphaera? spp.		+	+			+								+			+	+							
	Parasepsagon sp.								+																	
	Hindeosphaera spinulosa (Nakaseko and Nishimura)																+									
	Hindeosphaera sp.																					+				
	Muelleritortis cochleata (Nakaseko and Nishimura)																			+						
	Monostylosphaera? spp.														+							+				
	Entactinaria gen. et sp. indet.				+				+				+		+			+	+		+				+	
NASSELLARIA	*Tirodella*? sp.						+																			
	Bipedis sp.																	+								
	Napora mitrata Pessagno, Whalen and Yeh															+										
	Napora sp.															+										
	Haeckelicyrtium? spp.	+																								
	Celluronta sp.						+																			
	Paratriassocampe sp.																+									
	Triassocampe deweveri (Nakaseko and Nishimura)		+		+						+						+									
	Triassocampe sp. cf. *T. myterocorys* Sugiyama			+																+						
	Triassocampe sp. aff. *T. diordinisi* Bragin sensu Sugiyama (1992)																		+							
	Triassocampe spp.		+		+				+	+	+						+		+	+		+				
	Eucyrtidiellum nagaiae Dumitrica, Goričan and Matsuoka															+										
	Droltus sp. cf. *D. hecatensis* Pessagno and Whalen				+																					
	Parahsuum simplum Yao															+										
	Parahsuum ovale Hori and Yao															+										
	Parahsuum izeense (Pessagno and Whalen)															+										
	Parahsuum longiconicum Sashida															+										
	Parahsuum sp. cf. *P. longiconicum* Sashida																							+		
	Parahsuum spp.													+		+						+				+
	Parahsuum? sp. A																									+
	Hsuum sp. cf. *H. mulleri* Pessagno and Whalen													+												
	Hsuum sp. sensu Matsuoka (2004)															+										
	Hsuum? sp.																					+				
	Conoptum sp. cf. *C. anulatum* Pessagno and Poisson																					+				
	Conoptum sp. cf. *C. rugosum* Pessagno and Poisson															+										
	Multimonilis sp.			+																						
	Praeparvicingula gigantocornis (Kishida and Hisada)																								+	
	Praeparvicingula sp. cf. *P. nanoconica* (Hori and Otsuka)																								+	
	Praeparvicingula spp.																							+	+	
	Parvicingula sp.																								+	
	Lantus obesus (Yeh)															+										
	Lantus intermedius Carter															+										+
	Lantus? sp.													+												
	Dictyomitrella? sp. cf. *D.*? *kamoensis* Mizutani and Kido																								+	
	Minocapsa globosa Matsuoka															+										
	Poulpidae gen. et sp. indet.		+																		+					
	Favosyringiinae gen. et sp. indet.													+								+				
	Nassellaria gen. et sp. indet.				+	+	+	+	+	+	+			+		+						+	+	+		

Table. 2 List of radiolarian genera and their biostratigraphic ranges.

Genus	Range
Pantanellium	upper Carnian — lower Aptian
Zartus	lower Pliensbachian — upper Bajocian
Trillus	lower Pliensbachian — lower Bathonian
Archaeocenosphaera	middle Anisian — upper Campanian
Udalia	lower Hettangian — lower Pliensbachian
Protopsium	upper Hettangian — lower Toarcian
Spongoxystris	middle Anisian — Ladinian
Oertlispongus	upper Anisian — lower Carnian
Palaeosaturnalis	lower Carnian — upper Pliensbachian
Praemesosaturnalis	upper Norian — upper Rhaetian
Pentabelus	upper Olenekian — lower Carnian
Monostylosphaera	lower Carnian — upper Carnian
Spongostephanidium	upper Olenekian — upper Carnian
Cryptostephanidium	lower Anisian — upper Carnian
Eptingium	lower Anisian — upper Rhaetian
Pseudostylosphaera	upper Olenekian — lower Carnian
Parasepsagon	middle Anisian — upper Anisian
Hindeosphaera	middle Anisian — middle Norian
Muelleritortis	Ladinian — lower Carnian
Hozmadia	upper Olenekian — upper Carnian
Tirodella	lower Carnian
Bipedis	upper Norian — upper Pliensbachian
Napora	upper Sinemurian — lower Turonian
Haecklicyrtium	lower Carnian — upper Pliensbachian
Celluronta	lower Anisian — middle Anisian
Paratriassocampe	middle Anisian — upper Anisian
Triassocampe	lower Anisian — lower Norian
Yeharaia	middle Anisian — lower Carnian
Eucyrtidiellum	lower Pliensbachian — upper Tithonian
Droltus	lower Hettangian — lower Bajocian
Parahsuum	lower Hettangian — upper Kimmeridgian
Hsuum	lower Pliensbachian — lower Cenomanian
Canoptum	Ladinian — upper Bajocian
Multimonilis	Ladinian — middle Norian
Praeparvicingula	middle Toarcian — upper Barremian
Parvicingula	upper Bathonian — upper Hauterivian
Lantus	lower Pliensbachian — lower Kimmeridgian
Minocapsa	lower Pliensbachian — lower Toarcian

(5) Locality Kc-5 (Fig. 2a)
Location: Northeast of Masudani, Minamiechizen Town. (lat. 35º45’4.9” N, long. 136º15’55.1” E)
Sample number: KJ 0904a.
Lithology: Thinly bedded pale gray chert.
Fauna: *Archaeocenosphaera*? spp., *Triassocampe* sp., Nassellaria gen. et sp. indet. (Plate 3).
Age: Probably Middle Anisian – Early Norian.

Sample number: KJ 0904b.
Lithology: Thinly bedded pale gray chert.
Fauna: *Archaeocenosphaera*? spp., *Eptingium*? sp., *Pseudostylosphaera compacta* (Nakaseko and Nishimura), *Pseudostylosphaera helicata* (Nakaseko and Nishimura), *Triassocampe deweveri* (Nakaseko and Nishimura), *Triassocampe* spp., Spumellaria gen. et sp. indet., Nassellaria gen. et sp. indet. (Plate 3).
Age: Late Anisian – middle Late Ladinian.

Sample number: KJ 0904c.
Lithology: Thinly bedded pale gray chert.
Fauna: *Pseudostylosphaera* sp. aff. *P. tenuis* (Nakaseko and Nishimura), Spumellaria gen. et sp. indet. (Plate 3).
Age: Probably Middle Anisian or younger.

(6) Locality Kc-6 (Fig. 2a)
Location: Northeast of Masudani, Minamiechizen Town. (lat. 35º45’7.6” N, long. 136º16’5.5” E)
Sample number: KJ 0905b.
Lithology: Thinly bedded dark gray chert.
Fauna: Entactinaria gen. et sp. indet., Spumellaria gen. et sp. indet. (Plate 3).
Age: Unknown.

Sample number: KJ 0905c.
Lithology: Thinly bedded dark gray chert.
Fauna: *Trillus elkhornensis* Pessagno and Blome, *Hsuum* sp. cf. *H. mulleri* Pessagno and Whalen, *Parahsuum* spp., *Lantus*? sp., Favosyringiinae gen. et sp. indet., Nassellaria gen. et sp. indet. (Plate 3).
Age: Early Pliensbachian – Middle Bajocian?

(7) Locality Kc-7 (Fig. 2c)
Location: Southeast of Hirono, Minamiechizen Town. (lat. 35º42’5.5” N, long. 136º15’45.6” E)
Sample number: KJ 1904a.
Lithology: Thinly bedded dark gray chert.
Fauna: *Pantanellium*? *virgeum* Sashida, *Pseudostylosphaera*? spp., *Monostylosphaera*? sp., Spumellaria gen. et sp. indet., Entactinaria gen. et sp. indet. (Plate 4).
Age: Late Olenekian – Middle Anisian.

(8) Locality Kc-8 (Fig. 2a)
Location: Tarumi-gawa, Minamiechizen Town. (lat. 35º46’42.5” N, long. 136º17’1.9” E)
Sample number: KJ 2206a.
Lithology: Thinly bedded gray chert.
Fauna: *Udalia* spp., *Napora mitrata* Pessagno, Whalen and Yeh, *Napora* sp., *Eucyrtidiellum nagaiae* Dumitrica, Goričan and Matsuoka, *Parahsuum simplum* Yao, *Parahsuum ovale* Hori and Yao, *Parahsuum izeense* (Pessagno and Whalen), *Parahsuum longiconicum* Sashida, *Parahsuum* spp., *Hsuum* sp. sensu Matsuoka 2004, *Canoptum* sp. cf. *C. rugosum* Pessagno and Poisson, *Lantus obesus* (Yeh), *Lantus intermedius* Carter, *Minocapsa globosa* Matsuoka, Nassellaria gen. et sp. indet. (Plate 4).
Age: Early Toarcian.

Sample number: KJ 2206h.
Lithology: Thinly bedded gray chert.
Fauna: *Spongostephanidium* sp., *Cryptostephanidium*?

sp., *Pseudostylosphaera compacta* (Nakaseko and Nishimura), *Pseudostylosphaera* spp., *Hindeosphaera spinulosa* (Nakaseko and Nishimura), *Triassocampe deweveri* (Nakaseko and Nishimura), *Triassocampe* spp., *Paratriassocampe* sp. (Plate 5).
Age: Late Anisian.

Sample number: KJ 2206i.
Lithology: Thinly bedded gray chert.
Fauna: *Eptingium* sp., *Pseudostylosphaera*? spp., *Bipedis* sp., Spumellaria gen. et sp. indet., Entactinaria gen. et sp. indet. (Plate 5).
Age: Probably Carnian – Late Norian.

(9) Locality Kc-9 (Fig. 2a)
Location: South of Kōkuradani, Minamiechizen Town.
(lat. 35º46'12.1" N, long. 136º18'12" E)
Sample number: KJ 2412.
Lithology: Thinly bedded light gray chert.
Fauna: *Cryptostephanidium*? sp., *Pseudostylosphaera* spp., *Pseudostylosphaera*? spp., *Triassocampe* sp. aff. *T. diordinis* Bragin sensu Sugiyama 1992, *Triassocampe* spp., Entactinaria gen. et sp. indet. (Plate 5).
Age: Middle Anisian.

(10) Locality Kc-10 (Fig. 2a)
Location: South of Kōkuradani, Minamiechizen Town.
(lat. 35º46'4" N, long. 136º18'8.2" E)
Sample number: KJ 2413.
Lithology: Thinly bedded greenish gray chert.
Fauna: *Spongoxystris*? sp., *Pseudostylosphaera japonica* (Nakaseko and Nishimura), *Muelleritortis cochleata* (Nakaseko and Nishimura), *Triassocampe* sp. cf. *T. myterocorys* Sugiyama, *Triassocampe* spp. (Plate 6).
Age: Late Ladinian – earliest Carnian.

(11) Locality Kc-11 (Fig. 2d)
Location: Fujikuradani, Minamiechizen Town.
(lat. 35º48'21.5" N, long. 136º20'23.2" E)
Sample number: KJ 2902c.
Lithology: Thinly bedded dark gray chert.
Fauna: *Protopsium* spp., *Oertlispongus* sp., *Spongostephanidium* spp., *Eptingium*? sp., *Pentabelus* sp. cf. *P. furutanii* Sugiyama, *Pseudostylosphaera* sp., Poulpidae gen. et sp. indet., Spumellaria gen. et sp. indet., Entactinaria gen. et sp. indet. (Plate 6).
Age: Probably Late Anisian – Early Carnian.

(12) Locality Kc-12 (Fig. 2b)
Location: South of Kanmuri-tōge, Ibigawa Town.
(lat. 35º46'40.1" N, long. 136º23'13.4" E)
Sample number: KJ 3701.
Lithology: Thinly bedded light dark gray chert.
Fauna: *Parahsuum* spp., *Hsuum*? sp., *Canoptum* sp. cf. *C. anulatum* Pessagno and Poisson, Favosyringiinae gen. et sp. indet., Nassellaria gen. et sp. indet. (Plate 7).
Age: Probably Early Pliensbachian – early Late Toarcian.

(13) Locality Kc-13 (Fig. 2b)
Location: Northeast of Kanmuri-tōge, Ikeda Town.
(lat. 35º47'37.2" N, long. 136º24'23.3" E)
Sample number: KJ 3907.
Lithology: Thinly bedded light pale gray chert.
Fauna: *Eptingium nakasekoi* Kozur and Mostler, *Eptingium* sp., *Pseudostylosphaera japonica* (Nakaseko and Nishimura), *Hindeosphaera* sp., *Monostylosphaera*? sp. *Triassocampe* spp., Nassellaria gen. et sp. indet. (Plate 7).
Age: Middle Anisian – Late Anisian.

(14) Locality Kc-14 (Fig. 2b)
Location: Ichindani, Ibigawa Town.
(lat. 35º44'36.4" N, long. 136º23'20.2" E)
Sample number: KJ 4401a.
Lithology: Thinly bedded pale gray chert.
Fauna: *Palaeosaturnalis* sp., *Praemesosaturnalis* spp., Nassellaria gen. et sp. indet. (Plate 7).
Age: Late Norian – Late Rhaetian.

(15) Locality Kc-15 (Fig. 2b)
Location: Ichindani, Ibigawa Town.
(lat. 35º44'23.3" N, long. 136º23'21" E)
Sample number: KJ 4405
Lithology: Thinly bedded gray chert.
Fauna: *Pantanellium* spp., *Parahsuum* sp. cf. *P. longiconicum* Sashida, *Praeparvicingula* spp. (Plate 8).
Age: Probably Early Pliensbachian – Early Aalenian.

(16) Locality Kc-16 (Fig. 2b)
Location: Ichindani, Ibigawa Town.
(lat. 35º44'21.2" N, long. 136º23'21.3" E)
Sample number: KJ 4406a.
Lithology: Thinly bedded gray chert.
Fauna: *Zartus* sp., *Praeparvicingula gigantocornis* (Kishida and Hisada), *Praeparvicingula* sp. cf. *P. nanoconica* (Hori and Otsuka), *Praeparvicingula* spp., *Parvicingula* sp., *Dictyomitrella*? sp. cf. *D.*? *kamoensis* Mizutani and Kido, Patulibracchiidae gen. et sp. indet., Entactinaria gen. et sp. indet. (Plate 8).
Age: Late Toarcian – Bajocian.

(17) Locality Kc-17 (Fig. 2b)
Location: Southwest of Kanmuri-tōge, Ibigawa Town.
(lat. 35º46'44.2" N, long. 136º22'50" E)
Sample number: KJ 5904.
Lithology: Thinly bedded light gray chert.
Fauna: *Pantanellium* spp., *Parahsuum* spp., *Parahsuum*? sp. A, *Lantus intermedius* Carter (Plate 8).
Age: Latest Sinemurian – Early Toarcian.

4. Age determination

In order to determine the geological age of the radiolarian faunas detected from the chert samples of this report, the zonation schemes proposed by Sugiyama (1997) for Triassic (TR0 – TR8D), by Hori (1990) and Carter *et*

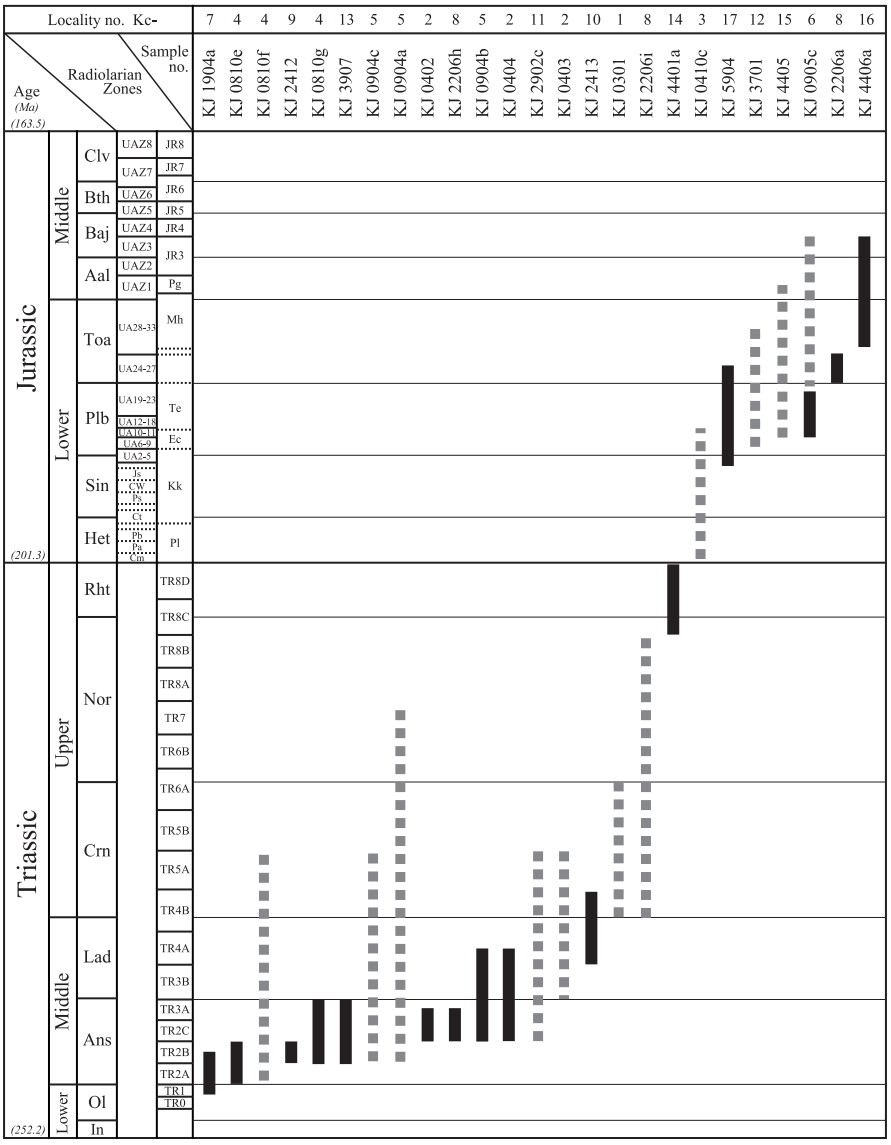

Fig. 3 Geologic age of each chert sample based on the detected radiolarians.
Radiolarian zonation schemes proposed by after-mentioned literatures are primarily adapted in this figure. These zones are arranged in ascending order: TR0 – TR8 for Triassic (Sugiyama, 1997); Pl, Kk, Ec, Te, Mh and Pg for Hettangian – lower Aalenian (Hori, 1990); Cm, Pa, Pb, Ct, Ps, CW, Js for Hettangian – Sinemurian (Carter *et al.*, 1998); UA2 – UA33 for uppermost Sinemurian – Toarcian (Carter *et al.*, 2010); JR3 – JR8 for Middle Jurassic (Matsuoka, 1995); UAZ1 – UAZ8 for Middle Jurassic (Baumgartner *et al.*, 1995b). Abbreviations are as follows. Pl: *Parahsuum aff. longiconicum*, Kk: *Katroma kurusuensis*, Ec: *Eucyrtidiellum*? sp. C, Te: *Trillus elkhornensis*, Mh: *Mesosaturnalis hexagonus*, Pg: *Parahsuum*? *grande*, Cm: *Canoptum merum*, Pa: *Protokatroma aquila*, Pb: *Pantanellium browni*, Ct: *Crucella hettangica*, Ps: *Parahsuum simplum*, CW: *Canutus rockfishensis* and *Wrangellium thurstonense*, Js: *Jacus*? *sandspitensis*, UAZ: Unitary Association Zone. Geologic time scale with ages (in Ma) is based on Gradstein *et al.* (2012).

al. (1998, 2010) for Lower Jurassic (UA1 – UA41), and by Baumgartner *et al.* (1995b) and Matsuoka (1995) for Middle Jurassic (UAZ1 – UAZ8), are primarily used. Biostratigraphic ranges of radiolarian genera fully and most-recently analyzed by O'Dogherty *et al.* (2009, 2010) are adapted to those of the radiolarian genera listed in Table 2. Furthermore, biostratigraphic ranges of the radiolarian species discussed below are partly based on Pessagno and Blome (1980), Pessagno and Whalen (1982), Sugiyama (1992), Sashida *et al.* (1993), Nishizono (1996), Yao (1997) and Matsuoka (2004), in addition to the above literatures.

4.1. Early – Middle Triassic

Ten samples (KJ0402, KJ0404, KJ0810e, KJ0810g, KJ0904b, KJ1904a, KJ2206h, KJ2412, KJ2413, and

KJ3907) taken from eight localities yielded Late Olenekian to Early Carnian (Early to Middle Triassic) radiolarian faunas; also five samples (KJ0403, KJ0810f, KJ0904a, KJ0904c and KJ2902c) contain faunas that have a much wider span ranging from the Anisian to Carnian or Norian ages.

Age-diagnostic species are rarely included in KJ0810e and KJ1904a, their ages however can be determined as follows; **KJ1904a** is assigned to TR1 – lower part of TR2B, ranging from the late Spathian (= late Late Olenekian) to Middle Anisian (Sugiyama, 1997), based on the presence of *Pantanellium*? *virgeum* Sashida, and **KJ0810e** is restricted in age to be the Early to Middle Anisian based on the occurrence of *Celluronta* sp.

Although the fauna is poorly preserved, the presence of *Triassocampe* sp. aff. *T. diordinis* Bragin sensu Sugiyama suggests that **KJ2412** is assigned to the Tc assemblage of Sugiyama (1992), indicating the Middle Anisian age. The presence of *Pseudostylosphaera compacta* (Nakaseko and Nishimura) and *Pseudostylosphaera japonica* (Nakaseko and Nishimura) suggests that **KJ0810g** and **KJ3907** are not older than the Middle Anisian (Sugiyama, 1992).

Moreover, the co-occurrence of *Parasepsagon* sp. in KJ0810g and *Eptingium nakasekoi* Kozur in KJ3907 supposed to be restricted to TR2A or TR2B – TR3A (Early or Middle Anisian – Late Anisian), were respectively found. Therefore, these samples are indicative of the Middle – Late Anisian age.

KJ0402 and **KJ2206h** are assigned to TR2C – lower part of TR3A (Late Anisian) based on the co-occurrence of following species: *Eptingium nakasekoi* Kozur and Mostler, *Pseudostylosphaera japonica* (Nakaseko and Nishinura) and *Triassocampe deweveri* (Nakaseko and Nishimura) in KJ0402; *Pseudostylosphaera compacta* (Nakaseko and Nishimura), *Triassocampe deweveri* (Nakaseko and Nishimura) and *Hindeosphaera spinulosa* (Nakaseko and Nishimura) in KJ2206h.

The fauna found in **KJ0904b** consists of *Pseudostylosphaera compacta* (Nakaseko and Nishimura), *Pseudostylosphaera helicata* (Nakaseko and Nishimura) and *Triassocampe deweveri* (Nakaseko and Nishimura). It is known that *Pseudostylosphaera helicata* (Nakaseko and Nishimura) had existed from T3 to lower part of T5 (Early Ladinian – Early Norian; Nishizono, 1996) or from Early Anisian to Late Ladinian (Sashida *et al.*, 1993), therefore KJ0904b is estimated to be a Late Anisian – middle Late Ladinian interval. *Triassocampe deweveri* (Nakaseko and Nishimura) is only an age-diagnostic species included in KJ0404, indicating a Late Anisian – middle Late Ladinian interval.

The fauna detected from **KJ2413** is characterized by the presence of *Muelleritortis cochleata* (Nakaseko and Nishimura) and *Pseudostylosphaera japonica* (Nakaseko and Nishimura), together with *Triassocampe* sp. cf. *T. myterocorys* Sugiyama. The former two co-existed during TR4A – TR4B (Late Ladinian and early Early Carnian), consequently suggesting that this sample is assigned to a Late Ladinian – earliest Carnian interval.

4.2. Late Triassic

Scarce and poorly preserved faunas were detected from Samples KJ0301, KJ2206i and K4401a. Ages of the former two samples are impossible to be determined precisely, due to the absence of age-diagnostic species. Remaining **KJ4401a** contains *Praemesosaturnalis* sp. and *Palaeosaturnalis* sp., therefore its age is estimated to be a Late Norian – Late Rhaetian interval.

4.3. Early – Middle Jurassic

Early to Middle Jurassic radiolarian faunas were found in seven samples (KJ0410c, KJ0905c, KJ2206a, KJ3701, KJ4405, KJ4406a and KJ5904).

A specimen comparable to *Droltus hecatensis* Pessagno and Whalen, ranging in age from Hettangian to Early Pliensbachian (Pessagno and Whalen, 1982), is an age-diagnostic species in **KJ0410c**. Thus, the inferred age-range probably is a Hettangian – Early Pliensbachian interval. **KJ5904** can be assigned to a latest Sinemurian – Early Toarcian interval (UA2 – UA26), based on the range of *Lantus intermedius* Carter.

Ages of **KJ3701** and **KJ4405** cannot be precisely determined because of their poorly preserved faunas. However, Early Pliensbachian – early Late Toarcian (UA6 – UA28) and Early Pliensbachian – Early Aalenian (UA10 – UA35) intervals are probably proposed respectively for the each age of KJ3701 and KJ4405, on the basis of the presence of *Canoptum* sp. cf. *C. anulatum* Pessagno and Poisson in KJ3701, and *Parahsuum* sp. cf. *P. longiconicum* Sashida in KJ4405.

KJ0905c contains *Trillus elkhornensis* Pessagno and Blome, which ranges from an Early or Late Pliensbachian to Middle Bajocian interval (Pessagno and Blome, 1980; Carter *et al.*, 2010). A specimen comparable to *Hsuum mulleri* Pessagno and Whalen is also included; its range is restricted in an interval of middle Early Pliensbachian – early Late Pliensbachian (UA10- UA20). For this sample, middle Early – early Late Pliensbachian age is indicated by the co-occurrence of the two species, although the maximum age may be extended up to the Middle Bajocian.

The fauna detected from **KJ2206a** is moderately preserved and relatively diverse. The co-occurrence of *Eucyrtidiellum nagaiae* Dumitrica, Goričan and Matsuoka and *Lantus intermedius* Carter suggests that this fauna compatible with an interval of Late Pliensbachian – Early Toarcian (UA19 – UA26). The presence of *Minocapsa globosa* Matsuoka, whose age-range is from Late Pliensbachian? – Early Toarcian (Yao, 1997; Matsuoka, 2004), is concordant with the age of the above co-occurrence. However, the range of *Napora mitrata* Pessagno, Whalen and Yeh is supposed to be restricted to the Early Toarcian age (Pessagno *et al.*, 1986), therefore the age of KJ2206a is within the Early Toarcian.

KJ4406a yielded poorly preserved fauna. On the basis of the presence of *Praeparvicingula gigantocornis* (Kishida and Hisada), together with *Praeparvicingula* sp. cf. *P. nanoconica* (Hori and Otsuka) and *Dictyomitrella*? sp. cf. *D.*? *kamoensis* Mizutani and Kido, an interval

between Late Toarcian and Middle Bajocian is inferred as the age of this sample.

5. Conclusion

The geological age inferred for all the twenty-six chert samples investigated in the Kanmuri Yama district, the Nanjō Mountains, spans a wide range from the Late Olenekian (Early Triassic) to Middle Bajocian (Middle Jurassic); age of one sample is still remain unknown (Fig. 3). This evidence strongly suggests that the cherts in this district records up to 80 m.y. of deposition.

6. Systematic Paleontology

Order **SPUMELLARIA** Ehrenberg 1875, *emend*. De Wever, Dumitrica, Caulet, Nigrini and Caridroit 2001
Family **Pantanelliidae** Pessagno 1977b

Genus ***Pantanellium*** Pessagno 1977a
Type species *Pantanellium riedeli* Pessagno 1977a

Pantanellium*? *virgeum Sashida 1991
(Plate 4, fig. 1)
1991 *Pantanellium*? *virgeum* n. sp.– Sashida, p.691-692, figs. 7.9-7.14.
1995 *Pantanellium*? *virgeum* Sashida – Kamata, figs. 6.6-6.7.
2010 *Pantanellium*? *virgeum* Sashida – Kuwahara, Sano, Ezaki and Yao, fig. 11.12.
Remarks: The illustrated specimen is characterized by a spherical shell and bipolar rod-like spines. The cortical shell, moderately-preserved, consists of large hexagonal pore frames that have rather high nodes at bars between pore frame vertices. The polar spines, longer and shorter ones, are circular in the axial section, but the proximal portion of the shorter spine is three-bladed. These diagnostic characters of this specimen are identical with those of *Pantanellium*? *virgeum* Sashida.
Range: Upper Olenekian – Middle Anisian (Sashida,1991; Sugiyama, 1997).

***Pantanellium* spp.**
(Plate 8, figs. 1-2, 17-19)
Remarks: Poorly- to moderately-preserved specimens were obtained. They consist of a spherical or ellipsoidal cortical shell with bipolar spines. Massive polygonal pore frames of the shell have small nodes at the vertices in the moderately-preserved specimens.

Genus ***Zartus*** Pessagno and Blome 1980
Type species *Zartus jonesi* Pessagno and Blome 1980

Zartus sp.
(Plate 8, fig. 9)
Remarks: A poorly-preserved specimen was obtained. It is similar to genus *Zartus* in having a spherical cortical shell with triradiate bipolar spines, and having secondary spines extended from raised median band.

Genus ***Trillus*** Pessagno and Blome 1980
Type species *Trillus seidersi* Pessagno and Blome 1980

Trillus elkhornensis Pessagno and Blome 1980
(Plate 3, fig. 26)
1980 *Trillus elkhornensis* n. sp. – Pessagno and Blome, p.249, pl.6, figs. 11-12, 16, 20, 25; pl.9, fig. 11.
1987 *Trillus elkhornensis* Pessagno and Blome – Yeh, p.37, pl.5, fig. 5.
1989 *Trillus elkhornensis* Pessagno and Blome – Hori and Otsuka, pl.4, fig. 15.
1990 *Trillus elkhornensis* Pessagno and Blome – Hori, fig. 8.30.
1992 *Trillus elkhornensis* Pessagno and Blome – Sashida, pl.2, figs. 21-22.
1996 *Trillus elkhornensis* Pessagno and Blome – Yeh and Cheng, p.98, pl.8, fig. 2.
1997 *Trillus elkhornensis* Pessagno and Blome – Yao, pl.3, fig. 147.
2004 *Trillus elkhornensis* Pessagno and Blome – Matsuoka, fig. 16.
Remarks: The examined specimen is moderately preserved, but is identical with *Trillus elkhornensis* Pessagno and Blome in having polygonal pore frames on the subspherical cortical shell and having triradiate bipolar spines.
Range: Lower Pliensbachian – Middle Bajocian (Pessagno and Blome, 1980; Carter *et al.*, 2010).

Family **Xiphostylidae** Haeckel 1881, *sensu* Pessagno and Yang *in* Pessagno, Six and Yang 1989, *emend*. De Wever, Dumitrica, Caulet, Nigrini and Caridroit 2001

Genus ***Archaeocenosphaera*** Pessagno and Yang *in* Pessagno, Six and Yang 1989
Type species *Archaeocenosphaera ruesti* Pessagno and Yang *in* Pessagno, Six and Yang 1989

***Archaeocenosphaera*? spp.**
(Plate 2, fig. 1; Plate 3, figs. 1-2, 5-6)
Remarks: The illustrated specimens are similar to genus *Archaeocenosphaera* in having a spherical shell and lacking spines. The outer lattice layer may be comprised of symmetrical polygonal pore frames, but it is not clear that two latticed layers are fused.

Family **Emiluviidae** Dumitrica 1995

Genus ***Udalia*** Whalen and Carter 1998
Type species *Udalia dennisoni* Whalen and Carter 1998

***Udalia* spp.**
(Plate 4, figs. 13-14)
Remarks: Overall form of the examined specimens is similar to those of genus *Udalia* in having a square spongy shell with four prominent spines, one of which is broken,

at each corner.

Family **Archaeospongoprunidae** Pessagno 1973

Genus ***Protopsium*** Pessagno and Poisson 1981
Type species *Protopsium ehrenbergi* Pessagno and Poisson 1981

***Protopsium* spp.**
(Plate 6, figs. 15-16)
Remarks: Overall form of the examined specimens is similar to those of genus *Protopsium* in having a subellipsoidal spongy shell and two rod-like polar spines.

Family **Spongotortilispinidae** Kozur and Mostler in Moix, Kozur, Stampfli and Mostler 2007

Genus ***Spongoxystris*** Sugiyama 1997
Type species *Spongoxystris hadra* Sugiyama 1997

***Spongoxystris*? sp.**
(Plate 6, fig. 2)
Remarks: The obtained specimen is similar to genus *Spongoxystris* in having two stout spines that are aligned in the major axis of the shell. However, it differs from the latter by the fact that a shorter spine dome-shaped.

Family **Oertlispongidae** Kozur and Mostler in Dumitrică, Kozur and Mostler 1980

Genus ***Oertlispongus*** Dumitrică, Kozur and Mostler 1980
Type species *Oertlispongus inaequispinosus* Dumitrică, Kozur and Mostler 1980

***Oertlispongus* sp.**
(Plate 6, fig. 21)
Remarks: The examined specimen is similar to genus *Oertlispongus* in general form and in having a subspherical shell with two long spines.

Family **Saturnalidae** Deflandre 1953, emend. Kozur and Mostler 1972

Genus ***Palaeosaturnalis*** Donofrio and Mostler 1978
Type species *Spongosaturnalis triassicus* Kozur and Mostler 1972

***Palaeosaturnalis* spp.**
(Plate 1, fig. 4; Plate 7, fig. 25)
Remarks: Two broken specimens were obtained. Their forms are characterized by a narrow and simple ring with radial spines of outside. Some of polar and radial spines lack due to poor preservation. However, they resemble genus *Palaeosaturnalis* in general form.

Genus ***Praemesosaturnalis*** Kozur and Mostler 1981
Type species *Spongosaturnalis bifidus* Kozur and Mostler 1972

***Praemesosaturnalis* spp.**
(Plate 7, figs. 23-24)
Remarks: These specimens are broken and composed of a wide ring and radial spines, which are short and massive, and therefore they belong to genus *Praemesosaturnalis*.

Order **ENTACTINARIA** Kozur and Mostler 1982

Family **Eptingiidae** Dumitrică 1978

Genus ***Spongostephanidium*** Dumitrică 1978
Type species *Spongostephanidium spongiosum* Dumitrică 1978

***Spongostephanidium* spp.**
(Plate 5, fig. 7, Plate 6, figs. 22-24)
Remarks: Moderately- to poorly-preserved specimens were examined. They resemble genus *Spongostephanidium* in general form, although one of the three rod-like horns is broken.

Genus ***Cryptostephanidium*** Dumitrică 1978
Type species *Cryptostephanidium cornigerum* Dumitrică 1978

***Cryptostephanidium*? spp.**
(Plate 1, fig. 5; Plate 2, figs. 24; Plate 5, figs. 8, 28)
Remarks: Moderately-preserved specimens were examined. They consist of a small subspherical shell and three spines. Thus, they are probably similar to genus *Cryptostephanidium* in general form.

Genus ***Eptingium*** Dumitrică 1978
Type species *Eptingium manfredi* Dumitrică 1978

Eptingium nakasekoi Kozur and Mostler 1994
(Plate 1, fig. 11; Plate 7, figs. 15-16)
1979 *Tripocyclia* sp. cf. *T. acythus* De Wever – Nakaseko and Nishimura, p.72-73, pl.4, fig. 2.
1994 *Eptingium nakasekoi* n. sp. – Kozur and Mostler, p.43, pl.1, fig. 5.
Remarks: Several moderately preserved specimens were examined. They consist of a cortical shell with three main spines. The shell is rounded subtriangular in lateral view, and its surface structure is characterized by large and irregular pore frames. The spines are stout and three-bladed in axial section. These features are quite similar to those of *Eptingium nakasekoi* Kozur and Mostler, although length of the spines are slightly shorter.
Range: Lower – Upper Anisian (Sugiyama, 1997).

***Eptingium* spp.**
(Plate 2, fig. 25; Plate 5, fig.20; Plate 7, fig. 17)
Remarks: Several poorly-preserved specimens were obtained. They are characterized by a rounded subtriangular cortical shell and three main spines that are three-bladed in axial section.

***Eptingium*? spp.**
(Plate 2, fig. 18; Plate 3, fig. 9; Plate 6, fig. 25)
Remarks: The illustrated specimens are broken due to poor preservation, but they are similar to *Eptingium* in having a rounded subtriangular shell and spines.

Family **Kungalariidae** Dumitrica and Carter 1999

Genus ***Pentabelus*** Sugiyama 1992
Type species *Pentabelus furutanii* Sugiyama 1992
Remarks: Sugiyama (1992) mentioned that the family assignment of genus *Pentabelus* is uncertain, and O'Dogherty *et al.* (2009) suggested that this genus belongs in Kungalariidae. In this report, *Pentabelus* is tentatively settled in Kungalariidae.

Pentabelus* sp. cf. *P. furutanii Sugiyama 1992
(Plate 6, fig. 17)
Remarks: Shell, primitive and spherical, is composed of coarse lattice work, with apical, primary lateral and secondary lateral spines. Thus, it is similar to *Pentabelus furutanii* Sugiyama.

Family **Hindeosphaeridae** Kozur and Mostler 1981

Genus ***Pseudostylosphaera*** Kozur and Mostler 1981
Type species *Pseudostylosphaera gracilis* Kozur and Mock in Kozur and Mostler 1981

Pseudostylosphaera compacta (Nakaseko and Nishimura) 1979
(Plate 2, fig. 22; Plate 3, fig. 8; Plate 5, fig. 1)
1979 *Archaeospongoprunum compactum* n. sp. – Nakaseko and Nishimura, p.68, pl.1, figs. 3, 7.
1981 *Pseudostylosphaera compacta* (Nakaseko and Nishimura) – Kozur and Mostler, p.30-31.
1990 *Pseudostylosphaera compacta* (Nakaseko and Nishimura) – Yeh, p.15, pl.4, figs. 3-4, 20.
1996 *Pseudostylosphaera compacta* (Nakaseko and Nishimura) – Nishizono, pl.3, fig. 6.
1996 *Pseudostylosphaera compacta* (Nakaseko and Nishimura) – Kozur, Krainer and Mostler, p.212, pl.6, fig. 17.
2001 *Pseudostylosphaera compacta* (Nakaseko and Nishimura) – Feng, Zhang and Ye, p.188-189, pl.5, figs. 7-12.
2011 *Pseudostylosphaera compacta* (Nakaseko and Nishimura) – Thassanapak, Feng, Grant-Mackie, Chonglakmani and Thanee, p.194, figs. 6O, 6Q.
Remarks: The illustrated specimens are not well preserved, but differ from *Pseudostylosphaera japonica* (Nakaseko and Nishinura) by having longer and slender polar spines. Then, they are identified with *Pseudostylosphaera compacta* (Nakaseko and Nishimura).
Range: Middle Anisian – Ladinian (Tumanda, 1991; Sugiyama,1992).

Pseudostylosphaera helicata (Nakaseko and Nishimura) 1979
(Plate 3. fig. 7)
1979 *Archaeospongoprunum helicatum* n. sp. – Nakaseko and Nishimura, p.68, pl.2, figs. 1-2; pl.12, fig. 3.
1981 *Pseudostylosphaera helicata* (Nakaseko and Nishimura) – Kozur and Mostler, p.30-31.
1992 *Pseudostylosphaera helicata* (Nakaseko and Nishimura) – Otsuka, Kajima and Hori, p.32, pl.3, figs. 3-4.
1992 *Pseudostylosphaera helicata* (Nakaseko and Nishimura) – Yeh, p.61, pl.7, fig. 1.
1993 *Pseudostylosphaera helicata* (Nakaseko and Nishimura) – Sashida, Nishimura, Igo, Kazama and Kamata, p.90, fig. 7.11.
1996 *Pseudostylosphaera helicata* (Nakaseko and Nishimura) – Nishizono, p.90, pl.3, fig. 7.
Remarks: The illustrated specimen possesses a subspherical shell and two opposite polar spines. The spines are slightly shorter than those of the type species, but are twisted in their distal part.
Range: Ladinian – Carnian or earliest Norian (Nishizono, 1996).

Pseudostylosphaera japonica (Nakaseko and Nishinura) 1979
(Plate 1, figs. 8-9; Plate 6, fig. 1; Plate 7, figs. 8-12)
1979 *Archaeospongoprunum japonicum* n. sp. – Nakaseko and Nishimura, p.67-68, pl.1, figs. 2, 4, 9.
1981 *Pseudostylosphaera japonica* (Nakaseko and Nishimura) – Kozur and Mostler, p.30-31.
1990 *Pseudostylosphaera japonica* (Nakaseko and Nishimura) – Yeh, p.15, pl.4, figs. 5-7.
1993 *Pseudostylosphaera japonica* (Nakaseko and Nishimura) – Sashida, Nishimura, Igo, Kazama and Kamata, p.89-90, figs. 7.9, 7.15
1996 *Pseudostylosphaera compacta* (Nakaseko and Nishimura) – Nishizono, pl.3, fig. 9.
1996 *Pseudostylosphaera japonica* (Nakaseko and Nishimura) – Kozur, Krainer and Mostler, p.212, pl.6, fig. 15.
1997 *Pseudostylosphaera japonica* (Nakaseko and Nishimura) – Sugiyama, p.186, fig. 48.15.
2001 *Pseudostylosphaera japonica* (Nakaseko and Nishimura) – Feng, Zhang and Ye, p.188, pl.5, figs. 1-6.
2011 *Pseudostylosphaera japonica* (Nakaseko and Nishimura) – Thassanapak, Feng, Grant-Mackie, Chonglakmani and Thanee, p.195, figs. 6P, 6S.
Remarks: The illustrated specimens are characterized by a globular shell with two polar spines. The spines are moderately long, massive and three-bladed in axial section. Their width slightly increase toward a distal direction and decrease near the terminus. Surface of the shell is rough and its spongy meshwork is indistinct due to poor preservation.
Range: Middle Anisian – Lower Carnian (Sugiyama,1997).

Pseudostylosphaera* sp. aff. *P. tenuis (Nakaseko and Nishimura) 1979
(Plate 3, fig. 19)
Remarks: The examined specimen is similar to *Pseudostylosphaera tenuis* (Nakaseko and Nishimura) in having a spherical shell and two polar spines that are unequal in length. However, length of the longer spine of the examined specimen is shorter than that of the type species (Nakaseko and Nishimura, 1979).

***Pseudostylosphaera* spp.**
(Plate 2, figs. 11-17; Plate 5, figs. 2-3, 23-24; Plate 6, fig. 14)
Remarks: The examined specimens seem to belong to genus *Pseudostylosphaera* on the basis of a subspherical shell with spongy meshwork and two polar spines although some of the specimens lack polar spines.

***Pseudostylosphaera*? spp.**
(Plate 1, figs. 10, 19; Plate 2, figs. 3-4; Plate 4, figs. 7, 12; Plate 5, figs. 17-18, 25-27)
Remarks: One of two polar spines of the examined specimens is lack or broken due to poor preservation. Therefore, it is questionable that they belong to genus *Pseudostylosphaera*.

Genus ***Parasepsagon*** Dumitrică, Kozur and Mostler 1980
Type species *Parasepsagon tetracanthus* Dumitrică, Kozur and Mostler 1980

***Parasepsagon* sp.**
(Plate 2, fig. 26)
Remarks: The examined specimen is not well preserved. It has a subspherical shell and four spines, one of which is broken. Outer shell consists of triangular meshes with small nodes at vertices. The spines are three-bladed and slightly twisted in distal part. This appearance is identical with genus *Parasepsagon*.

Genus ***Hindeosphaera*** Kozur and Mostler 1979
Type species *Hindeosphaera foremanae* Kozur and Mostler 1979

Hindeosphaera spinulosa (Nakaseko and Nishimura) 1979
(Plate 5, figs. 4-6)
1979 *Archaeospongoprunum spinulosum* n. sp. – Nakaseko and Nishimura, p.69, pl.2, figs. 3-4, 6.
1989 *Pseudostylosphaera* sp. cf. *P. spinulosa* (Nakaseko and Nishimura) – Cheng, p.143, pl.6, fig. 2; pl.7, figs. 8-9.
1989 *Hindeosphaera spinulosa* (Nakaseko and Nishimura) – Martini, De Wever, Zaninetti, Denelian and Kito, p.150, pl.3, fig. 8.
1990 *Pseudostylosphaera spinulosa* (Nakaseko and Nishimura) – Yeh, p.15, pl.4, fig. 14.
1993 *Pseudostylosphaera spinulosa* (Nakaseko and Nishimura) – Sashida, Nishimura, Igo, Kazama and Kamata, p.92, figs. 7.16-7.17.
1995 *Hindeosphaera*? *spinulosa* (Nakaseko and Nishimura) – Ramovš and Goričan, p.185, pl.3, figs. 6-8.
1996 *Pseudostylosphaera spinulosa* (Nakaseko and Nishimura) – Nishizono, pl.3, figs. 10-12.
1996 *Hindeosphaera spinulosa* (Nakaseko and Nishimura) – Kozur, Krainer and Mostler, p.210, pl.4, figs. 4, 8.
2001 *Hindeosphaera spinulosa* (Nakaseko and Nishimura) – Feng, Zhang and Ye, p.190, pl.5, figs. 15, 21.
2011 *Hindeosphaera spinulosa* (Nakaseko and Nishimura) – Thassanapak, Feng, Grant-Mackie, Chonglakmani and Thanee, p.194, fig. 6K.
Remarks: The illustrated specimens possess an ellipsoidal shell and two polar spines. One spine is broad and three-bladed, and is considerably larger than the opposite spine.
Range: Lower – Upper Anisian (Sugiyama, 1997).

***Hindeosphaera* sp.**
(Plate 7, fig. 14)
Remarks: This specimen consists of a spherical shell with spongy meshwork and spikes. One massive and stout spike, which is not spirally rotated as in other species of genus *Hindeosphaera*, is quite longer than the others.

Family **Muelleritortiidae** Kozur 1988

Genus ***Muelleritortis*** Kozur 1988
Type species *Emiluvia*? *cochleata* Nakaseko and Nishimura 1979

Muelleritortis cochleata (Nakaseko and Nishimura) 1979
(Plate 6, figs. 3-10)
1979 *Emiluvia*? *cochleata* n. sp. – Nakaseko and Nishimura, p.70, pl.3, figs. 2-4, 6.
1979 *Staurocontium minoense* n. sp. – Nakaseko and Nishimura, p.71, pl.2, figs. 7, 9-10; pl.12, fig. 4.
1988 *Muelleritortis cochleata cochleata* (Nakaseko and Nishimura) – Kozur, p.53, pl.l, figs. 1-8; pl.2, figs. 1-2; pl.3, fig. 1.
1993 *Emiluvia*? *cochleata* Nakaseko and Nishimura – Sashida, Nishimura, Igo, Kazama and Kamata, p.93, figs. 8.5-8.6, 8.8, 8.15-8.16.
1996 *Plafkerium cochleatum* (Nakaseko and Nishimura) – Nishizono, pl.3, figs. 20-21.
Remarks: The examined specimens are grouped into two types; one has four main spines, and the other has two spines. Based on Kozur and Mostler (1996), the latter type is included into genus *Ditortis*, but it is not clear whether two of four spines were lacked or not. These examined specimens consist of a spherical to subellipsoidal shell and four or two main spines. The outer shell structures are indistinct due to poor preservation, but polygonal pore frames are observed in the case of moderately-preserved specimen. One of the main spines straightly extends, whereas the remaining three or one spines are strongly

twisted. These characters are identical with those of *Muelleritortis cochleata* (Nakaseko and Nishimura).
Range: Upper Ladinian – lowest Carnian (Sugiyama, 1997).

ENTACTINARIA *Incertae sedis*

Genus ***Monostylosphaera*** Xu 1992
Type species *Monostylosphaera sinensis* Xu 1992

***Monostylosphaera*? spp.**
(Plate 4, figs. 11; Plate 7, fig. 13)
Remarks: The illustrated specimens are similar to genus *Monostylosphaera* in having a spherical shell with one polar spine, but it is unclear that the spine is three-bladed in the axial section, due to poor preservation.

Order **NASSELLARIA** Ehrenberg 1875

Family **Ultranaporidae** Pessagno 1977b

Genus ***Tirodella*** Kozur and Mostler 1981
Type species *Tirodella goestlingensis* Kozur and Mostler 1981

***Tirodella*? sp.**
(Plate 2, fig. 7)
Remarks: This poorly-preserved specimen lacks its apical horn, but resembles genus *Tirodella* in having thin thoracic feet that connect to strong ribs on the wall of the very large thorax. However, other diagnostic features of this specimen are unclear, due to poor preservation.

Genus ***Bipedis*** De Wever 1982
Type species *Bipedis calvabovis* De Wever 1982

***Bipedis* sp.**
(Plate 5, fig. 21)
Remarks: The examined specimen is similar to genus *Bipedis* in having a two-segmented small test with strong apical horn and two feet, one of which is lost.

Genus ***Napora*** Pessagno 1977a, *emend*. Pessagno, Whalen and Yeh 1986
Type species *Napora bukryi* Pessagno 1977a

Napora mitrata Pessagno, Whalen and Yeh 1986
(Plate 4, fig. 16)
1986 *Napora mitrata* n. sp. – Pessagno, Whalen and Yeh, p.42-43, pl.5, figs. 8, 15; pl.11, figs. 11-12.
1987 *Napora mitrata* Pessagno, Whalen and Yeh – Yeh, pl.13, figs. 6, 11.
Remarks: The figured specimen consists of a two-segmented test, cephalis and thorax, with an apical horn and three feet, two of which are lost. Cephalis is small and imperforate. The apical horn is bladed in axial section with three ridges alternating with three grooves. It terminates with moderately long subsidiary spines. Thorax is hemispherical in outline and is composed of pentagonal and hexagonal pore frames. The remaining foot occurs at the base of thorax and is triradiate in axial section with alternating three ridges and grooves.
Range: Lower Toarcian (Pessagno, Whalen and Yeh 1986)

***Napora* sp.**
(Plate 4, fig. 17)
Remarks: A strongly broken specimen was obtained and is composed of cephalis and thorax with a three-bladed apical horn. It seems to belong to genus *Napora* on the basis of the above morphologic features.

Family **Deflandrecyrtiidae** Kozur and Mostler 1979

Genus ***Haeckelicyrtium*** Kozur and Mostler 1979, *emend*. Carter 1993
Type species *Haeckelicyrtium austriacum* Kozur and Mostler 1979

***Haeckelicyrtium*? spp.**
(Plate 1, figs. 1-3)
Remarks: Genus *Haeckelicyrtium* consists of hot-shaped shell with three segments and skirt (Kozur and Mostler, 1979). Preservation of the detected specimens is extremely poor; they are a fragment of the skirt which has subcircular or subhexagonal pores. Therefore, it is doubtful that these specimens belong to genus *Haeckelicyrtium*.

Family **Acropyramididae** Haeckel 1881

Genus ***Celluronta*** Sugiyama 1997
Type species *Celluronta donax* Sugiyama 1997

***Celluronta* sp.**
(Plate 2, fig. 8)
Remarks: The illustrated specimen possesses a long test probably consisting of more than seven segments. Pores on the lower part of the test are large in size and subcircular in shape. These characters are identical with those of genus *Celluronta*.

Family **Ruesticyrtiidae** Kozur and Mostler 1979

Genus ***Paratriassocampe*** Kozur and Mostler 1994
Type species *Paratriassocampe gaetanii* Kozur and Mostler 1994

***Paratriassocampe* sp.**
(Plate 5, fig. 15)
Remarks: Genus *Paratriassocampe* is similar to genus *Triassocampe* in general shape of their test, but the former differs from the latter by having two rings of pores on the well-developed circumferential ridges. The illustrated specimen is characterized by the above two rings of pores.

Genus ***Triassocampe*** Dumitrică, Kozur and Mostler 1980
Type species *Triassocampe scalaris* Dumitrică, Kozur and

Mostler 1980

Triassocampe deweveri (Nakaseko and Nishimura) 1979
(Plate 1, figs. 14, 22; Plate 3, fig. 12; Plate 5, figs. 9-12)
1979 *Dictyomitrella deweveri* n. sp. – Nakaseko and Nishimura, p.77, pl.10, figs. 8-9.
1982 *Triassocampe deweveri* (Nakaseko and Nishimura) – Yao, pl.1, figs. 1-3.
1989 *Triassocampe deweveri* (Nakaseko and Nishimura) – Cheng, p.148, pl.6, figs. 13-14; pl.7, figs. 10-11.
1990 *Triassocampe deweveri* (Nakaseko and Nishimura) – Yeh, p.28-29, pl.7, figs. 7, 18, 20; pl.11, figs. 2-3, 7-8, 13-14.
1993 *Triassocampe deweveri* (Nakaseko and Nishimura) – Sashida, Nishimura, Igo, Kazama and Kamata, p.86, figs. 5.3-5.7.
2001 *Triassocampe deweveri* (Nakaseko and Nishimura) – Feng, Zhang and Ye, p.182, pl.3, figs. 1-6.
2011 *Triassocampe deweveri* (Nakaseko and Nishimura) – Thassanapak, Feng, Grant-Mackie, Chonglakmani and Thanee, p.198, figs. 8I, 8J, 8L.
Remarks: The examined specimens are characterized by dome-shaped cephalis without an apical horn and by well-developed circumferential ridges. One row of small knobs and two or three rows of circular pores are arranged respectively on and below each circumferential ridge. These specimens are identical with the type specimen reported by Nakaseko and Nishimura (1979).
Range: Upper Anisian – middle Upper Ladinian (Sugiyama, 1997).

Triassocampe* sp. cf. *T. myterocorys Sugiyama 1992
(Plate 1, fig. 20; Plate 6, fig. 11)
Remarks: The main character of the examined specimens is two rows of large pores that are aligned below a strong circumferential ridge on each post-abdominal segment. However, it differs from *Triassocampe myterocorys* Sugiyama by having a conical test.

Triassocampe* sp. aff. *T. diordinis Bragin 1991 sensu Sugiyama 1992
(Plate 5, fig. 37)
1992 *Triassocampe* sp. aff. *T. diordinis* Bragin 1991 – Sugiyama, p.1199, figs. 11.7-11.8.
Remarks: The examined specimen is quite poorly-preserved. But it is similar to *Triassocampe* sp. aff. *T. diordinis* Bragin described by Sugiyama (1992) in having a single row of pores, which are indistinct, just beneath the poorly developed circumferential ridges.
Range: Middle Anisian (Sugiyama, 1992).

***Triassocampe* spp.**
(Plate 1, figs. 15-18, 23; Plate 2, figs. 28-30; Plate 3, figs. 3, 13-16; Plate 5, figs. 13-14, 16, 31-36; Plate 6, figs. 12-13; Plate 7, figs. 18-20)
Remarks: Preservation of most specimens obtained is so poor that diagnostic features characterizing genus *Triassocampe* are not identified. However, they consist of a long and slightly conical to subcyrindrical multisegmented shell without an apical horn. This appearance is similar to that of *Triassocampe*.

Family **Eucyrtidiellidae** Takemura 1986

Genus ***Eucyrtidiellum*** Baumgartner 1984
Type species *Eucyrtidium*? *unumaensis* Yao 1979

Eucyrtidiellum nagaiae Dumitrica, Goričan and Matsuoka in Goričan, Carter, Dumitrică, Whalen, Hori, De Wever, O'Dogherty, Matsuoka and Guex 2006
(Plate 4, figs. 18-19)
1986 *Eucyrtidiellum* sp. C group – Nagai, p.12, pl.2, figs. 11-12.
1987 *Eucyrtidiellum* sp. C_2 – Hattori, pl.12, fig. 12.
1990 *Eucyrtidiellum* sp. C_2 – Nagai, pl.4, figs. 1a-1c.
1995 *Eucyrtidiellum* sp. C_2 – Nagai, p.12, pl.4, figs. 7-8.
2004 *Eucyrtidiellum* – Matsuoka, fig. 2-8.179.
2006 *Eucyrtidiellum nagaiae* Dumitrica, Goričan and Matsuoka n. sp. – Goričan, Carter, Dumitrică, Whalen, Hori, De Wever, O'Dogherty, Matsuoka and Guex, p.158, pl.EUC06.
Remarks: The figured specimens are composed of three segments and characterized by a stout apical horn and strong longitudinal costae on their abdominal surfaces. Cephalis is imperforate and is incorporated into the apical horn. Thorax is perforated with polygonal pore frames. Abdomen is inflated and porous, and is ornamented with the continuous vertical costae.
Range: Upper Pliensbachian – Upper Toarcian (Carter *et al.*, 2010).

Family **Bagotidae** Pessagno and Whalen 1982

Genus ***Droltus*** Pessagno and Whalen 1982
Type species *Droltus lyellensis* Pessagno and Whalen 1982

Droltus* sp. cf. *D. hecatensis Pessagno and Whalen 1982
(Plate 1, fig. 30)
Remarks: The examined specimen is poorly-preserved, but is similar to *Droltus hecatensis* Pessagno and Whalen in having a conical test and in the state of pore frames. Pore frames of the upper portion of the test including abdomen and first several post-abdominal segments are irregular in size and shape; tetragonal pore frames of the lower portion are more uniform in size and aligned in longitudinal rows.

Family **Hsuidae** Pessagno and Whalen 1982

Genus ***Parahsuum*** Yao 1982
Type species *Parahsuum simplum* Yao 1982

Parahsuum simplum Yao 1982
(Plate 4, figs. 24-26)
1982 *Parahsuum simplum* n. sp. – Yao, p.61, pl.4, figs.

1-8.
1990 *Parahsuum simplum* Yao – Kozur and Mostler, p.222, pl.17, fig. 2.
1991 *Parahsuum simplum* Yao – Tumanda, pl.7, fig. 20; pl.8, fig. 5.
1994 *Parahsuum simplum* Yao – Goričan, p.79, pl.17, figs. 9-10, 12.
1998 *Parahsuum simplum* Yao – Whalen and Carter, p.67, pl.16, fig. 6.
1998 *Parahsuum simplum* Yao – Yeh and Cheng, p.26, pl.4, fig. 14.
2002 *Parahsuum simplum* Yao – Whalen and Carter, p.126, pl.12, figs. 3-4, 12-13; pl.17, figs. 14-15.
2002 *Parahsuum simplum* Yao – Tekin, p.189, pl.4, fig. 3.
2004 *Parahsuum simplum* Yao – Ishida, Shimakawa, Kozai, and Yao, pl.5, figs. 1-2.

Remarks: Considerable variation in overall form and size has been recognized in *Parahsuum simplum* Yao (Hori and Yao, 1988). The illustrated specimens, lacking an apical horn, are short in length rather than the type species, but resemble *Parahsuum simplum* Yao in having an elongate conical shell with six or more segments, and also having continuous costae.
Range: Hettangian – Lower Aalenian (Hori, 1990; Carter *et al.*, 2010).

Parahsuum ovale Hori and Yao 1988
(Plate 4, figs. 27-28)
1982 *Parahsuum* sp. C – Yao, pl.4, figs. 9-11.
1988 *Parahsuum ovale* n. sp. – Hori and Yao, p.51, pl.1, figs. 3a-3e.
1988 *Parahsuum takarazawaense* n. sp. – Sashida, p.19, pl.1, figs. 6-13, 18-19.
1990 *Parahsuum ovale* Hori and Yao – Hori, fig. 8.16.
1994 *Parahsuum ovale* Hori and Yao – Goričan, p.79, pl.17, fig. 13.
2010 *Parahsuum ovale* Hori and Yao – Uchino and Hori, figs. 5.3-5.4.

Remarks: The examined specimens are characterized by an oval-shaped shell. Cephalis is slightly flattened conical in shape without an apical horn. Based on these characters, they are identical with *Parahsuum ovale* Hori and Yao.
Range: Sinemurian – Upper Toarcian (Hori 1990).

Parahsuum izeense (Pessagno and Whalen) 1982
(Plate 4, fig. 30)
1982 *Canutus izeensis* n.sp. – Pessagno and Whalen, p.129, pl.6, figs. 8, 10, 15.
1982 *Canutus giganteus* n.sp. – Pessagno and Whalen, p.127, pl.4, figs. 5, 13.
1995a *Parahsuum izeense* (Pessagno and Whalen) – Baumgartner *et al.*, p.378, pl.2012, figs. 1-2.
2003 *Parahsuum izeense* (Pessagno and Whalen) – Goričan, Šmuc and Baumgartner, p.296, pl.5, figs. 18-19.

Remarks: Shell of each specimen obtained is short and inflated conical in shape. The last two segments slightly decrease in width. Based on these characters, it is identical with *Parahsuum izeense* (Pessagno and Whalen).
Range: Lower Pliensbachian – Bajocian (Carter *et al.*, 2010).

Parahsuum longiconicum Sashida 1988
(Plate 4, fig. 31-33)
1988 *Parahsuum longiconicum* n. sp. – Sashida, p.20, pl.2, figs. 1-4, 16-17.
1996 *Parahsuum longiconicum* Sashida – Tumanda, Sashida and Igo, p.178, fig. 4.2.
2003 *Parahsuum longiconicum* Sashida – Goričan, Šmuc, and Baumgartner, p.296, pl.V, fig. 16.
2004 *Parahsuum longiconicum* Sashida – Ishida, Shimakawa, Kozai and Yao, figs. 5.3-5.4.

Remarks: The illustrated specimens are characterized by a conical test that consists of eight to ten segments, and by a massive conical horn on the cephalis with wide and deep grooves at the base of the horn. Longitudinal continuous edged costae and weak circumferential ridges are visible on the outer layer of these specimens. Based on the above, they are identical with *Parahsuum longiconicum* Sashida.
Range: Lower Pliensbachian – Lower Aalenian (Carter *et al.*, 2010).

Parahsuum* sp. cf. *P. longiconicum Sashida 1988
(Plate 8, fig. 3)
Remarks: The examined specimen is similar to *Parahsuum longiconicum* Sashida in general shell shape. However, the apical horn is broken and the grooves at the base of the horn are not visible.

***Parahsuum* spp.**
(Plate 3, fig. 29-31; Plate 4, figs. 29, 34; Plate 7, figs. 2-4; Plate 8, figs. 20-27)
Remarks: As originally described by Yao (1982), conical to spindle-shaped multisegmented Nassellaria lacking well-developed strictures and having continuous edged costae is included into species of genus *Parahsuum*. A wide range in variation of the examined specimens is recognized.

***Parahsuum*? sp. A**
(Plate 8, fig. 28)
1997 *Parahsuum* sp. A – Yao, pl.14, fig. 658.
2004 *Archaeodictyomitra*? sp. – Hori, pl.1, fig. 55.

Description: Test is elongate and conical with probably six post-abdominal segments, lacking well-developed strictures. Pore frames of post-abdominal segments are square in shape with circular pores. Cephalis, without a horn, is dome-shaped and remaining segments are trapezoidal in outline, increasing moderately in width and more rapidly in length as added. Thin circumferential ridges present at joints between post-abdominal segments. Pore frames on post-abdominal segments are aligned in a transverse and vertical directions; three or four rows of pore frames are transversally arranged between the ridges, and single row of pore frames is longitudinally arranged

between the costae. Costae are not continuous, due to development of the ridges.
Remarks: *Parahsuum*? sp. A is questionably assigned to genus *Parahsuum*, because it is different from the latter by having thin circumferential ridges although it has single row of pore frames that is arranged between costae. This species resembles *Parahsuum* sp. A of Yao (1997) and *Archaeodictyomitra*? sp. of Hori (2004) in having the same diagnostic features.

Genus ***Hsuum*** Pessagno 1977a, *emend*. Takemura 1986
Type species *Hsuum cuestaense* Pessagno 1977a

Hsuum* sp. cf. *H. mulleri Pessagno and Whalen 1982
(Plate 3, fig. 32)
Remarks: The illustrated specimen has an elongate conical test with discontinuous costae. The costae which indicate few branches laterally and are developed over the abdomen and post-abdominal segments. This appearance is similar to that of *Hsuum mulleri* Pessagno and Whalen, but an apical horn is not developed in this specimen.

***Hsuum* sp.** sensu Matsuoka 2004
(Plate 4, fig. 23)
2004 *Hsuum* sp. – Matsuoka, p.77, fig. 2-9.224.
Remarks: Test of the examined specimen is elongated conical in shape and much wider than other species of genus *Hsuum*. Relatively thin costae developed over the test are continuous, and are inserted between rows of pore frames.
Range: Toarcian (Matsuoka, 2004).

***Hsuum*? sp.**
(Plate 7, fig. 6)
Remarks: Test of the examined specimen is an inflated conical in shape with probably five segments. These segments are separated by strictures and rapidly increase in width. Cephalis is dome-shaped without an apical horn. The test is composed of polygonal pore frames with circular pores and with continuous costae. The costae extend throughout the test. Two rows of pores are arranged between two adjacent costae. This specimen is questionably assigned to genus *Hsuum*, due to strictures between segments.

Family **Canoptidae** Pessagno in Pessagno, Finch and Abbott 1979, *emend*. Yeh 1987

Genus ***Canoptum*** Pessagno in Pessagno, Finch and Abbott 1979
Type species *Canoptum poissoni* Pessagno in Pessagno, Finch and Abbott 1979

Canoptum* sp. cf. *C. anulatum Pessagno and Poisson 1981
(Plate 7, fig. 7)
Remarks: As originally described by Pessagno and Poisson (1981), *Canoptum anulatum* has a slender and more elongate test with closely spaced post-abdominal segments; post-abdominal segments are eleven to fifteen in number with short and discontinuous costae. These costae are visible on each circumferential ridge. The obtained specimen is poorly-preserved, but it is similar to *Canoptum anulatum* Pessagno and Poisson in slender and elongate outer form. Discontinuous costae are slightly recognized.

Canoptum* sp. cf. *C. rugosum Pessagno and Poisson 1981
(Plate 4, fig. 35)
Remarks: *Canoptum rugosum* Pessagno and Poisson is characterized by having a short and broad test that is ornamented by circumferential ridges between post-abdominal segments, and also having post-abdominal segments with a rugose surface. Nevertheless, the rugose surface is indistinct in the examined specimen, because of its poor preservation.

Genus ***Multimonilis*** Yeh 1989
Type species *Multimonilis pulcher* Yeh 1989

***Multimonilis* sp.**
(Plate 1, fig. 21)
Remarks: The examined specimen is similar to genus *Multimonilis* in overall form that consists of a conical and multicyrtid test. Especially, this specimen possesses narrow elevated circumferential ridges that modified by well-developed nodes. According to Yeh (1989), this is a characteristic feature of genus *Multimonilis*.

Family **Parvicingulidae** Pessagno 1977a, *emend*. Pessagno and Whalen 1982

Genus ***Praeparvicingula*** Pessagno, Blome and Hull in Pessagno, Blome, Hull and Six 1993
Type species *Parvicingula profunda* Pessagno and Whalen 1982

Praeparvicingula gigantocornis (Kishida and Hisada) 1985
(Plate 8, fig. 13)
1982 *Parvicingula* sp. A – Kishida and Sugano, pl.7, fig. 8.
1985 *Parvicingula gigantocornis* n. sp. – Kishida and Hisada, p.118, pl.4, figs. 1-5.
1988 *Parvicingula gigantocornis* Kishida and Hisada – Sashida, p.22, pl.2, figs. 5, 10-12, 20-21; pl.3, figs. 4-5.
2001 *Praeparvicingula gigantocornis* (Kishida and Hisada) – Kashiwagi, fig. 6.6.
2004 *Parvicingula gigantocornis* Kishida and Hisada – Ishida, Shimakawa, Kozai and Yao, pl.5, fig. 14.
Remarks: The illustrated specimen is characterized by a slightly slender conical test with a long massive apical horn. Moreover, Each circumferential ridge is widely spaced and separated by three rows of small pores; center row of pores is poorly developed. Based on these features,

it is identical with *Praeparvicingula gigantocornis* (Kishida and Hisada).
Range: Upper Toarcian – Bajocian (Carter *et al.*, 2010).

Praeparvicingula* sp. cf. *P. nanoconica (Hori and Otsuka) 1989
(Plate 8, fig. 12)
Remarks: The illustrated specimen is similar to *Praeparvicingula nanoconica* (Hori and Otsuka) in general shape and especially having a long apical horn. However, it is not clear that this specimen is identical with *Praeparvicingula nanoconica* (Hori and Otsuka), because of its poorly preservation.

***Praeparvicingula* spp.**
(Plate 8, figs. 4-7, 14-15)
Remarks: The illustrated specimens are moderately- to poorly-preserved. They are characterized by a conical- to subcylindrical-shaped test. Their final post-abdominal segments lack narrow terminal tube.

Genus ***Parvicingula*** Pessagno 1977a, *emend*. Pessagno, Blome, Hull and Six 1993
Type species *Parvicingula santabarbarensisa* Pessagno 1977a

***Parvicingula* sp.**
(Plate 8, fig. 16)
Remarks: The poorly-preserved specimen was obtained. It is characterized by a spindle-shaped test and final post-abdominal segment terminates in a narrow tube.

NASSELLARIA *Incertae sedis*

Genus ***Lantus*** Yeh 1987
Type species *Lantus sixi* Yeh 1987

Lantus obesus (Yeh) 1987
(Plate 4, fig. 21)
1987 *Pseudoristola obesa* n. sp. – Yeh, p.96-97, pl. 14, figs. 11-12.
1997 *Pseudoristola obesa* Yeh – Yao, pl. 15, fig. 724.
2001 *Stichocapsa obesa* (Yeh) – Gawlick, Suzuki and Missoni, fig. 5.6.
2006 *Lantus obesus* (Yeh) – Goričan, Carter, Dumitrică, Whalen, Hori, De Wever, O'Dogherty, Matsuoka and Guex, p.234, pl. LAN01, figs. 1-10.
2010 *Lantus obesus* (Yeh) – Uchino and Hori, figs. 5.16-5.17.
Remarks: Moderately preserved specimen was obtained. Its test is conical with a large bulbous expansion, and without circumferential ridges. It is not clear that cephalis is perforate, but thorax, abdomen and post-abdominal segments are perforate; post-abdominal segments consist of pentagonal or hexagonal pore frames.
Range: Uppermost Simenurian – Upper Toarcian (Carter *et al.*, 2010).

Lantus intermedius Carter in Goričan, Carter, Dumitrică, Whalen, Hori, De Wever, O'Dogherty, Matsuoka and Guex 2006
(Plate 4, fig. 22; Plate 8, fig. 29)
1988 *Hemicryptocephalis dengqensis* n. sp. – Li, p.327, p.330, pl. 1, figs. 5-6.
1997 *Parahsuum* sp. NB – Yao, pl. 13, fig. 642.
2006 *Lantus intermedius* n. sp. – Goričan, Carter, Dumitrică, Whalen, Hori, De Wever, O'Dogherty, Matsuoka and Guex, p.232, pl. LAN05, figs. 1-7.
Remarks: The obtained specimens are identical with *Lantus intermedius* Carter on the basis of general shape of their conical tests. Post-abdominal segments increase in width as added, and the final segment is closed with an ellipsoidal cap. These specimens possess weakly circumferential ridges, which are recognized between segments.
Range: Uppermost Simenurian – Lower Toarcian (Carter *et al.*, 2010).

***Lantus*? sp.**
(Plate 3, fig. 33)
Remarks: Because of extremely poor preservation, the examined specimen questionably belongs to genus *Lantus*.

Genus ***Dictyomitrella*** Haeckel 1887
Type species *Eucyrtidium articulatum* Ehrenberg 1873

Dictyomitrella*? sp. cf. *D.*? *kamoensis Mizutani and Kido 1983
(Plate 8, fig. 11)
Remarks: Poorly-preserved specimen was obtained. It consists of a test that is conical at the upper portion and subcylindrical at the lower portion. Post-abdominal segments are separated by nodose circumferential ridges; each one row of pores are faintly observed below and above the ridges, but tetragonally-arranged two rows of circular pits are indistinct on the abdomen and post-abdominal segments. This specimen is similar to *Dictyomitrella*? *kamoensis* Mizutani and Kido in possessing each one row of pores below and above the nodose circumferential ridges, but is different by the absence of two rows of circular pits.

Genus ***Minocapsa*** Matsuoka 1991
Type species *Minocapsa cylindrica* Matsuoka 1991

Minocapsa globosa Matsuoka 1991
(Plate 4, fig. 20)
1991 *Minocapsa globosa* n. sp. – Matsuoka, p.736, figs. 11.1a-11.4b.
1997 *Minocapsa globosa* Matsuoka – Yao, pl.10, fig. 451.
2004 *Minocapsa globosa* Matsuoka – Matsuoka, fig. 90.
Remarks: The obtained specimen has a pyriform test consisting of four segments; proximal part including cephalis, thorax and abdomen is conical, and distal part composed of fourth segment is large and subspherical

without aperture. Circular pores are set in pentagonal to hexagonal pore frames and arranged irregularly rather than longitudinally. This specimen is slightly slender; change in contour from the conical proximal part to subspherical distal part is not rapid than the type species of *Minocapsa globosa* Matsuoka.

Range: Upper Pliensbachian? – Lower Toarcian (Yao, 1997; Matsuoka, 2004).

Acknowledgements: This report is based on results of the study "Geology of the Kanmuri Yama district" which has been conducted by the Geological Survey of Japan, AIST. Thanks are extended to Dr. M. Saito (GSJ) for his comments on the radiolarian identification. Associate Prof. Y. Kamata (Univ. Tsukuba) is gratefully acknowledged for thorough review of the manuscript.

References

Baumgartner, P.O. (1984) A Middle Jurassic–Early Cretaceous low-latitude radiolarian zonation based on Unitary Associations and age of Tethyan radiolarites. *Eclogae Geologicae Helvetiae*, **77**, 729-837.

Baumgartner, P.O., O'Dogherty, L., Gorican, S., Dumitrica-Jud, R., Dumitrica, P., Pillevuit, A. Urquhart, E., Matsuoka, A., and Danelian, T. (1995a) Radiolarian catalogue and systematics of Middle Jurassic to Early Cretaceous Tethyan genera and species. *In* Baumgartner, P. O., O'Dogherty, L., Gorican, S., Urquhart, E., Pillevuit, A. and De Wever, P. eds., *Middle Jurassic to Early Cretaceous Radiolaria of Tethys: occurrence, systematics, biochronology. Mémoires de Géologie (Lausanne)*, no.23, Institut de Géologie et Paléontologie, Université de Lausanne, Switzerland, 37-688.

Baumgartner, P.O., Bartolini, A., Carter, E.S., Conti, M., Cortese, G., Danelian, T., De Wever, P., Dumitrica, P., Dumitrica-Jud, R., Gorican, S., Guex, J., Hull, D.M., Kito, N., Marcucci, M., Matsuoka, A., Murchey, B., O'Dogherty, L., Savary, J., Vishnevskaya, V., Widz, D. and Yao, A. (1995b) Middle Jurassic to Early Cretaceous radiolarian biochronology of Tethys based on Unitary Association. *In* Baumgartner, P. O., O'Dogherty, L., Gorican, S., Urquhart, E., Pillevuit, A. and De Wever, P. eds., *Middle Jurassic to Early Cretaceous Radiolaria of Tethys: occurrence, systematics, biochronology. Mémoires de Géologie (Lausanne)*, no.23, Institut de Géologie et Paléontologie, Université de Lausanne, Switzerland, 1013-1048.

Bragin, N.Yu. (1991) Ралиолярии и Нижнемезозойские Толщи Востока СССР. Доклады Академии Наук, *СССР*, **469**, 1-122.

Carter, E.S. (1993) Biochronology and paleontology of uppermost Triassic (Rhaetian) radiolarians, Queen Charlotte Islands, British Columbia, Canada. *Mémoires de Géologie (Lausanne)*, no.11, Institut de Géologie et Paléontologie, Université de Lausanne, Switzerland, 1-175.

Carter, E.S., Whalen, P.A. and Guex, J. (1998) Biochronology and paleontology of Lower Jurassic (Hettangian and Sinemurian) radiolarians, Queen Charlotte Islands, British Columbia. *Geol. Surv. Canada Bull*., no.496, 1-162.

Carter, E.S., Goričan, Š., Guex, J., O'Dogherty, L., De Wever, P., Dumitrica, P., Hori, R.S., Matsuoka, A and Whalen, P.A. (2010) Global radiolarian zonation for the Pliensbachian, Toarcian and Aalenian. *Palaeogeography, Palaeoclimatology, Palaeoecology*, **297**, 401-419.

Cheng, Y-N. (1989) Upper Paleozoic and Lower Mesozoic radiolarian assemblages from the Busuanga Islands, North Palawan block, Philippines. *Bull. National Museum of Natural Science, Taiwan*, no.1, 129-175.

Deflandre, G. (1953) Radiolaires fossils. *In* Grassé, P.P. ed., *Traite de zoologie*. Masson, Paris, 389-436.

De Wever, P. (1981) Une nouvelle sous-famille, les Poulpinae, et quatre nouvelles espèces de *Saitoum* radiolarires mésozoïques téthysiens. *Géobios*, **14**, 5-15.

De Wever, P. (1982) Nassellaria (Radiolarires polycystines) du Lias de Turquie, *Revue de Micropaléontologie*, **24**, 189-232.

De Wever, P., Dumitrica, P., Caulet, J.P., Nigrini, C. and Caridroit, M. (2001) *Radiolarians in the sedimentary record*. Gordon and Breach Science Publishers, 533p.

Donofrio, D. and Mostler, H. (1978) Zur Verbreitung der Saturnalidae (Radiolaria) im Mesozoikum der Nordlichen Kalkalpan und Sudalpen. *Geologisch Pläontologische mitteilungen Innsbruck*, **7**, 1-55.

Dumitrică, P. (1978) Family Eptingiidae n. fam., extinct Nassellaria (Radiolaria) with sagittal ring. *Deri di Seama ale sedintelor, Institutul de Geologie si Geofizica, Bucuresti*, **64**, 27-38.

Dumitrica, P. (1995) Upper Jurassic and Lower Cretaceous radiolarians at Svinita (Romania). *In* Baumgartner, P.O., O'Dogherty, L., Gorican, S., Urquhart, E., Pillevuit, A. and De Wever, P. eds., *Middle Jurassic to Early Cretaceous Radiolaria of Tethys: occurrence, systematics, biochronology. Mémoires de Géologie (Lausanne)*, no.23, Lausanne, Switzerland, 897-905.

Dumitrica, P. and Carter, E.S. (1999) Family Kungalariidae, n. fam., new Mesozoic entactinarian Radiolaria with a nassellarian-type initial spicule. *Micropaleontology*, **45**, 418-428.

Dumitrică, P., Kozur, H. and Mostler, H. (1980) Contribution to the radiolarian fauna of the Middle Triassic of the Southern Alps. *Geologisch Pläontologische mitteilungen Innsbruck*, **10**, 1-46.

Ehrenberg, C.G. (1873) Grössere Felsproben des Polycystine – Mergels von Barbados mit weiteren Erläuterungen. *Monatsberichte der Königlichen Preussischen Akademie der Wissenschaften zu Berlin*, 213-263.

Ehrenberg, C.G. (1875) Fortsetzung der mikrogeologischen Studien als Gesammt-Ubersichtder mikroskopischen

Palaontologie gleichartig analysirter Gebirgsarten der Erde, mit specieller Rucksicht auf den Polycystinen-Mergel von Barbados. *Abhandlungen der Königlichen Preussischen Akademie der Wissenschaften zu Berlin*, Abhandlungen, Jahre 1875, 1-225.

Feng, Q., Zhang, Z. and Ye, M. (2001) Middle Triassic radiolarian fauna from southwest Yunnan, China. *Micropaleontology*, **47**, 173-204.

Gawlick, H.-J., Suzuki, H. and Missoni, S. (2001) Nachweis von unterliassischen Beckensedimenten in Hallstätter Fazies (Dürrnberg-Formation) im Bereich der Hallein-Berchtesgadener Hallstätter Zone und des Lammer Beckens (Hettangium – Sinemurium). *Mitteilungen der Gesellschaft der Geologie und Bergbaustudenten in Österreich*, **45**, 39-55. (in German with English abstract)

Goričan, Š. (1994) Jurassic and Cretaceous radiolarian biostratigraphy and sedimentary evolution of the Budva zone (Dinarides, Montenegro). *Mémoires de Géologie (Lausanne)*, no.18, Institut de Géologie et Paléontologie, Université de Lausanne, Switzerland, 177p.

Goričan, Š., Šmuc, A. and Baumgartner, P.O. (2003) Toarcian Radiolaria from Mt. Mangart (Slovenian – Italian border) and their paleoecological implications. *Marine Micropaleontology*, **49**, 275-301.

Goričan, Š., Carter, E. S., Dumitrică, P., Whalen, P. A., Hori, R.S., De Wever, P., O'Dogherty, L., Matsuoka, A. and Guex, J. (2006) *Catalogue and systematics of Pliensbachian, Toarcian and Aalenian radiolarian genera and species*. Založba ZRC/ZRC Publishing, ZRC SAZU, Ljubljana, 446p.

Gradstein, F. M., Ogg, J. G., Schmitz, M. and Ogg. G. (2012) *The Geologic Time Scale 2012*. Elsevier.

Haeckel, E. (1881) Entwurf eines Radiolarien–Systems auf Grund von Studien der Challenger–Radiolarien. *Jenaische Zeitschrift für Naturwissenschaft*, **15**, 418-472.

Haeckel, E. (1887) Report on the Radiolaria collected by H.M.S. Challenger during the years 1873-1876. *Report on the Scientific Results of the Voyage of the H.M.S. Challenger, Zoology*, **18**, 1803p.

Hattori, I. (1987) Jurassic radiolarian fossils from the Nanjo massif, Fukui Prefecture, central Japan. *Bull. Fukui Municipal Museum of Natural History*, no.34, 29-101. (in Japanese with English abstract)

Hattori, I. and Yoshimura, M. (1982) Lithofacies distribution and radiolarian fossils in the Nanjo area in Fukui Prefecture, central Japan. *News of Osaka Micropaleontologists, spec. vol*., no.5, 103-116. (in Japanese with English abstract)

Hori, N. (2004) Jurassic radiolarians from chert and clastic rocks of the Chichibu belt in the Toyohashi district, Aichi Prefecture, Southwest Japan. *Bull. Geological Survey of Japan*, **55**, 335-388. (in Japanese with English abstract)

Hori, R. (1990) Lower Jurassic radiolarian zones of SW Japan. *Trans. Proc. Paleont. Soc. Japan. New series*, no.159, 562-586.

Hori, R. and Otsuka, T. (1989) Early Jurassic radiolarians from the Mt. Norikuradake area, Mino terrane, central Japan. *Jour. Geosciences, Osaka City Univ*., **32**, 175-199.

Hori, R. and Yao, A. (1988) *Parahsuum* (Radiolaria) from the Lower Jurassic of the Inuyama area, central Japan. *Jour. Geosciences, Osaka City Univ*., **31**, 47-61.

Ishida, K., Shimakawa, M., Kozai, T. and Yao, A. (2004) Oceanic-plate stratigraphy and radiolarian zonation of the Hegawa section in northern South Chichibu belt (Kurano subbelt), east Shikoku. *News of Osaka Micropaleontologists, spec. vol*., no.13, 181-195. (in Japanese with English abstract)

Kamata, Y. (1995) Early Triassic radiolarians from black siliceous shale and black chert in the Kuzu area of the Ashio terrane, central Japan. *FOSSILS*, **59**, 23-31. (in Japanese with English abstract)

Kashiwagi, K. (2001) The Inumodorikyo Complex of the Chichibu terrane, eastern Kii Peninsula, Southwest Japan: Jurassic accretionary complex as characterized by chert–clastics sequence. *Jour. Geological Society of Japan*, **107**, 640-658. (in Japanese with English abstract)

Kishida, Y. and Hisada, K. (1985) Late Triassic to Early Jurassic radiolarian assemblages from the Ueno-mura area, Kanto Mountains, central Japan. *Mem. Osaka Kyoiku Univ., ser. III (Natural Science)*, **34**, 103-129. (in Japanese with English abstract)

Kishida, Y. and Sugano, K. (1982) Radiolarian zonation of Triassic and Jurassic in outer side of Southwest Japan. *News of Osaka Micropaleontologists, spec. vol*., no.5, 271-300. (in Japanese with English abstract)

Kozur, H. (1988) Muelleritortiidae n. fam., eine charakteristische longobardische (oberladinische) Radiolarienfamilie, Teil I. *Freiberger Forschungshefte, Geowissenschaften-Paläontologie*, **C419**, 51-61.

Kozur, H. and Mostler, H. (1972) Beiträge zur Erforschung der mesozoischen Radiolarien. Teil I: Revision der Oberfamilie Coccodiscacea Haeckel 1862 emend. und Beschreibung ihrer triassischen Vertreter. *Geologisch Pläontologische mitteilungen Innsbruck*, **2**, 1-60.

Kozur, H. and Mostler, H. (1979) Beiträge zur Erforschung der mesozoischen Radiolarien. Teil III: Die Oberfamilien Actinommacea Haeckel 1862 emend., Artiscacea Haeckel 1882, Multiarcusellacea nov. der Spumelllaria und triassische Nassellaria. *Geologisch Pläontologische mitteilungen Innsbruck*, **9**, 1-132.

Kozur, H. and Mostler, H. (1981) Beiträge zur Erforschung der mesozoischen Radiolarien. Teil IV: Thalassosphaeracea Hackel, 1862, Hexastylacea Haeckel, 1882 emend. Petruševskaja, 1979, Sponguracea Haeckel, 1862 emend. und weitere triassische Lithocycliacea, Trematodiscacea, Actinommacea und Nassellaria. *Geologisch Pläontologische mitteilungen Innsbruck, Sonderband*, 1-208.

Kozur, H. and Mostler, H. (1982) Entactinaria subordo

Nov., a new radiolarian suborder. *Geologisch Pläontologische mitteilungen Innsbruck*, **11**, 399-414.
Kozur, H. and Mostler, H. (1990) Saturnaliacea Deflandre and some other stratigraphically important Radiolaria from the Hattangian of Lenggries/Isar (Bavaria, Northern Calcareous Alps). *Geologisch Pläontologische mitteilungen Innsbruck*, **17**, 179-248.
Kozur, H. and Mostler, H. (1994) Anisian to Middle Carnian radiolarian zonation and description of some stratigraphically important radiolarians. *Geologisch Pläontologische mitteilungen Innsbruck, Sonderband*, **3**, 39-255.
Kozur, H. and Mostler, H. (1996) Longobardian (Late Ladinian) Muelleritortiidae (Radiolaria) from the Repablic of Bosnia-Hercegowina. *Geologisch Pläontologische mitteilungen Innsbruck, Sonderband*, **4**, 83-103.
Kozur, H., Krainer, K. and Mostler, H. (1996) Radiolarians and facies of the Middle Triassic Loibl Formation, South Alpine Karawanken Mountains (Carpathia, Austria). *Geologisch Pläontologische mitteilungen Innsbruck, Sonderband*, **4**, 195-269.
Kuwahara, K., Sano, H., Ezaki, Y. and Yao, A. (2010) Discovery of Triassic siliceous rocks within a large Permian oceanic-rock mass in the Mt. Funafuse-yama area, western Mino terrane, and geologic implication. *Jour. Geological Society of Japan*, **116**, 159-173. (in Japanese with English abstract)
Li, Hong-shen (1988) Early Jurassic (Late Pliensbachian) Radiolaria from the Dengqen area, Xizang (Tibet). *Acta Micropalaeontologica Sinica*, **5**, 323-330. (in Chinese with English abstract)
Martini, R., De Wever, P., Zaninetti, L., Denelian, T. and Kito, N. (1989) Les radiolarites triasiques de la Formation du Monte Facito *Auct*. (Bassin de Lagonegro, Italieméridionale). *Revue de Paléobiologie*, **8**, 143-161.
Matsuoka, A. (1991) Early Jurassic radiolarians from the Nanjo massif in the Mino terrane, central Japan. *Trans. Proc. Paleont. Soc. Japan. New series*, no.161, 720-738.
Matsuoka, A. (1995) Middle Jurassic – Lower Cretaceous radiolarian zonation in Japan and the western Pacific, and age assignments based on the Unitary Associations method. *In* Baumgartner, P. O., O'Dogherty, L., Gorican, S., Urquhart, E., Pillevuit, A. and De Wever, P. eds., *Middle Jurassic to Early Cretaceous Radiolaria of Tethys: occurrence, systematics, biochronology. Mémoires de Géologie (Lausanne)*, no.23, Lausanne, Switzerland, 1049-1057.
Matsuoka, A. (2004) Toarcian (Early Jurassic) radiolarian fauna from the Nanjo massif in the Mino terrane, central Japan. *News of Osaka Micropaleontologists, spec. vol*., no.13, 69-87.
Mizutani, S. and Kido, S. (1983) Radiolarians in Middle Jurassic siliceous shale from Kamiaso, Gifu Prefecture, central Japan. *Trans. Proc. Paleont. Soc. Japan. New series*, no.132, 253-262.
Moix, P., Kozur, H.W., Stampfli, G.M. and Mostler, H. (2007) New paleontological, biostratigraphic and paleographic results from the Triassic of the Mersin Melange, SE Turkey. *In* Lucas, S.G. and Spielmann, J.A. eds., *Bull. New Mexico Museum of Natural History and Science*, New Mexico, **41**, 282-305.
Nagai, H. (1986) Jurassic *Eucyrtidiellum* (Radiolaria) from central Japan. *Bull. Nagoya Univ. Museum*, no.2, 1-22.
Nagai, H. (1990) Jurassic (Lower Toarcian) radiolarians from the Hyde Formation, central Oregon, North America. *Bull. Nagoya Univ. Museum*, no.6, 1-7. (in Japanese with English abstract)
Nagai, H. (1995) History and significance of radiolarian biostratigraphic study on the Mesozoic of Mino terrane. *Bull. Nagoya Univ. Furukawa Museum, special report*, no.4, 89p. (in Japanese with English abstract)
Nakae, S. (2012) Geology of the Permian Higashimata Complex in the Nanjō Mountains, Fukui Prefecture, Southwest Japan. *Bull. Geological Survey of Japan*, **63**, 269-281.
Nakae, S. (2013) Triassic to Middle Jurassic radiolarians from pelagic cherts in the Nanjō Mountains, Southwest Japan – Part 1. Imajō district. *Bull. Geological Survey of Japan*, **64**, 85-112.
Nakae, S., Komatsubara, T. Takahashi, Y. and Yoshikawa, T. (2013) *Geology of the Imajō and Takenami district*. Quadrangle Series, 1:50000, Geological Survey of Japan, AIST, 110p. (in Japanese with English abstract, 4p.)
Nakaseko, K. and Nishimura, A. (1979) Upper Triassic Radiolaria from Southwest Japan. *Sci. Rep., Col. Educ., Osaka Univ*., **28**, 61-109.
Nishizono, Y. (1996) Mesozoic convergent process of the Southern Chichibu terrane in West Kyushu, Japan, on the basis of Triassic to Early Cretaceous radiolarian biostratigraphy. *Kumamoto Jour. Science (Earth Sciences)*, **14**, 45-226. (in Japanese with English abstract)
O'Dogherty, L., Carter, E.S., Dumitrica, P., Goričan, Š. and De Wever, P. (2009) An illustrated and revised catalogue of Mesozoic radiolarian genera – objectives, concepts and guide for users. *Geodiversitas*, **31**, 191-356.
O'Dogherty, L., Carter, E.S., Gorican, S. and Dumitrica, P. (2010) Triassic radiolarian biostratigraphy. *In* Licas, S.G. ed., *The Triassic timescale*. Geol. Soc. London, Special publications, **334**, 163-200.
Otsuka, T., Kajima, M. and Hori, R. (1992) The Batinah olistostrome of the Oman Mountains and Mesozoic radiolarians. *News of Osaka Micropaleontologist, Special Volume*, no.8, 21-34. (in Japanese with English abstract)
Pessagno, E.A. (1973) Upper Cretaceous Spumellariina from the Great Valley Sequence, California Coast Ranges. *Bull. American Paleontology*, **63**, 49-102.
Pessagno, E.A. (1977a) Upper Jurassic Radiolaria and

radiolarian biostratigraphy of the California Coast Ranges. *Micropaleontology*, **23**, 56-113.

Pessagno, E.A. (1977b) Lower Cretaceous radiolarian biostratigraphy of the Great Valley Sequence and Franciscan Complex, California Coast Ranges. *Cushman Foundation for Foraminiferal Research, Special publication*, no.15, 87p.

Pessagno, E.A. and Blome, C.D. (1980) Upper Triassic and Jurassic Pantanelliinae from California, Oregon and British Columbia. *Micropaleontology*, **26**, 225-273.

Pessagno, E.A. and Poisson, A. (1981) Lower Jurassic Radiolaria from the Gümüşlü Allochton of southwestern Turkey (Taurides occidentals). *Bull. Mineral Research and Exploration Inst. Turkey*, **92**, 47-69.

Pessagno, E.A. and Whalen, P.A. (1982) Lower and Middle Jurassic Radiolaria (multicyrtid Nassellariina) from California, east-central Oregon and the Queen Charlotte Islands, B.C.. *Micropaleontology*, **28**, 111-169.

Pessagno, E.A., Finch, W. and Abbott, P.L. (1979) Upper Triassic Radiolaria from the San Hipólito Formation, Baja California. *Micropaleontology*, **25**, 160-197.

Pessagno, E.A., Whalen, P.A. and Yeh, K.-Y. (1986) Jurassic Nassellariina (Radiolaria) from North American geologic terranes. *Bulletins of American paleontology*, **91**, 5-75.

Pessagno, E.A., Six, W.M. and Yang, Q. (1989) The Xiphostylidae Haeckel and Parvivaccidae, n. fam. (Radiolaria) from the North America Jurassic. *Micropaleontology*, **35**, 138-255.

Pessagno, E.A., Blome, C.D., Hull, D.M. and Six, W.M. (1993) Jurassic Radiolaria from the Josephine ophiolite and overlying strata, Smith River subterrane (Klamath Mountains), northwestern California and southwestern Oregon. *Micropaleontology*, **39**, 93-166.

Ramovš, A. and Goričan, Š. (1995) Late Anisian-Early Ladinian radiolarians and conodonts from Šmarma Gora near Ljublana, Slovenia. *Razprave IV. Razreda SAZU*, **36**, 179-221.

Sashida, K. (1988) Lower Jurassic multisegmented Nassellaria from the Itsukaichi area, western part of Tokyo Prefecture, central Japan. *Science Report, Institute of Geosciences, University of Tsukuba, sec.B*, **9**, 1-27.

Sashida, K. (1991) Early Triassic radiolarians from the Ogamata Formation, Kanto Mountains, central Japan. Part 2. *Trans. Proc. Paleont. Soc. Japan. New series*, no.161, 681-696.

Sashida, K. (1992) Early Jurassic radiolarians from the Shomaru Pass–Higashiagano area, Hanno City, Saitama Prefecture, central Japan. *News of Osaka Micropaleontologists, spec. vol*., no.8, 35-46. (in Japanese with English abstract)

Sashida, K., Nishimura, H., Igo, H., Kazama, S. and Kamata, Y. (1993) Triassic radiolarian faunas from Kiso-fukushima, Kiso Mountains, central Japan. *Science Report, Institute of Geosciences, Univ. Tsukuba, sec.B*, **14**, 77-97.

Sugiyama, K. (1992) Lower and Middle Triassic radiolarians from Mt. Kinkazan, Gifu Prefecture, central Japan. *Trans. Proc. Paleont. Soc. Japan. New series*, no.167, 1180-1223.

Sugiyama, K. (1997) Triassic and Lower Jurassic radiolarians biostratigraphy in the siliceous claystone and bedded chert units of the southeastern Mino Terrane, central Japan. *Bull. Mizunami Fossil Museum*, no.24, 79-193.

Taga, H. (1997) Paleozoic and Mesozoic radiolarian fossils found in chert of the Nanjo massif, central Japan. *Bull. Fukui City Museum of Natural History*, no.44, 35-55. (in Japanese)

Takamura, Y. and Hayami, T. (1985) On the Paleozoic and Mesozoic strata in the eastern area of Imajo-cho, Fukui Prefecture, central Japan. *Bull. Fukui City Museum of Natural History*, no.31, 1-16. (in Japanese)

Takemura, A. (1986) Classification of Jurassic nassellarians (Radiolaria). *Palaeontographica. Abteilung A: Palaeozoologie-Stratigraphie*, **195**, 29-74.

Tekin, U.K. (2002) Lower Jurassic (Hettangian-Sinemurian) radiolarians from the Antaya Nappes, central Taurids, Southern Turkey. *Micropaleontology*, **48**, 177-205.

Thassanapak, H., Feng, Q.-L., Grant-Mackie, J., Chonglakmani, C. and Thanee, N. (2011) Middle Triassic radiolarian faunas from Chiang Dao, Northern Thailand. *Palaeoworld*, **20**, 179-202.

Tumanda, F. (1991) Radiolarian biostratigraphy in central Busuanga Island, Palawan, Philippines. *Jour. Geological Society of Philippines*, **46**, 49–104.

Tumanda, F.M., Sashida, K. and Igo, H. (1996) Some Jurassic radiolarians from Busuanga Island, Calamian Island Group, Palawan, Philippines. *In* Noda, H. and Sashida, K. eds., *Professor Hisayashi Igo Commemorative volume on Geology and Paleontology of Japan and Southeast Asia*, 165-192.

Uchino, T. and Hori, R.S. (2010) Early Jurassic radiolarian fossils from mudstone of the Ashio terrane in the Kambara Mountains, Niigata Prefecture, Japan. *Jour. Geological Society of Japan*, **116**, 441-446. (in Japanese with English abstract)

Umeda, M. and Taga, H. (2003) Note of occerrence of radiolarian fossils in the Nanjo massif, Fukui Prefecture, central Japan – No. 7 – Takura-gawa area. *Bull. Fukui City Museum of Natural History*, no.50, 27-36. (in Japanese)

Umeda, M., Taga, H. and Hattori, I. (1996) Discovery and its geologic significance of Permian radiolarians from clastic rocks at the northern margin of the Nanjo massif, Fukui Prefecture, central Japan. *Jour. Geological Society of Japan*, **102**, 635-638. (in Japanese with English abstract)

Wakita, K. (1988) Origin of chaotically mixed rock bodies in the Early Jurassic to Early Cretaceuos sedimentary

complex of the Mino terrane, central Japan. *Bull. Geological Survey of Japan*, **39**, 675-757.

Whalen, P.A. and Carter, E.S. (1998) Part II. Systematic paleontplogy. *In* Carter, E. S., Whalen, P. A. and Guex, J. eds., Biochronology and paleontology of Lower Jurassic (Hettangian and Sinemurian) radiolarians, Queen Charlotte Islands, British Columbua. *Geological Survey of Canada Bull*., no.496, 36-162.

Whalen, P.A. and Carter, E.S. (2002) Pliensbachian (Lower Jurassic) Radiolaria from Baja Californian Sur, Mexico. *Micropaleontology*, **48**, 97-151.

Xu, X. (1992) Triassic faunas and stratigraphic subdivision and correlation of Qinling and neibouring areas. 1. Triassic marine faunas and stratigraphic subdivision and correlation of Qinling region. 1. Triassic faunas and fossil zonations. (6). Radiolarians. *In* Yin, H., Yang, F., Huang, Q., Yang, H. and Lai, X. eds., *The Triassic of Qinling Mountains and neibouring area*. Press of the China University of Geosciences, 68-69.

Yao, A. (1979) Radiolarian fauna from the Mino belt in the northern part of the Inuyama area, central Japan. Part II: Nassellaria 1. *Jour. Geosci., Osaka City Univ*., **22**, 21-72.

Yao, A. (1982) Middle Triassic to Early Jurassic radiolarians from the Inuyama area, central Japan. *Jour. Geosci., Osaka City Univ*., **25**, 53-70.

Yao, A. (1997) Faunal change of Early – Middle Jurassic radiolarians. *News of Osaka Micropaleontologists, spec. vol*., no.10, 155-182. (in Japanese with English abstract)

Yeh, K.-Y. (1987) Taxonomic studies of Lower Jurassic Radiolaria from east–central Oregon. *Special Publication, National Museum of Natural Science, Taiwan*, no.2, 169p.

Yeh, K.-Y. (1989) Studies of Radiolaria from the Fields Creek Formation, east-central Oregon, U.S.A.. *Bull. National Museum of Natural Science, Taiwan*, no.1, 43-109.

Yeh, K.-Y. (1990) Taxonomic studies of Triassic Radiolaria from Busuanga Island, Philippines. *Bull. National Museum of Natural Science, Taiwan*, no.2, 1-63.

Yeh, K.-Y. (1992) Triassic Radiolaria from Uson Island, Philippines. *Bull. National Museum of Natural Science, Taiwan*, no.3, 51-91.

Yeh, K.-Y. and Cheng, Y.-N. (1996) Jurassic radiolarians from the northwest coast of the Busuanga Island, North Palawan block, Philippines. *Micropaleontology*, **42**, 93-124.

Yeh, K.-Y. and Cheng, Y.-N. (1998) Radiolarians from the Lower Jurassic of the Busuanga Island, Philippines. *Bull. National Museum of Natural Science, Taiwan*, no.11, 1-65.

Received May 13, 2013
Accepted August 21, 2013

Plate

Plate 1 SEM images of Triassic to Middle Jurassic radiolarians from the Kanmuri Yama district.

KJ0301 (Locality Kc-1: Tarumi-gawa)
1-3: *Haeckelicyrtium*? sp. (1: GSJ F18132-002, 2: -003, 3: -001)
4: *Palaeosaturnalis* sp. (GSJ F18132-005)
5: *Cryptostephanidium*? sp. (GSJ F18132-004)

KJ0402 (Locality Kc-2: Northeast of Masudani)
6-7: Spumellaria gen. et sp. indet. (6: GSJ F18136-013, 7: -014)
8-9: *Pseudostylosphaera japonica* (Nakaseko and Nishinura) (8: GSJ F18136-011, 9: -010)
10: *Pseudostylosphaera*? sp. (GSJ F18136-012)
11: *Eptingium nakasekoi* Kozur and Mostler (GSJ F18136-009)
12-13: Poulpidae gen. et sp. indet. (12: GSJ F18136-006, 13: -008)
14: *Triassocampe deweveri* (Nakaseko and Nishimura) (GSJ F18136-003)
15-18: *Triassocampe* sp. (15: GSJ F18136-002, 16: -001, 17: -004, 18: -005)

KJ0403 (Locality Kc-2: Northeast of Masudani)
19: *Pseudostylosphaera*? sp. (GSJ F18137-003)
20: *Triassocampe* sp. cf. *T. myterocorys* Sugiyama (GSJ F18137-002)
21: *Multimonilis* sp. (GSJ F18137-01)

KJ0404 (Locality Kc-2: Northeast of Masudani)
22: *Triassocampe deweveri* (Nakaseko and Nishimura) (GSJ F18138-008)
23: *Triassocampe* sp. (GSJ F18138-001)
24-28: Nassellaria gen. et sp. indet. (24: F18138-002, 25: -003, 26: -004, 27: -005, 28: -007)

KJ0410c (Locality Kc-3: East of Masudani)
29: Entactinaria gen. et sp. indet. (GSJ F18139-003)
30: *Droltus* sp. cf. *D. hecatensis* Pessagno and Whalen (GSJ F18139-001)
31: Nassellaria gen. et sp. indet. (GSJ F18139-002)

All scale bars equal to 0.1 mm.

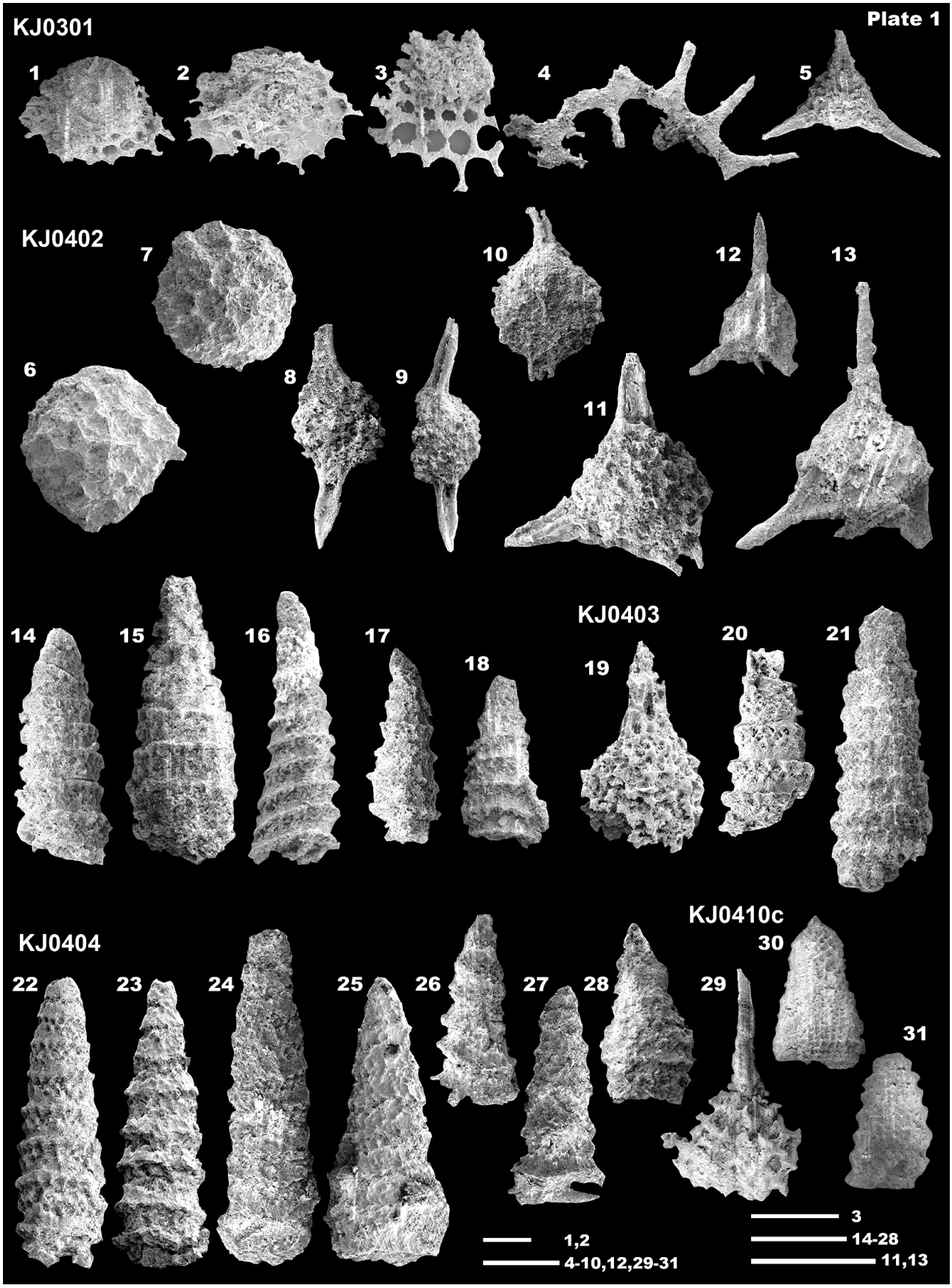
KJ0301
Plate 1
1
2
3
4
5
KJ0402
7
10
12
13
6
8
9
11
14
15
16
17
18
KJ0403
19
20
21
KJ0404
22
23
24
25
26
27
28
KJ0410c
29
30
31
1,2
4-10,12,29-31
3
14-28
11,13

Plate 2 SEM images of Triassic to Middle Jurassic radiolarians from the Kanmuri Yama district.

KJ0810e (Locality Kc-4: Masudani)
1: *Archaeocenosphaera*? sp. (GSJ F18141-008)
2: Spumellaria gen. et sp. indet. (GSJ F18141-009)
3-4: *Pseudostylosphaera*? sp. (3: GSJ F18141-006, 4: -005)
5-6: Spumellaria gen. et sp. indet. (GSJ F18141-003, 6: -004)
7: *Tirodella*? sp. (GSJ F18141-007)
8: *Celluronta* sp. (GSJ F18141-001)
9: Nassellaria gen. et sp. indet. (GSJ F18141-002)

KJ0810f (Locality Kc-4: Masudani)
10: Spumellaria gen. et sp. indet. (GSJ F18142-013)
11-17: *Pseudostylosphaera* sp. (11: GSJ F18142-008, 12: -011, 13: -005, 14: -010, 15: -009, 16: -007, 17: -012)
18: *Eptingium*? sp. (GSJ F18142-006)
19-20: Spumellaria gen. et sp. indet. (19: GSJ F18142-004, 20: -003)
21: Nassellaria gen. et sp. indet. (GSJ F18142-002)

KJ0810g (Locality Kc-4: Masudani)
22: *Pseudostylosphaera compacta* (Nakaseko and Nishimura) (GSJ F18143-010)
23: Spumellaria gen. et sp. indet. (GSJ F18143-005)
24: *Cryptostephanidium*? sp. (GSJ F18143-008)
25: *Eptingium* sp. (GSJ F18143-007)
26: *Parasepsagon* sp. (GSJ F18143-009)
27: Entactinaria gen. et sp. indet. (GSJ F18143-006)
28-30: *Triassocampe* sp. (28: GSJ F18143-003, 29: -002, 30: -001)
31: Nassellaria gen. et sp. indet. (GSJ F18143-004)

All scale bars equal to 0.1 mm.

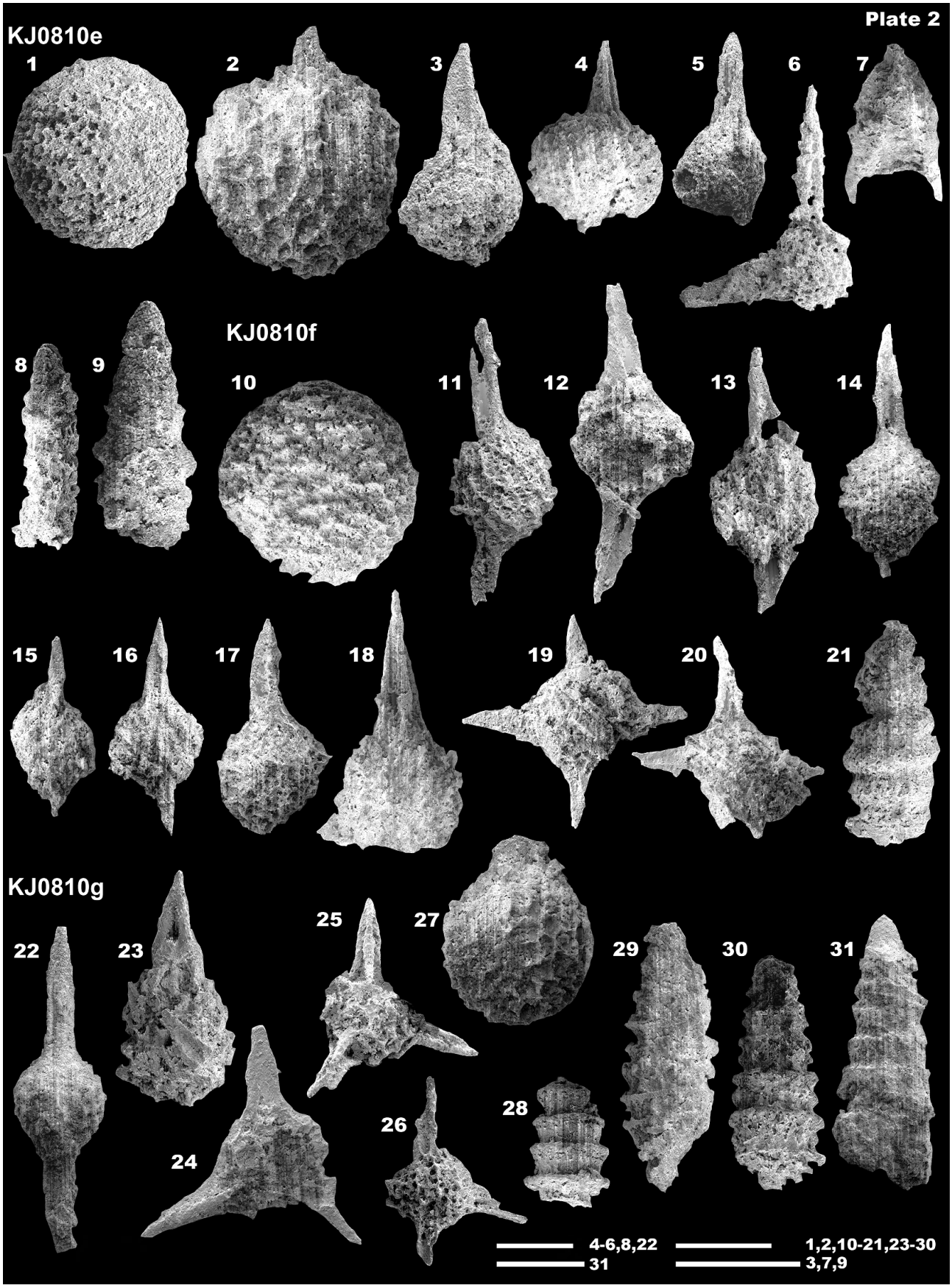
Plate 2
KJ0810e
1
2
3
4
5
6
7
KJ0810f
8
9
10
11
12
13
14
15
16
17
18
19
20
21
KJ0810g
22
23
24
25
26
27
28
29
30
31
4-6,8,22
31
1,2,10-21,23-30
3,7,9

Plate 3 SEM images of Triassic to Middle Jurassic radiolarians from the Kanmuri Yama district.

KJ0904a (Locality Kc-5: Northeast of Masudani)
1-2: *Archaeocenosphaera*? sp. (1: GSJ F18144-004, 2: -005)
3: *Triassocampe* sp. (GSJ F18144-001)
4: Nassellaria gen. et sp. indet. (GSJ F18144-002)

KJ0904b (Locality Kc-5: Northeast of Masudani)
5-6: *Archaeocenosphaera*? sp. (5: GSJ F18145-013, 6: -012)
7: *Pseudostylosphaera helicata* (Nakaseko and Nishimura) (GSJ F18145-008)
8: *Pseudostylosphaera compacta* (Nakaseko and Nishimura) (GSJ F18145-011)
9: *Eptinguium*? sp. (GSJ F18145-010)
10: Spumellaria gen. et sp. indet. (GSJ F18145-009)
11: Nassellaria gen. et sp. indet. (GSJ F18145-007)
12: *Triassocampe deweveri* (Nakaseko and Nishimura) (GSJ F18145-003)
13-16: *Triassocampe* sp. (13: GSJ F18145-004, 14: -002, 15: -001, 16: -005)

KJ0904c (Locality Kc-5: Northeast of Masudani)
17-18: Spumellaria gen. et sp. indet. (17: GSJ F18146-009, 18: -003)
19: *Pseudostylosphaera* sp. aff. *P. tenuis* (Nakaseko and Nishimura) (GSJ F18146-004)
20-23: Spumellaria gen. et sp. indet. (20: GSJ F18146-001, 21: -007, 22: -002, 23: -008)

KJ0905b (Locality Kc-6: Northeast of Masudani)
24: Entactinaria gen. et sp. indet. (GSJ F18147-001)
25: Spumellaria gen. et sp. indet. (GSJ F18147-002)

KJ0905c (Locality Kc-6: Northeast of Masudani)
26: *Trillus elkhornensis* Pessagno and Blome (GSJ F18148-008)
27: Favosyringiinae gen. et sp. indet. (GSJ F18148-006)
28: Nassellaria gen. et sp. indet. (GSJ F18148-007)
29-31: *Parahsuum* sp. (29: GSJ F18148-003, 30: -005, 31: -001)
32: *Hsuum* sp. cf. *H. mulleri* Pessagno and Whalen (GSJ F18148-004)
33: *Lantus*? sp. (GSJ F18148-002)

All scale bars equal to 0.1 mm.

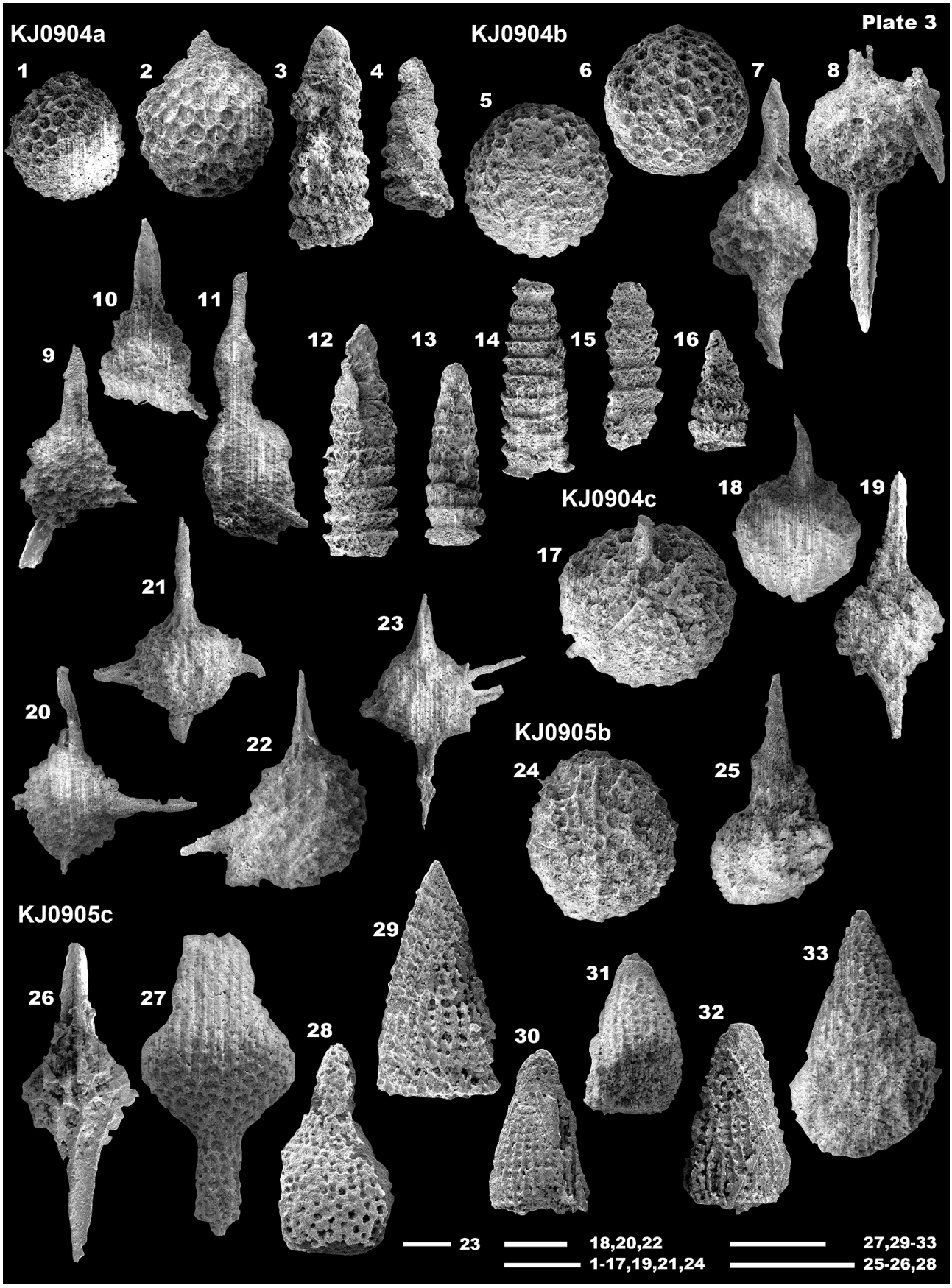
Plate 3
KJ0904a
KJ0904b
KJ0904c
KJ0905b
KJ0905c
1
2
3
4
5
6
7
8
9
10
11
12
13
14
15
16
17
18
19
20
21
22
23
24
25
26
27
28
29
30
31
32
33
23
18,20,22
1-17,19,21,24
27,29-33
25-26,28

Plate 4 SEM images of Triassic to Middle Jurassic radiolarians from the Kanmuri Yama district.

KJ1904a (Locality Kc-7: Southeast of Hirono)
1: *Pantanellium*? *virgeum* Sashida (GSJ F18157-014)
2-6: Spumellaria gen. et sp. indet. (2: GSJ F18157-009, 3: -017, 4: -004, 5: -003, 6: -012)
7: *Pseudostylosphaera*? sp. (GSJ F18157-007)
8-10: Entactinaria gen. et sp. indet. (8: GSJ F18157-008, 9: -005, 10: -013)
11: *Monostylosphaera*? sp. (GSJ F18157-002)
12: *Pseudostylosphaera*? sp. (GSJ F18157-001)

KJ2206a (Locality Kc-8: Tarumi-gawa)
13-14: *Udalia* sp. (13: GSJ F18159-038, 14: -039)
15: Nassellaria gen. et sp. indet. (GSJ F18159-028)
16: *Napora mitrata* Pessagno, Whalen and Yeh (GSJ F18159-037)
17: *Napora* sp. (GSJ F18159-034)
18-19: *Eucyrtidiellum nagaiae* Dumitrica, Goričan and Matsuoka (18: GSJ F18159-030, 19: -031)
20: *Minocapsa globosa* Matsuoka (GSJ F18159-025)
21: *Lantus obesus* (Yeh) (GSJ F18159-026)
22: *Lantus intermedius* Carter (GSJ F18159-015)
23: *Hsuum* sp. sensu Matsuoka 2004 (GSJ F18159-012)
24-26: *Parahsuum simplum* Yao (24: GSJ F18159-006, 25: -018, 26: -013)
27-28: *Parahsuum ovale* Hori and Yao (27: GSJ F18159-009, 28: -023)
29: *Parahsuum* sp. (GSJ F18159-021)
30: *Parahsuum izeense* (Pessagno and Whalen) (GSJ F18159-011)
31-33: *Parahsuum longiconicum* Sashida (31: GSJ F18159-002, 32: -007, 33: -020)
34: *Parahsuum* sp. (GSJ F18159-001)
35: *Canoptum* sp. cf. *C. rugosum* Pessagno and Poisson (GSJ F18159-019)

All scale bars equal to 0.1 mm.

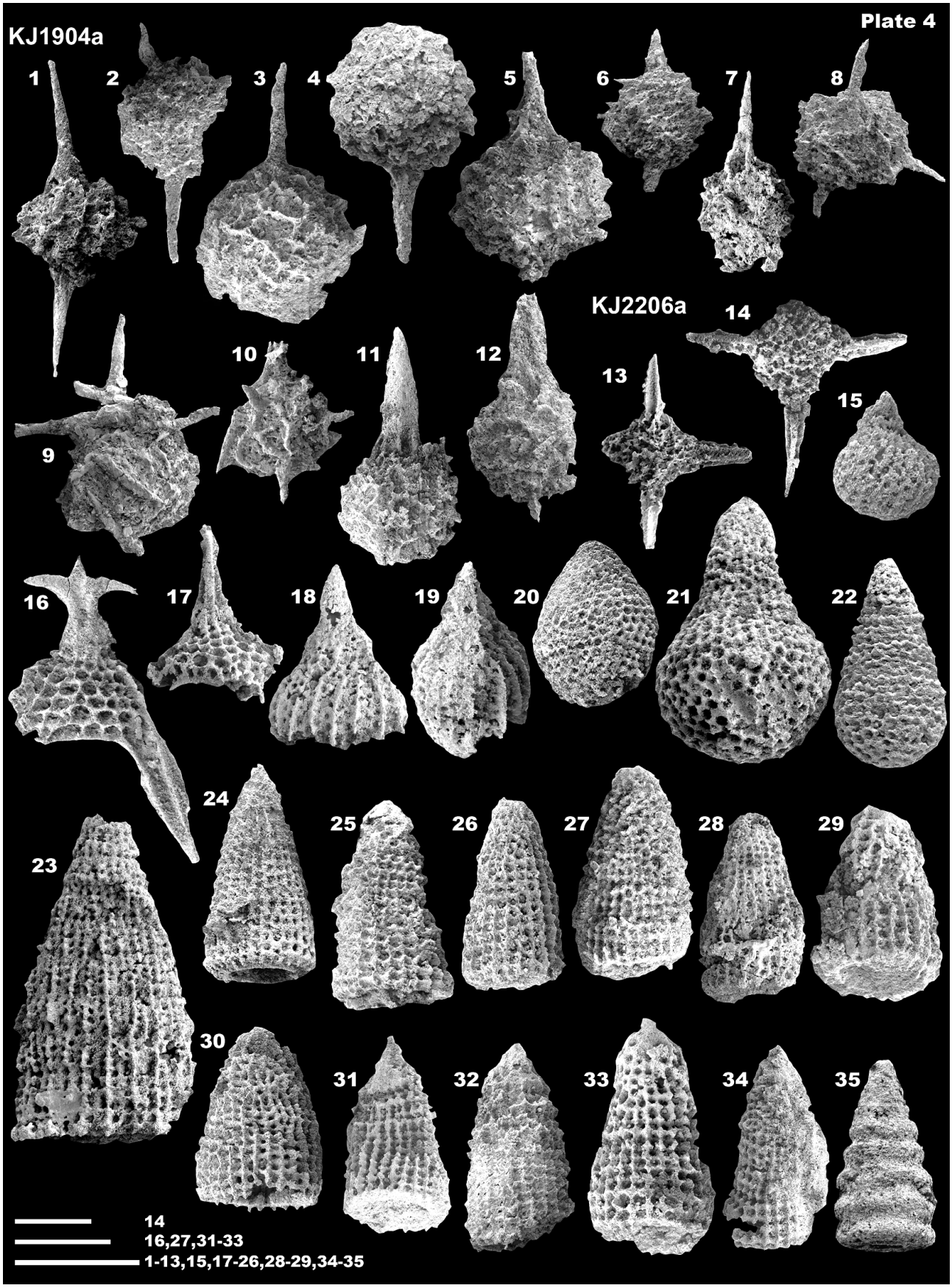
Plate 4
KJ1904a
KJ2206a
1
2
3
4
5
6
7
8
9
10
11
12
13
14
15
16
17
18
19
20
21
22
23
24
25
26
27
28
29
30
31
32
33
34
35
14
16,27,31-33
1-13,15,17-26,28-29,34-35

Plate 5 SEM images of Triassic to Middle Jurassic radiolarians from the Kanmuri Yama district.

KJ2206h (Locality Kc-8: Tarumi-gawa)
1: *Pseudostylosphaera compacta* (Nakaseko and Nishimura) (GSJ F18160-011)
2-3: *Pseudostylosphaera* sp. (2: GSJ F18160-010, 3: -015)
4-6: *Hindeosphaera spinulosa* (Nakaseko and Nishimura) (4: GSJ F18160-014, 5: -017, 6: -016)
7: *Spongostephanidium* sp. (GSJ F18160-018)
8: *Cryptostephanidium*? sp. (GSJ F18160-021)
9-12: *Triassocampe deweveri* (Nakaseko and Nishimura) (9: GSJ F18160-004, 10: -005, 11: -003, 12: -008)
13-14: *Triassocampe* sp. (13: GSJ F18160-007, 14: -001)
15: *Paratriassocampe* sp. (GSJ F18160-006)
16: *Triassocampe* sp. (GSJ F18160-002)

KJ2206i (Locality Kc-8: Tarumi-gawa)
17-18: *Pseudostylosphaera*? sp. (17: GSJ F18161-006, 18: -005)
19: Entactinaria gen. et sp. indet. (GSJ F18161-007)
20: *Eptingium* sp. (GSJ F18161-001)
21: *Bipedis* sp. (GSJ F18161-004)
22: Spumellaria gen. et sp. indet. (GSJ F18161-002)

KJ2412 (Locality Kc-9: South of Kōkuradani)
23-24: *Pseudostylosphaera* sp. (23: GSJ F18167-009, 24: -014)
25-27: *Pseudostylosphaera*? sp. (25: GSJ F18167-013, 26: -010, 27: -008)
28: *Cryptostephanidium*? sp. (GSJ F18167-018)
29-30: Entactinaria gen. et sp. indet. (29: GSJ F18167-017, 30: -016)
31-36: *Triassocampe* sp. (31: GSJ F18167-001, 32: -002, 33: -003, 34: -004, 35: -005, 36: -007)
37: *Triassocampe* sp. aff. *T. diordinis* Bragin sensu Sugiyama 1992 (GSJ F18167-006)

All scale bars equal to 0.1 mm.

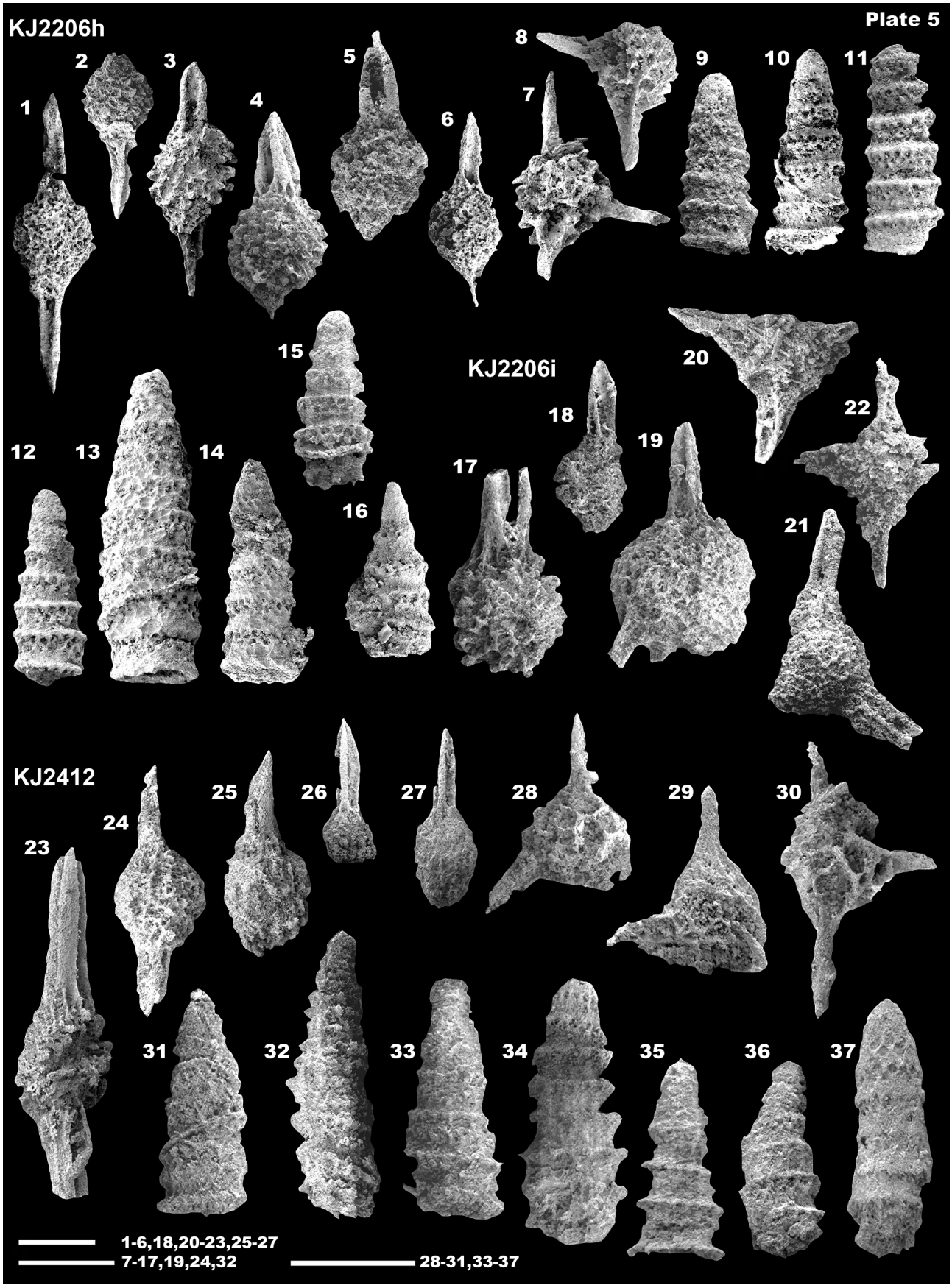
KJ2206h
Plate 5
1
2
3
4
5
6
7
8
9
10
11
KJ2206i
12
13
14
15
16
17
18
19
20
21
22
KJ2412
23
24
25
26
27
28
29
30
31
32
33
34
35
36
37
1-6,18,20-23,25-27
7-17,19,24,32
28-31,33-37

Plate 6 SEM images of Triassic to Middle Jurassic radiolarians from the Kanmuri Yama district.

KJ2413 (Locality Kc-10: South of Kōkuradani)
1: *Pseudostylosphaera japonica* (Nakaseko and Nishimura) (GSJ F18168-005)
2: *Spongoxystris*? sp. (GSJ F18168-009)
3-10: *Muelleritortis cochleata* (Nakaseko and Nishimura) (3: GSJ F18168-014, 4: -012, 5: -016, 6: -013, 7: -012, 8: -008, 9: -006, 10: -011)
11: *Triassocampe* sp. cf. *T. myterocorys* Sugiyama (GSJ F18168-003)
12-13: *Triassocampe* sp. (12: GSJ F18168-004, 13: -001)

KJ2902c (Locality Kc-11: Fujikuradani)
14: *Pseudostylosphaera* sp. (GSJ F18173-034)
15-16: *Protopsium* sp. (15: GSJ F18173-012, 16: -040)
17: *Pentabelus* sp. cf. *P. furutanii* Sugiyama (GSJ F18173-011)
18: Spumellaria gen. et sp. indet. (GSJ F18173-007)
19: Entactinaria gen. et sp. indet. (GSJ F18173-008)
20: Spumellaria gen. et sp. indet. (GSJ F18173-039)
21: *Oertlispongus* sp. (GSJ F18173-031)
22-24: *Spongostephanidium* sp. (22: GSJ F18173-003, 23: -001, 24: -023)
25: *Eptingium*? sp. (GSJ F18173-005)
26: Entactinaria gen. et sp. indet. (GSJ F18173-029)
27: Poulpidae gen. et sp. indet. (GSJ F18173-044)
28: Entactinaria gen. et sp. indet. (GSJ F18173-013)

All scale bars equal to 0.1 mm.

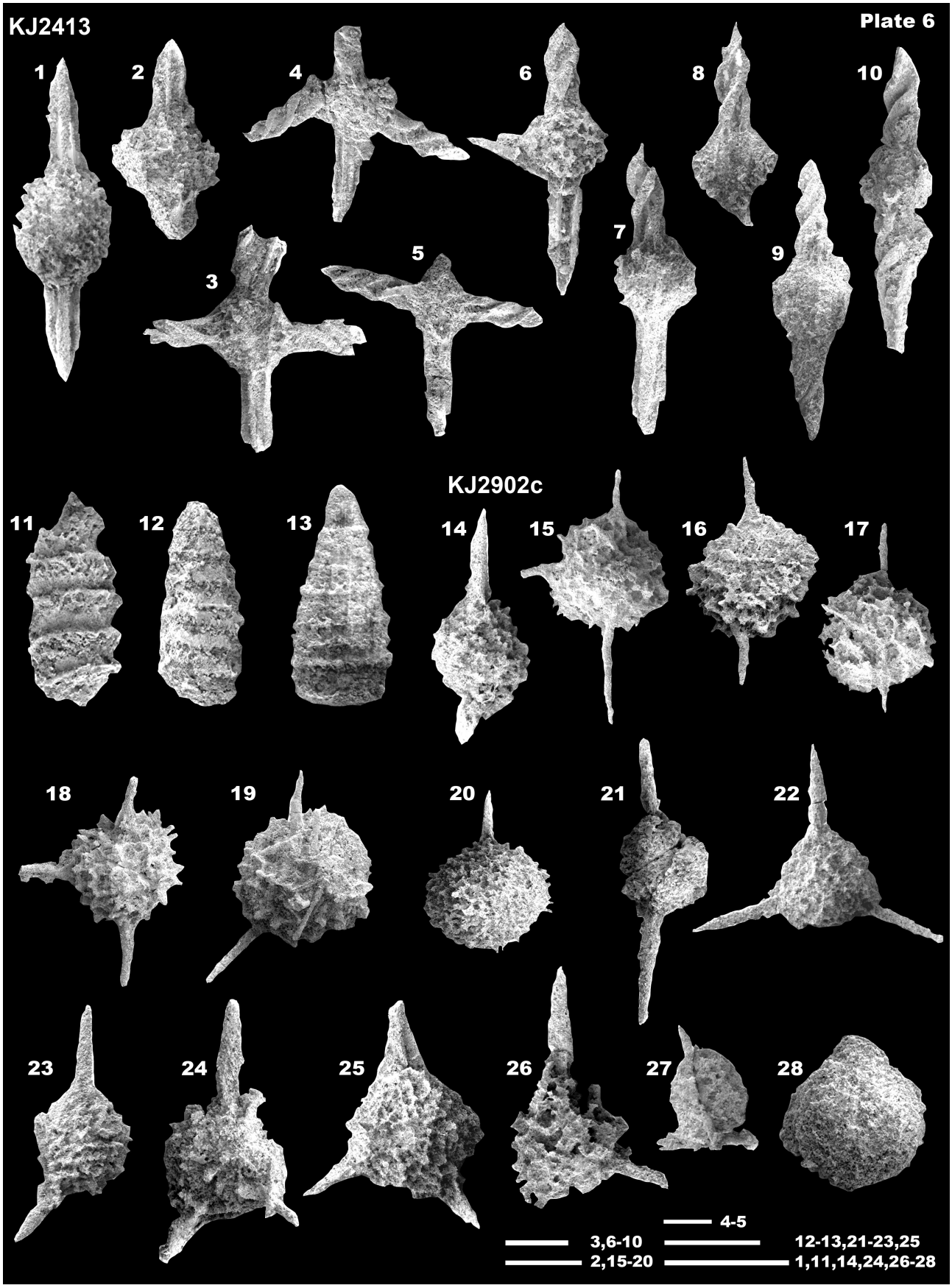
KJ2413
Plate 6
1
2
4
6
8
10
3
5
7
9
KJ2902c
11
12
13
14
15
16
17
18
19
20
21
22
23
24
25
26
27
28
4-5
3,6-10
12-13,21-23,25
2,15-20
1,11,14,24,26-28

Plate 7 SEM images of Triassic to Middle Jurassic radiolarians from the Kanmuri Yama district.

KJ3701 (Locality Kc-12: South of Kanmuri-tōge)
1: Favosyringiinae gen. et sp. indet. (GSJ F18177-011)
2-4: *Parahsuum* sp. (2: GSJ F18177-004, 3: -001, 4: -006)
5: Nassellaria gen. et sp. indet. (GSJ F18177-005)
6: *Hsuum*? sp. (GSJ F18177-009)
7: *Canoptum* sp. cf. *C. anulatum* Pessagno and Poisson (GSJ F18177-002)

KJ3907 (Locality Kc-13: Northeast of Kanmuri-tōge)
8-12: *Pseudostylosphaera japonica* (Nakaseko and Nishimura) (8: GSJ F18178-007, 9: -008, 10: -009, 11: -010, 12: -011)
13: *Monostylosphaera*? sp. (GSJ F18178-012)
14: *Hindeosphaera* sp. (GSJ F18178-014)
15-16: *Eptingium nakasekoi* Kozur and Mostler (15: GSJ F18178-013, 16: -017)
17: *Eptingium* sp. (GSJ F18178-015)
18-20: *Triassocampe* sp. (18: GSJ F18178-004, 19: -005, 20: -006)
21-22: Nassellaria gen. et sp. indet. (21: GSJ F18178-001, 22: -003)

KJ4401a (Locality Kc-14: Ichindani)
23-24: *Praemesosaturnalis* sp. (GSJ F18194-005, 24: -004)
25: *Palaeosaturnalis* sp. (GSJ F18194-006)
26-28: Nassellaria gen. et sp. indet. (26: GSJ F18194-001, 27: -002, 28: -003)

All scale bars equal to 0.1 mm.

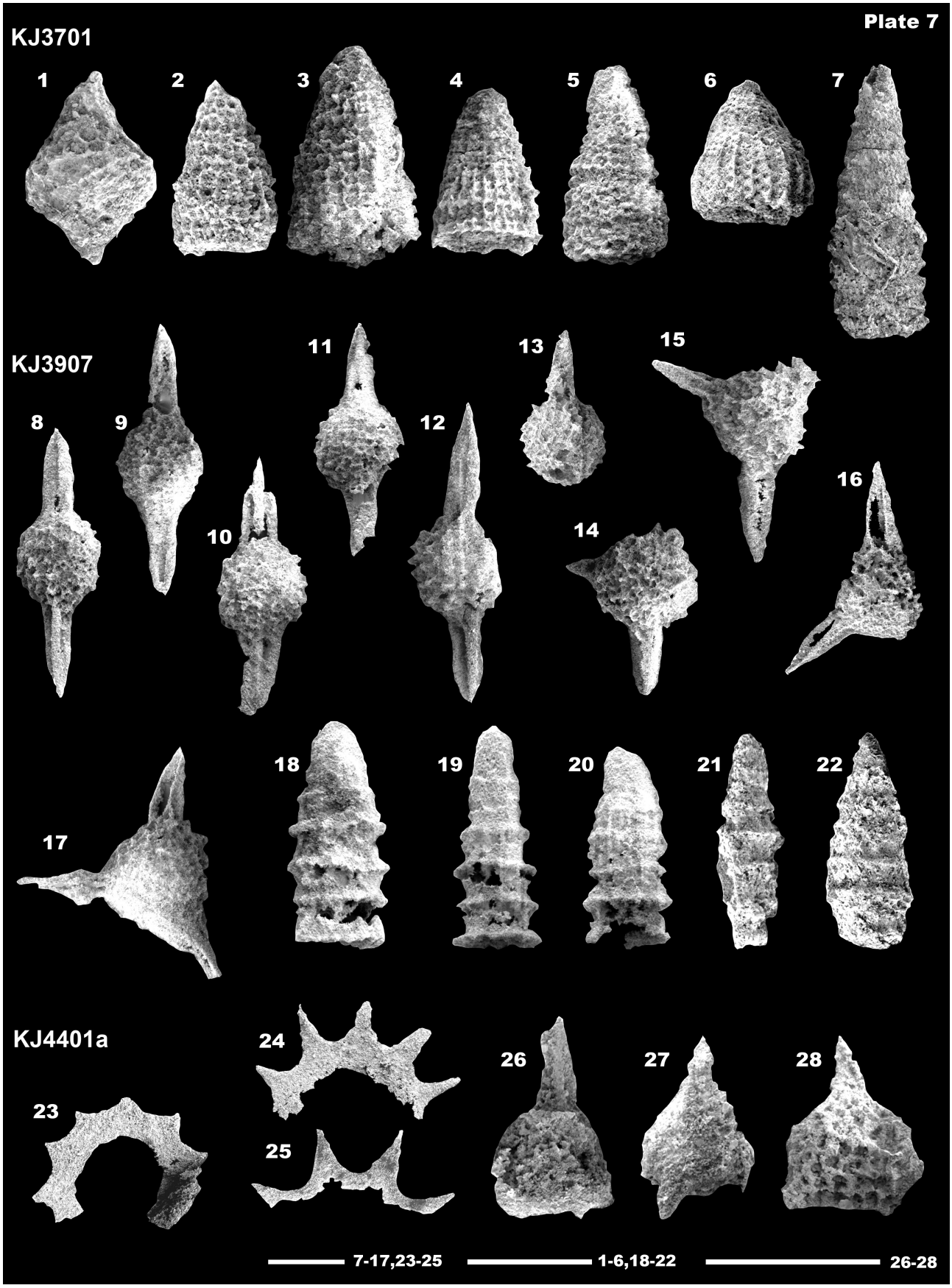
Plate 7
KJ3701
1
2
3
4
5
6
7
KJ3907
8
9
10
11
12
13
14
15
16
17
18
19
20
21
22
KJ4401a
23
24
25
26
27
28
7-17,23-25
1-6,18-22
26-28

Plate 8 SEM images of Triassic to Middle Jurassic radiolarians from the Kanmuri Yama district.

KJ4405 (Locality Kc-15: Ichindani)
1-2: *Pantanellium* sp. (1: GSJ F18195-013, 2: -009)
3: *Parahsuum* sp. cf. *P. longiconicum* Sashida (GSJ F18195-007)
4-7: *Praeparvicingula* sp. (4: GSJ F18195-004, 5: -006, 6: -005, 7: 001)

KJ4406a (Locality Kc-16: Ichindani)
8: Entactinaria gen. et sp. indet. (GSJ F18196-015)
9: *Zartus* sp. (GSJ F18196-012)
10: Patulibracchiidae gen. et sp. indet. (GSJ F18196-013)
11: *Dictyomitrella*? sp. cf. *D.*? *kamoensis* Mizutani and Kido (GSJ F18196-007)
12: *Praeparvicingula* sp. cf. *P. nanoconica* (Hori and Otsuka) (GSJ F18196-004)
13: *Praeparvicingula gigantocornis* (Kishida and Hisada) (GSJ F18196-006)
14-15: *Praeparvicingula* sp. (14: GSJ F18196-002, 15: -001)
16: *Parvicingula* sp. (GSJ F18196-008)

KJ5904 (Locality Kc-17: Southwest of of Kanmuri-tōge)
17-19: *Pantanellium* sp. (17: GSJ F18215-015, 18: -019, 19: -016)
20-27: *Parahsuum* sp. (20: GSJ F18215-009, 21: -005, 22: -008, 23: -007, 24:-002, 25: -003, 26: -006, 27: -004)
28: *Parahsuum*? sp. A (GSJ F18215-011)
29: *Lantus intermedius* Carter (GSJ F18215-012)

All scale bars equal to 0.1 mm.

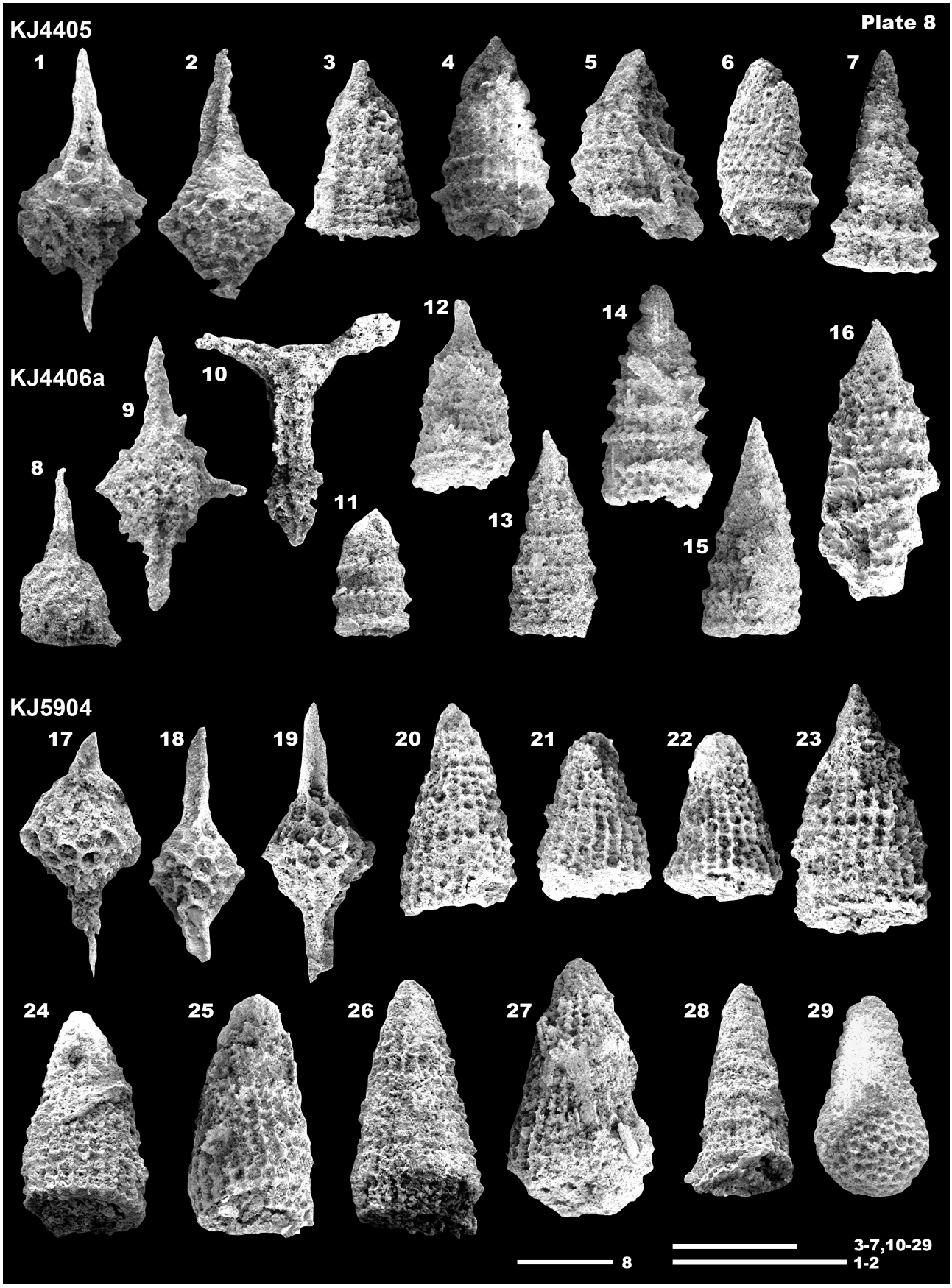
KJ4405
Plate 8
1
2
3
4
5
6
7
KJ4406a
8
9
10
11
12
13
14
15
16
KJ5904
17
18
19
20
21
22
23
24
25
26
27
28
29
8
3-7,10-29
1-2

西南日本南条山地における遠洋性チャートから産出した三畳紀–中期ジュラ紀放散虫 ー 第２部．冠山地域

中江　訓

要　旨

西南日本福井県中央部に位置する南条山地の主要域には，玄武岩・石灰岩・チャート・泥岩・砂岩などの多様な岩石から構成される堆積岩複合岩体が分布する．南条山地におけるこれらの岩石のうち 27 地点の露頭から採取したチャートについて，含有される放散虫化石の検討を行った．その結果，冠山地域では 17 地点 26 試料から Spumellaria 目ならびに Entactinaria 目が卓越する三畳紀群集と Nassellaria 目が卓越するジュラ紀群集が産出した．本報告ではこれらの放散虫化石群集を記載するとともに，その種構成に基づき冠山地域に分布するチャートの地質時代は前期三畳紀（Olenekian）～中期ジュラ紀（Bajocian）に至ると結論した．

難読・重要地名

Fujikuradani：藤倉谷，Fukui：福井，Hirono：広野，Ichindani：イチン谷，Imajō：今庄，Kanmuri-tōge：冠峠，Kanmuri Yama：冠山，Kōkuradani：高倉谷，Masudani：桝谷，Minamiechizen：南越前，Mino：美濃，Tarumi-gawa：多留美川．

地質調査総合センター研究資料集

571	次世代 20 万分の 1 日本シームレス地質図凡例	斎藤　眞・西岡芳晴・宮崎一博・渡辺真人・水野清秀・宝田晋治・森尻理恵・吉川敏之・利光誠一・中江　訓・内野隆之・原　英俊・野田　篤・松浦浩久・高橋　浩・山崎　徹・佐藤大介・小松原琢・植木岳雪・中島　礼・宮地良典・兼子尚知・尾崎正紀・田辺　晋・中野　俊・竹内圭史・青矢睦月
572	産技連地質関係合同研究会地質地盤および地圏環境に関する最近の成果	産技連地質関係合同研究会事務局
573	地質調査総合センター第 19 回シンポジウム「地質学は火山噴火の推移予測にどう貢献するか」	地質調査総合センター　編
574	第 10 回水文学的・地球化学的手法による地震予知研究についての日台国際ワークショップ予稿集	謝　正倫・小泉尚嗣・松本則夫　編
575	第 11 回水文学的・地球化学的手法による地震予知研究についての日台国際ワークショップ予稿集	小泉尚嗣、松本則夫、謝　正倫　編
576	第 1 回アジア太平洋大規模地震・火山噴火リスク対策 (G-EVER) シンポジウム講演要旨集	宝田晋治・石川有三・小泉尚嗣・内田利弘・桑原保人・高田亮・吾妻　崇・田村　亨・古川竜太・吉見雅行　編
577	地質情報展 2012 おおさか　ー過去から学ぼう大地のしくみー	川畑　晶・中島和敏・大熊洋子・百目鬼洋平　編
578	第 3 回火山巡回展霧島火山ーボラ（軽石）が降ってきた！新燃岳の噴火とその恵みー	及川輝樹・筒井正明・田島靖久・芝原暁彦・古川竜太・斎藤元治・池辺伸一郎･佐藤　公･小林知勝･下司信夫・西来邦章・東宮昭彦・宮城磯治・中野　俊・渡辺真人
580	十和田火山御倉山溶岩ドームの反射電子像	宮城磯治・工藤　崇
581	第 3 回火山巡回展　霧島火山ーボラが降ってきた！新燃岳の噴火とその恵みー資料映像「霧島火山新燃岳 2011 年噴火」	芝原暁彦・及川輝樹
582	非常に古い地下水年代測定のための日本列島の帯水層岩石を対象にしたヘリウム同位体生成速度および放射性塩素同位体放射平衡値データ集	森川徳敏・戸崎裕貴
583	第 1 回アジア太平洋大規模地震・火山噴火リスク対策 (G-EVER) シンポジウムプロシーディングス	宝田晋治・石川有三・小泉尚嗣・内田利弘・桑原保人・高田　亮・吾妻　崇・重松紀生・田村　亨・丸山　正・安藤亮輔・古川竜太・吉見雅行　編
584	地質標本館特別展「地球の恵み地熱・地中熱エネルギーを活用しよう」	石戸恒雄・唐澤廣和・水垣桂子・大熊茂雄・阪口圭一・佐脇貴幸・杉原光彦・高倉伸一・内田洋平・柳澤教雄・安川香澄・吉岡真弓

地質調査総合センターの最新出版物

200 万分の 1 地質編集図	No. 4	日本地質図（第 5 版）
	No. 11	日本の火山（第 3 版）
20 万分の 1 地質図幅	伊勢・静岡及び御前崎（第2版）・与論島及び那覇・八代及び野母崎の一部・新潟（第2版）	
5 万分の 1 地質図幅	熱海・榛名山・阿仁合（第2版）・足助・京都東南部・新居浜・青森西部・今庄及び竹波	
海外地球科学図	アジア地質図（1:500 万）	
	中央アジア鉱物資源図（1:300 万）	
海洋地質図	No. 81	日高舟状海盆表層堆積図　（1:20 万）
	No. 82	奥尻海盆表層堆積図　（1:20 万）
構造図	No. 14	全国主要活断層活動確率地図
火山地質図	No. 1	桜島火山地質図（第 2 版）（1:3 万）
	No. 16	十勝岳火山地質図（1:3 万）
	No. 17	諏訪之瀬島火山地質図（1:3 万）
鉱物資源図	No. 7	南西諸島（1:50 万）
特殊地質図	No. 39	千葉県清和県民の森周辺の地質図
重力図	No. 29	姫路地域重力図（ブーゲー異常）
	No. 30	徳島地域重力図（ブーゲー異常）
	S3	甲府地域重力構造図（ブーゲー異常）
空中磁気図	No. 44	岩手火山地域高分解能空中磁気異常図
	No. 45	福井平野地域高分解能空中磁気異常図
数値地質図	G-16	20 万分の 1 日本シームレス地質図　DVD 版
	G-17	九州地質ガイド
	FR-2	燃料資源地質図「東部南海トラフ」
	GT-4	全国地熱ポテンシャルマップ
	S-2	海陸シームレス地質情報集「新潟沿岸域」 DVD 版
	S-3	海陸シームレス地質情報集「福岡沿岸域」 DVD 版
	V-3	口永良部島火山地質データベース
	P-2	日本重力データベース　DVD 版
	G20-1	20 万分の 1 数値地質図幅集「北海道北部」第 2 版
	G20-2	20 万分の 1 数値地質図幅集「北海道南部」第 2 版
	E-5	表層土壌評価基本図　～富山県地域～
その他	日本の熱水系アトラス	
	海と陸の地球化学図	

地質調査研究報告 第64巻 第5/6号
平成25年9月30日　発行

独立行政法人 産業技術総合研究所
地質調査総合センター
〒305-8567 茨城県つくば市東1-1-1
つくば中央第7

Bulletin of the Geological Survey of Japan
Vol.64 No.5/6 Issue September 30, 2013

National Institute of Advanced Industrial
Science and Technology
Geological Survey of Japan
AIST Tsukuba Central 7, 1-1, Higashi 1-chome,
Tsukuba, Ibaraki 305-8567 Japan

AIST13-G68683

Online ISSN : 2186-490X
Print ISSN : 1346-4272
CODEN : CCKHA7

地質調査研究報告

BULLETIN OF THE GEOLOGICAL SURVEY OF JAPAN

Vol. 64 No. 5/6 2013

CONTENTS

GEOLOGICAL SURVEY OF JAPAN
National Institute of Advanced Industrial Science and Technology

1-1, Higashi 1-chome, Tsukuba, Ibaraki, 305-8567 Japan

地 調 研 報
Bull. Geol. Surv. Japan
Vol. 64, No. 5/6, 2013

Bulletin of the Geological Survey of Japan
Vol. 64, No. 5/6, P. 121–190 2013